DOTTORATO DI RICERCA IN SCIENZE CLINICHE

CICLO XXXIII

COORDINATORE Prof. Lorenzo Cosmi

Advanced Magnetic Resonance Imaging in cardiothoracic and abdominal imaging

Settore Scientifico Disciplinare MED/37

Dottorando
Dott. Grazzini Giulia

(firma)

Tutore
Prof. Fainardi Enrico

(firma)

Coordinatore
Prof. Cosmi Lorenzo

(firma)

Prof. COSMI LORENZO
Matr. 999314

Anni 2017/2021

A mio figlio che mi ha donato la gioia più grande
A mio marito che mi ha sempre supportato e consigliato
Ai miei genitori che mi hanno sempre spronato a dare il massimo
G.G.

General Introduction **3**
Advanced MRI in Thoracic Imaging 3
Advanced MRI in Cardiac Imaging 6
Advanced MRI in Abdominal Imaging 8
Radiomics **9**
Cardiac Magnetic Resonance **17**
Basic Physics of CMR 18
Spatial Encoding and Image Construction 22
Motion Compensation 23
Imaging Planes for Cardiac Structures 27
Main sequences in CMR 32
Image analysis 43
T1 mapping 47
T2 and T2* mapping 54
Indications for CMR 55
Myocardial ischemic disease 56
Myocardial non ischemic disease 58
Quantification of nonviable tissue in Late Gadolinium Enhancement **65**
The prognostic role of the Late Gadolinium Enhancement 65
Myocardial segmentation techniques on late gadolinium enhancement sequence 67
Our experience **71**
Introduction **71**
Material and Methods **73**
Results **87**
Discussion **97**
References **110**

General Introduction

Magnetic Resonance Imaging (MRI) has now entered in clinical practice as a radiation-free diagnostic imaging thanks to the increasingly availability of MR scanner and the ongoing technical improvement. Moreover, the development of innovative sequence techniques, such as Perfusion imaging (PwI), Diffusion imaging (DwI) and mapping techniques, allowed to progress from morphological MRI to functional MRI and from qualitative evaluation to quantitative analysis. Therefore, advanced MRI is able to provide new and useful diagnostic data in cardiothoracic and abdominal imaging. The most recent advanced MRI technique is the Radiomics, which deserves its own chapter.

Advanced MRI in Thoracic Imaging

In the study of the lung, current MRI techniques enable functional imaging allowing for a comprehensive assessment of lung disease. PwI can quantitatively evaluate the combined effects of plasma blood flow, permeability, and capillary surface area. Therefore, PwI of the lung is revealing as an alternative to nuclear medicine in the assessment of pulmonary perfusion. This technique is suitable for the quantitative analysis of regional pulmonary blood flow in order to obtain an objectively assessment. Pulmonary blood flow (PBF), mean transit time (MTT), and pulmonary blood volume (PBV) can be calculated (Henzler et al. Eur J Radiol 2010).

Indications for the assessment of pulmonary perfusion are various. Perfusion MRI showed a higher diagnostic accuracy for the detection of pulmonary embolism when compared to multi-detector CT and ventilation-perfusion scintigraphy (Ohno et al. AJR Am J Roentgenol 2004). Perfusion MRI has an application also in patients with cystic fibrosis in order to study changes in regional lung perfusion due to the hypoxic vasoconstriction; perfusion MRI showed a good agreement to pulmonary function tests and radionuclide lung scintigraphy (Eichinger et al. Eur Radiol 2006). In patients with chronic obstructive pulmonary disease, quantitative perfusion MRI shows a reduction of mean PBF, MTT, and PBV and it is more accurate than radionuclide scintigraphy in detecting perfusion abnormalities in these patients (Fink et al. Radiology 2004). Finally, MR perfusion may be used to improve therapy planning and to predict the postoperative lung function (Henzler et al. Eur J Radiol 2010).

In the last years, DwI of the thorax has become feasible thanks to the developments of innovative techniques allowing a significant reduction of the artifacts from respiratory and cardiac motion. DwI is able to provide an assessment of tumor cellular cramming. In chest imaging, the mainly application of DwI is for the characterization of lung cancer, lymph nodes and pulmonary metastases (Henzler et al. Eur J Radiol 2010). As other malignant tumors, lung cancer is characterized by increased cellularity so that the diffusion of water molecules is restricted, resulting in decreased apparent diffusion coefficient (ADC) (Padhani et al. Neoplasia 2009). Ohba et al. showed that DwI is equivalent to PET in differentiating malignant and benign lung nodules (Ohba et al. J Thorac Cardiovasc Surg 2009). DwI may be also used to the M- and N-staging of lung cancer.

The whole- body MRI with DwI showed a good accuracy for M-stage assessment in patients with non-small cell lung cancer (Ohno et al. Radiology 2008). In differentiating metastatic and non-metastatic lymph node stations DwI is more accurate than PET-CT because of fewer false-positive results (Naruke et al. J Thorac Cardiovasc Surg 1978).

DwI and PwI are promising tools for evaluation of early response to chemotherapy or radiotherapy, in particular for the assessment of mediastinal residual masses in patients with Hodgkin's and non-Hodgkin's lymphoma (Henzler et al. Eur J Radiol 2010). Our research group carried out a prospective study to compare the diagnostic performance of advanced MRI (DwI and PwI) with PET/CT in the assessment of residual masses in patients with lymphoma. In particular, we aimed to investigate whether MRI can decrease the false-positive or false-negative rate and can be a valid alternative to PET/CT evaluations. We enrolled 25 consecutive patients (17 females and 8 males aged 40.5 ±16 years) with a histological diagnosis of lymphoma, and who had residual disease of ≥ 3 cm at the end of therapy. All patients underwent MRI and PET/CT 3–4 months after the end of immuno-chemotherapy and chemotherapy plus radiotherapy. The residual masses were analyzed by 2 radiologists experienced in MRI. They evaluated 3 parameters: morphological-contrastographic (MC) features, DwI, and PwI. The residual disease was defined as being active if 2 or 3 of the parameters were positive and inactive if 2 or 3 parameters were negative. PET/CT used a 5-point scale (based on the Deauville criteria) for the end-of-therapy response assessment of residual disease. Scores of 1–3 were considered negative for residual disease. The diagnostic accuracy of MRI and PET/CT was calculated by

considering the 6-month follow-up as the standard of reference. According to the histology data of the 25 patients, 8 (32%) had HL, 5 (20%) had gray-zone lymphoma (GZL), and 12 (48%) had NHL (8 with primary mediastinal large B cell lymphoma, 2 with diffuse large B cell lymphoma, and 2 with follicular lymphoma). At the 6-month follow-up, 22 patients showed a complete remission and 3 had a partial remission. No statistically significant differences were found between the false-positive or false-negative errors on MRI and PET/CT ($p = 0.46$ and $p = 1$, respectively). The agreement between the 2 radiologists for the MRI evaluation was excellent ($\kappa = 1$).

The specificity, negative predictive value, and accuracy were 86, 95, and 84% and 73, 89, and 68% for MRI and PET/CT, respectively. MRI and PET/CT results correlated in 19 of 25 cases (agreement rate = fair; $\kappa = 0.35$). Upon review of the 6 discrepant cases, 4 were false-positive PET/CT errors, 1 was a false-positive MRI error, and 1 was a false-negative PET/CT error. In conclusion, our results showed that advanced MRI had greater diagnostic accuracy than PET/CT for the evaluation of the residual masses in lymphoma at the 6-month follow-up (84 vs. 68%). At the end of therapy, it could be used to confirm a positive or negative PET/CT result. During long-term follow-up, it could be an alternative technique when the first check-up of the residual mass on PET/CT is negative (Calistri et al. Acta Haematol 2018).

Advanced MRI in Cardiac Imaging

Cardiac MRI is currently considered the gold standard for myocardial characterization (Cummings et al. RadioGraphics 2009). In spite of this potential capability, the traditional Cardiac MR sequences provide only a subjective qualitative analysis of signal intensity.

Newer T1 and T2 myocardial mapping techniques offer a quantitative assessment of the myocardium (by using T1 and T2 relaxation times), which can be helpful in focal disease and especially in the evaluation of diffuse myocardial disease (e.g. edema and fibrosis) (Hamlin et al. Radiographics 2014).

Myocardial edema can be evaluated using T2 mapping techniques. These have shown a superior performance compared to the traditional T2-weighted and STIR sequences (Ferreira et al. J Thorac Imaging 2014). T2 mapping can detect edematous myocardial territories in a variety of cardiac pathologies, including acute myocardial infarction, myocarditis, Tako-tsubo cardiomyopathy, and heart transplant rejection.

T1 mapping techniques, performed both with and without contrast medium, enable to quantify diffuse myocardial fibrosis and to assess myocardial edema and infiltration. Native myocardial T1 values have been reported to be elevated in a lot of cardiac diseases including myocardial infarction, myocarditis, hypertrophic and dilated cardiomyopathy and cardiac amyloidosis. Reduced T1 times in the myocardium have been reported in presence of fat inside cardiac masses, in Anderson-Fabry disease, and in myocardial siderosis (Ferreira et al. J Thorac Imaging 2014).

In addition, non-enhanced and contrast-enhanced T1 mapping are useful, in conjunction with the hematocrit value, for calculating the extracellular volume fraction (ECV), a measure of the proportion of extracellular space within the myocardium. ECV quantification is more reproducible across different vendors and different acquisition techniques than T1 values. ECV can be used to identify and characterize diffuse fibrosis or subtle myocardial abnormalities (Hamlin et al. Radiographics 2014).

In our retrospective study to evaluate the incidence of late-gadolinium-enhancement (LGE) in mitral valve prolapse (MVP), and its association with the degree of mitral regurgitation (MR) and/or with complex ventricular arrhythmia (ComVA), we also analysed the role of T1 mapping in the evaluation of MVP patients. We found that patients with MVP had higher native T1-values, lower post-contrast T1-values and increased ECV-values compared with controls (p=0.01, 0.01 and 0.00, respectively). T1 mapping significantly confirmed LGE and it was more sensitive in identifying alterations in one patient. However, no significant associations between the MR severity and ComVA and T1/ECV values were found (Pradella et al. European Radiology 2018).

Perfusion CMR imaging has been shown to be an important method to diagnose myocardial ischemia, to predict the hemodynamic significance of coronary stenosis and to determine the prognosis after myocardial reperfusion. Stress myocardial perfusion MRI has a diagnostic accuracy similar to PET in ruling out hemodynamically significant coronary artery disease (Takx et al. Circ Cardiovasc Imaging. 2015).

Advanced MRI in Abdominal Imaging

DwI and PwI techniques are increasingly used in the abdomen particularly in the evaluation of diffuse and focal liver diseases. Thanks to its high tissue contrast, DwI allows the detection of hepatic focal lesions with a great sensitivity and it has been considered an alternative to gadolinium-enhanced T1 weighted imaging for detection of liver metastases. Furthermore, several studies showed that DwI in association with gadolinium-enhanced MRI increases

sensitivity for detection of hepatocellular carcinomas (Li et al. PLoS One. 2015). DwI may be helpful in lesion characterization, differentiating between benign from malignant lesions on the base of ADC values. In our retrospective study on 25 patients with pathologically proven primary hepatic lymphoma (PHL) we found that all the PHLs showed restricted diffusion on DwI with ADC values lower than of the other hepatic lesions (Colagrande et al. Abdom Radiol 2018).

ADC measurements have also a potential predictive value of treatment response, because mean ADC increases in metastases or tumor with at least a partial response to chemotherapy (Koh et al. Am J Roentgenol 2007). DwI plays a role also in diffuse liver disease. Lewin et al. found an excellent correlation between ADC values and FibroScan® (sonographic elastography technique) and serum markers of fibrosis; ADC values are lower in patients with moderate-to-severe fibrosis than those with mild fibrosis and healthy volunteers (Lewin et al. Hepatology 2007).

Liver perfusion MRI is currently being actively investigated as a functional imaging technique that allows the characterization of the angiogenic activity of HCC and liver metastases, especially helpful for predicting and monitoring treatment response to antiangiogenic therapy (Chandarana et al. Eur J Radiol. 2010).

Radiomics

Radiomics is a novel image analysis technique, whereby digital images are converted to data that can be analysed to derive multiple numerical quantifiers of shape and tissue character—referred to as 'radiomics features'. With radiomics, it is now possible to rapidly

extract innumerable quantitative features from tomographic images (computed tomography [CT], magnetic resonance [MR], or positron emission tomography [PET] images). Radiomics is motivated by the concept that biomedical images contain information that reflects underlying pathophysiology and that these relationships can be revealed via quantitative image analyses. Thus, radiomics features may be used as predictor variables in statistical models for diagnosis or outcome prediction. Radiomics has been initiated in oncology studies, but it is potentially applicable to all diseases. Quantitative image features based on intensity, shape, size or volume, and texture offer information on tumor phenotype and microenvironment (or habitat) that is distinct from that provided by clinical reports, laboratory test results, and genomic or proteomic assays. Radiomics models have had notable success in oncology, where their utility in classification of tumours, prediction of treatment response, and prognostication has been demonstrated in multiple cohorts (Gillies et al. Radiology 2016).

For a clinical radiologist, radiomics has the potential to help with the diagnosis of both common and rare tumors. Visualization of tumor heterogeneity may prove critical in the assessment of tumor aggressiveness and prognosis. For example, research has already shown the capacity of radiomics analyses to help distinguish prostate cancer from benign prostate tissue or add information about prostate cancer aggressiveness (Wibmer et al. Eur Radiol 2015). In the evaluation of lung cancer and in the evaluation of glioblastoma multiforme, radiomics has been shown to be a tool with which to assess patient prognosis (Coroller et al. Radiother Oncol 2015). Many studies revealed that radiomics can help predict tumor grade. (Shiradkar et al. J Magn Reson Imaging 2018; Lambin et al. Eur J

Cancer 2012; Kumar et al. Magn Reson Imaging 2012). Good results have been achieved in terms of grading classification by radiomics in clear cell renal cell carcinoma, colorectal adenocarcinoma, and gliomas (Ding et al. European journal of radiology 2018; Huang et al. Academic radiology vol. 25,10 2018; Tian et al. Journal of magnetic resonance imaging 2018).

However, radiomics can be applied to a large number of conditions and there is a growing interest in using it in cardiac imaging where experience with radiomics is still limited. Texture analysis is the most common type of radiomic analysis performed in CMR imaging (Hassani et al. AJR Am J Roentgenol. 2020). Some studies showed that texture analysis of unenhanced CMR images could be successfully used to identify, differentiate, and diagnose cardiomyopathies (Schofield et al. Clin Radiol 2019; Shao et al. Medicine Baltimore 2018). On this background, we chose to focus our study on radiomics in cardiac imaging because the experience in this field is still limited.

The practice of radiomics involves discrete steps each with its own challenges. These steps include: (a) image acquisition, (b) volumes of interest identification, (c) segmentation (ie, delineating the borders of the volume), (d) feature extraction from the volume, (e) feature selection, and (f) mining these data to develop classifier models to predict outcomes either alone or in combination with additional information, such as demographic, clinical, comorbidity, or genomic data.

Image acquisition. Radiomics analysis can be applied to standard, routinely acquired clinical images. However, Modern CT, MR imaging, and combined PET/CT units allow for wide variations in acquisition and image reconstruction protocols, and standardization

of these protocols across medical imaging centers is typically lacking. These are technical challenges to the individual steps in the process of radiomics because variations in acquisition and image reconstruction parameters can introduce changes that are not due to underlying biologic effects. CT-based studies of reproducibility have shown that differences in acquisition and reconstruction settings can significantly alter radiomic results (Midya et al. J Med Imaging Bellingham 2018; Kim et al. PLoS One 2016). Others studies do report significant differences in radiomic reproducibility depending on differences in MR image acquisition, which type of MRI sequence, and which radiomic feature is being analyzed (Traverso et al. Int J Radiat Oncol Biol Phys 2018; Shiri et al. Iran J Radiol 2017). Thus, reproducibility of any given radiomic study is a constant challenge. The most rigorous radiomics investigation requires a prospective multicenter trial wherein acquisition and image reconstruction protocols are standardized.

Volume of Interest Identification and Segmentation. Once the image to be used is selected, the area for radiomics analysis is defined by contouring a region of interest (ROI). The ROI may be a limited area or multiple areas. As the radiomics features are extracted from the defined areas, variations in contouring that alter the ROI will change the values of the radiomics features. Thus, segmentation is the most critical, challenging, and contentious component of radiomics. There are ongoing debates over whether to seek ground truth or reproducibility and how much to rely on manual or automatic segmentation. However, a consensus is emerging that truth is elusive and that optimum reproducible segmentation is achievable with computer-aided edge detection followed by manual curation. It is well recognized that interoperator variability of manually contoured

tumors is high (Rios Velazquez et al. Radiother Oncol 2012). Segmentation of normal structures, such as skeletal elements and organs, can now be achieved with full automation. However, any disease, especially cancer, requires operator input because of inter- and intrasubject morphologic and contrast heterogeneity at the initial examination (Gillies et al. Radiology 2016).

Feature Extraction. The heart of radiomics is the extraction of high-dimension feature data to quantitatively describe attributes of volumes of interest. Extraction of radiomics features from the segmented ROI can be performed through dedicated pipelines developed by individual centres or using open-source packages, such as 3D-slicer. Radiomics features include Shape features and agnostic features that can be divided into first-, second-, or higher order statistical outputs (subsumed under the term "texture analysis" [TA]). Radiomics shape features quantify the 3D size and shape of the segmented volume. Radiomics shape features include conventional indices (e.g. volume), as well as additional parameters, such as surface area and dimensions in multiple planes. There are also descriptors of the overall shape of the ROI, such as compactness, sphericity, elongation, and flatness. Texture features are derived by assigning a signal intensity (SI) level to each voxel in the region of interest and considering the pattern and relationships between different voxel signal intensities through application of various mathematical processes. This is a slightly more abstract concept in comparison to the shape analysis. The first step to performing radiomics texture analysis is construction of a 'SI matrix', whereby each voxel within the ROI is assigned a number (level/value) depending on the intensity of signal in that voxel. The SI value for every voxel in the ROI is then tabulated to form a simple matrix. All

SI-based radiomics features are derived from analysis of the SI matrix. The most straightforward analysis of the SI matrix involves creating a histogram of the SI levels identified in the ROI and the frequency with which they are observed. From this, first-order histogram-based statistics can be computed. This includes simple descriptive summary statistics, such as mean, median, and standard deviation, as well as less familiar measures of skewness (asymmetry), kurtosis (flatness), and entropy (randomness or disorder). These histogram-based texture features describe the distribution of values of individual voxels without concern for spatial relationships. In order to consider the relationship of neighbouring voxel SIs, more complex mathematical approaches to analysis of the SI matrix are required. These features are derived by considering the spatial distribution of SIs within the ROI and aim to quantify heterogeneity, repeatability, and complexity of the SI matrix. For instance, a common approach for considering the relationship between voxel pairs is through construction of a grey-level co-occurrence matrix (GLCM). The GLCM is constructed by tabulating the frequency of different SI pairings occurring within the SI matrix. Different mathematical processes are then applied to the GLCM to compute, according to agreed definitions, measures, such as angular second moment (homogeneity), contrast (local variation), and entropy (disorder or randomness). These features reflect the probability of certain SI pairings, the level of greylevel variation interdependencies, and the extent of disorder within the ROI. The grey-level run length matrix (GLRLM) is another commonly constructed matrix. It can be used to consider the spatial relationship of any number of voxels (not just pairs). A GLRLM is constructed by recording the number of times a voxel with a specific SI is seen in an uninterrupted run within the

image SI matrix in a specified direction. The GLRLM is used to calculate a number of features such as short-run emphasis, run-length non-uniformity, and run entropy. A number of other matrices, tabulated according to different rules, are also available for calculation of additional features [grey-level size zone matrix (GLSZM), grey-level difference matrix (GLDM), and neighbouring grey tone difference matrix (NGTDM)] (Raisi-Estabragh et al. European Heart Journal - Cardiovascular Imaging 2020). Thus, Second-order statistical descriptors describe statistical interrelationships between voxels with similar (or dissimilar) contrast values. Finally, Higher-order statistical methods impose filter grids on the image to extract repetitive or nonrepetitive patterns. These include fractal analyses, wherein patterns are imposed on the image and the number of grid elements containing voxels of a specified value is computed; Minkowski functionals, which assess patterns of voxels whose intensity is above a threshold; wavelets, which are filter transforms that multiply an image by a matrix of complex linear or radial "waves"; and Laplacian transforms of Gaussian bandpass filters that can extract areas with increasingly coarse texture patterns from the image (Gillies et al. Radiology 2016).

Feature selection. The process of feature extraction will yield a large number of radiomics features (100–1000 s). The aim is to use the extracted features as predictor variables within a statistical model for disease classification or outcome prediction. The number of extracted radiomics features often far exceeds the sample size of cohorts used for model building. Using all the extracted features in a statistical model would lead to overfitting. Therefore, we need to select a reduced number of features for model building. The purpose of feature selection is to identify the optimal set of radiomics features to

be taken forward for model building. We would aim to include in the model features that are most informative and robust and remove those that are unstable or provide repetitive information. Various methods may be used to identify such highly correlated features and select the most informative.

The most popular approaches are unsupervised machine learning methods such as clustering and principal component analysis.

Clustering algorithms group features into clusters based on high correlation with each other (inter-cluster correlation) and low correlation with other features (extra-cluster correlation). The algorithm then identifies the most defining feature from each cluster for inclusion in the model and removes the rest. Principal component analysis through different methods reduces the extracted features to a subset that provides nearly as much information as the whole feature-set. Regardless of the method used for feature selection, the common goal is identification of a reduced set of radiomics features that are robust, informative, and non-redundant for inclusion in the predictive model (Raisi-Estabragh et al. European Heart Journal - Cardiovascular Imaging 2020).

Model building. Once we have identified the final set of radiomics features through feature selection, we can begin to build our classification model. The predictor/discriminatory variables will be the radiomics features (input) and the output will be the desired label. To build the model, we require a sample (training set) of example cases (training examples) with known inputs and outputs, from which we have extracted and selected our features. In some cases, logistic regression will be adequate to address a simple classification problem. More commonly, machine learning algorithms are used to train different models, from these, the model with the best

performance is selected. Support vector machines (SVMs) are a commonly used machine learning algorithm for addressing classification problems with capability of modelling both linear and non-linear (SVMwith kernels) relationships. The SVM identifies all the hyperplanes that could separate the different classes within the training set and selects the one that maximizes the margins between classes (Raisi-Estabragh et al. European Heart Journal - Cardiovascular Imaging 2020).

Cardiac Magnetic Resonance

In 1977, the first magnetic resonance scan of a human body was accomplished, but the required scan time of almost 5 hours prevented use of this technology as a clinical tool (Damadian et. al FONAR image of the live human body 1977). Further refinement of the technique in the 1980's resulted in electrocardiography (ECG)-gated Cardiovascular Magnetic Resonance imaging (CMR) of the heart (Didier et al Thieme 2003). As a result of various developments in terms of hardware, pulse sequences, and the ability of post-processsing techniques, CMR nowadays allows us to depict cardiovascular anatomy with a high spatial and temporal resolution. These image sequences permit not only the morphological examination of the heart, including left ventricular dimensions, but they also make functional assessment possible, including accurate and reproducible assessment of left ventricular (LV) function. This has enabled CMR to emerge as a powerful tool for physicians to diagnose various cardiac pathologies, guide therapies, and predict outcome and prognosis (Bruder et al. J Cardiovasc Magn Reson 2013).

Furthermore, CMR is able to characterize myocardial tissue after the administration of gadolinum, so-called Late Gadolinium-Enhanced CMR (LGE-CMR) (Shulz-Menger et al. J Cardiovasc Magn Reson 2013), which previously has been referred to as Contrast-Enhanced CMR (CE-CMR) or Delayed-Enhanced CMR (DE-CMR). This technical approach can be valuable for the evaluation of both patients with ischemic heart disease, who developed a myocardial infarction, as well as for patients with non-ischemic heart diseases, as for instance myocarditis. Currently, CMR is considered the "gold" standard for non-invasive assessment of LV function and tissue characterization (Pilz et al. Minerva Cardioangiol 2009). CMR is undergoing a rapid, continuous evolution and other new CMR techniques, such as T1 and T2 mapping, are available.

Basic Physics of CMR

The basic principles of MRI are the same irrespective of the part of the body. However, there are specific areas of MRI physics that are particularly important for CMR (i.e. motion compensation and cardiac relevant MRI sequences).

MRI is based on nuclear magnetic resonance, the phenomenon of the resonance of atomic nuclei in response to radiofrequency (RF) waves. The presence of an external magnetic field (B_0) is used to align the nuclear magnetization of hydrogen atoms (H+, protons), which are abundant in the human body. In quantum terms, nuclei align either parallel or antiparallel to the B_0 field due to the fact that protons can occupy multiple energy states. Low-energy protons line up parallel to B_0 while high-energy protons line up antiparallel. There

is always a small excess of parallel protons and thus the net magnetic vector (NMV) is in the direction of the B_0 field.

In the presence of a B_0 field the protons do not simply line up, they actually precess around the B_0 axis (Fig. 1a). The precessional frequency (ω) of a MR active nucleus is given by the Larmor equation: $\omega = \gamma B0$, where γ is the gyromagentic constant, a nuclei specific constant. Hydrogen exposed to a 1.5T field precess around the B_0 axis at approximately 64 MHz. When protons precess in synchrony they are said to be in-phase. When they are out of phase with each other, the NMV does not precess and only has a component in the direction of the B_0 field.

These hydrogen nuclei are then excited intermittently by pulses of radiofrequency (RF) waves (a magnetic resonance [MR] sequence), and the signal emitted from the body in return is detected with MR receiver coils. Specifically, the RF energy, inputted into the system, causes moving of NMV (M_0) toward a plane perpendicular to the B_0 field (Fig. 1b).

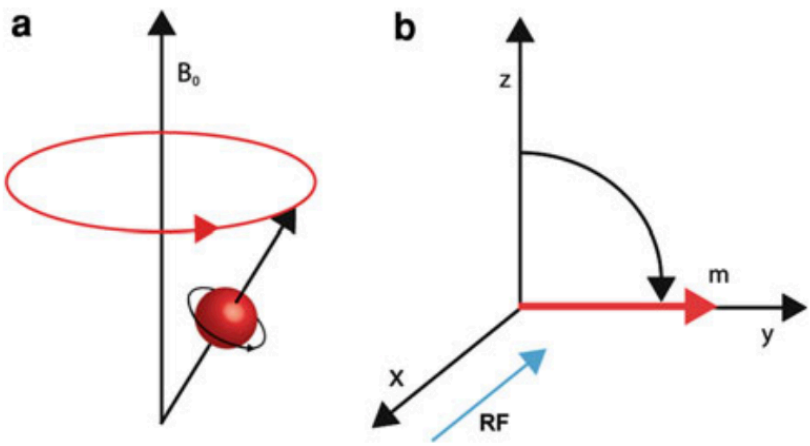

Fig 1. A) Proton spinning around its own axis while precessing around the z-axis (i.e. the direction of the static field). B) RF excitation causing flipping of z magnetization into the x–y plane

Therefore, if the B_0 field is assumed to be in the z direction (along the bore of the MR scanner), RF excitation cause the flipping of M_0 from z to the the x–y plane (Fig. 1b). The flip angle is dependent on the strength and duration of RF pulse, with a 90° flip placing all the longitudinal magnetization into the transverse plane. The flipped magnetization vector now has a transverse component, which forms the basis of the MR signal.

Faraday's law of electromagnetic induction states voltage will be induced in a conductor exposed to a changing magnetic field. Longitudinal magnetization does not change and therefore it cannot induce a voltage. Transverse magnetization on the other hand rotates in the x–y plane and therefore it will induce a voltage in a conductor. This is an important point to note: only the transverse component of M_0 induces voltage. However this signal does not stay the same indefinitely, but rather relaxes back to its resting state. It is this relaxation that forms the basis of MRI contrast. Relaxation is the process by which magnetization returns to its resting state after RF excitation. There are two processes involved (T1 and T2 relaxation), both of which are dependent on the atomic arrangement within tissues. Thus, the rate of relaxation is tissue specific and can be used to develop tissue contrast.

T1 relaxation times measure the time after excitation to recover the longitudinal magnetisation found in the equilibrium state. Transverse magnetisation decays at a rate measured by T2, which is faster than the rate of T1 recovery. T1 and T2 relaxation vary according to the environment of the H^+ atom within tissues and imaging sequences can be designed with different preference (or weighting) to one of these relaxation parameters for tissue characterisation, known as T1-weighted (T1W) and T2-weighted (T2W) acquisitions. T1 relaxation (longitudinal relaxation) is due to transfer of energy from high-

energy protons to the surrounding lattice (spin-lattice relaxation). This causes the NMV to flip back into the z direction; during this process longitudinal magnetization recovers exponentially. As T1 depends on the atomic structure of the tissue, it is a tissue-specific constant. In tissues with a short T1 (such as fat) longitudinal magnetization will be recovered more quickly (hyperintensity signal) than in tissue with a longer T1 (such as muscle) (hypointesity signal). The nature of the exponential recovery curve means that when time equals T1, 63% of z magnetization will have recovered (Fig. 2).

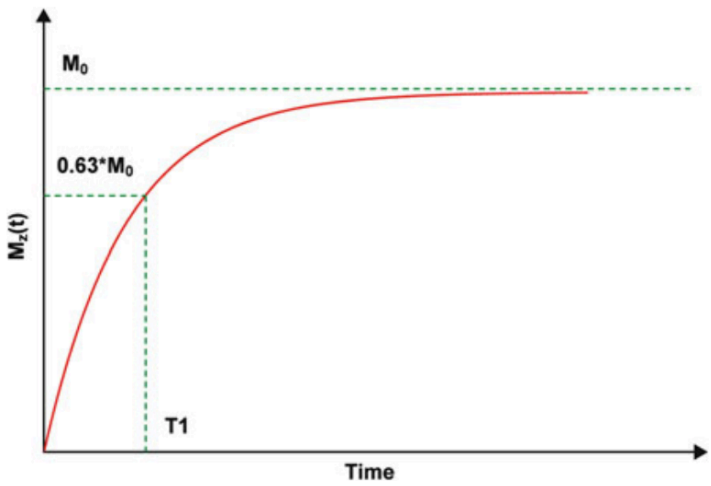

Fig 2. T1 relaxation curve.

The other relaxation process is T2 relaxation (transverse relaxation) and is due to dephasing of the individual spins leading to a reduction in coherent transverse magnetization. This is due to the interaction between the magnetic fields of adjacent protons (spin–spin interactions) and results in different protons precessing at different rates. In the rotating frame of reference, this variation in frequency is seen as dephasing. Thus, the coherent magnetization vector in the x–y plane starts to fan out resulting in a reduction in the net transverse magnetization. Transverse relaxation results in exponential decay of coherent transverse magnetization at a rate governed by T2 (Fig.3).

Thus, when time equals T2, transverse magnetization will have decayed to 37% of its original value. Much like T1, T2 also depends on the atomic structure of the tissue, and is therefore an independent tissue-specific constant. In tissues with a long T2 (such as tissue with a high water content) transverse magnetization will persist longer (hyperintense signal) than tissue in tissue with a shorter T2 (such as fat) (hypointense signal). However, there is a second process that results in loss of transverse magnetization. This is B_0 field inhomogeneity, which also results in dephasing. This accelerated dephasing is encapsulated in the time constant T2*. The T2* value is dependant on the underlying T2 and any field inhomogeneity and is therefore not purely a tissue constant.

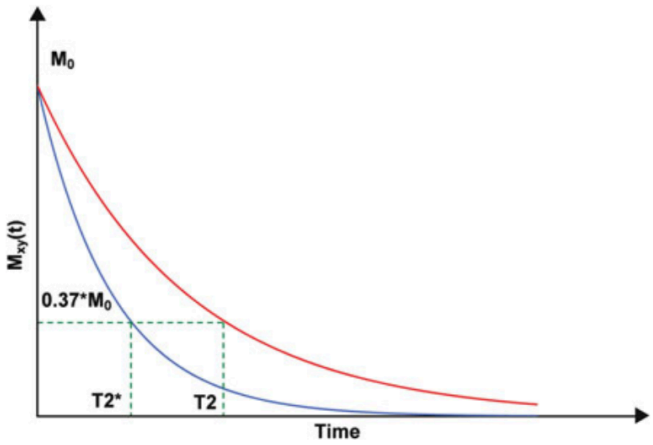

Fig 3. T2 and T2* relaxation curves

Spatial Encoding and Image Construction

The basic purpose of imaging is to understand how an object occupies space. In all cases this requires interaction with the object and subsequent collection of spatially encoded measurements. In MRI, the induced signal is spatially encoded by magnetic gradient fields (a magnetic field whose strength varies with space). As we know the precessional frequency is directly proportional to the

magnetic field. Thus, a magnetic gradient results in a spatially varying precessional frequency. In the rotating frame of reference, a magnetic gradient results in a spatial variation in the phase of the MR signal from different areas. The total MR signal is the vectoral sum of the signals from each area and will now be dependant on the spatial distribution of protons. Because there is more than one distribution of protons that will give the same total MR signal we need to perform more 'experiments' with different gradients. In this way we reach a point where there was only one possible distribution that fits all the collected MR signals. In fact, to create an image with x number of pixels we have to perform x number of experiments or independent measurements. Each independent measurement requires an MR signal to be acquired under a different magnetic gradient (producing different amounts of spatially dependant dephasing).

Motion Compensation

More than any other type of MRI, CMR has to compensate for motion in order to achieve acceptable image quality. Therefore, MRI sequences must be adjusted to account for cardio-respiratory motion. To prevent artifacts from cardiac motion, most CMR images are generated with fast sequences gated to the R-wave of the electrocardiogram. Respiratory motion, another source of artifacts, is usually eliminated by acquiring CMR images in end-expiratory breath-hold.

The purpose of ECG gating is to 'freeze' cardiac motion and this is possible with "segmented k-space acquisition".

MRI signals are stored in a structure called k-space. A position in k-space is proportional to the gradient moment, with the center of k-space coinciding with a zero moment (i.e. no gradient applied) and the edge with the highest moment. Therefore, K-space is a spatial

frequency domain. Thus, a point in k-space represents a given spatial frequency, and not a point in the image. The central portions of k-space encode the low spatial frequencies that equate to the broad contrast in the image, essentially blobs of signal rather than defined objects. The outer portions of k-space encode the higher spatial frequencies that define the edge of an image—the higher the frequency the sharper the edge.

One-way to freeze motion when performing traditional k-space filling is to divide k-space into segments and fill each segment in successive R–R intervals. This is called a segmented k-space acquisition (Finn and Edelman 1993). If the time taken to fill a segment is short or the myocardium is relatively still, motion is essentially frozen. Reducing the number of lines per segment should improve image sharpness. However, reducing the number of lines per segment increases the number of k-space segments. As each segment is acquired in a single R–R interval, increasing the number of segments increases total acquisition time. The segmented k-space approach is the basis of cardiac gating for both single-phase and multi-phase acquisitions.

Single-Phase Acquisitions are used in many types of CMR, such as morphological imaging (e.g. coronary CMR angiography) or tissue characterization (e.g. late gadolinium enhancement) in order to obtain a static image of the heart. CMR data must therefore be acquired at a certain point of the cardiac cycle. The traditional approach is to image during diastasis, as this is the period in the cardiac cycle when the myocardium is most at rest. Diastasis occurs during mid to-late diastole and its length is inversely related to heart rate.

In multi-phase acquisitions, multiple k-spaces are acquired throughout the R–R interval. After inverse Fourier transformation this produces a multi-frame cine of cardiac motion. The easiest way to perform cine MRI is prospective gating. This can be understood by

considering single-phase techniques in which data is acquired in a certain part of the cardiac cycle. If the trigger delay was set at 0 ms the single-phase technique would only acquire the first part of the cardiac cycle (Fig. 4). However, if data acquisition was continued another segment would be acquired and a second k-space would be filled in the same number of R–R intervals. Obviously this would represent the second frame in the cardiac cycle. Consequently, if data was acquired during the whole R–R interval, one could produce a multi-phase cine loop of cardiac motion. In multi-phase sequences, the number of frames acquired depends on the time it takes to fill a segment (i.e. the line per segment). As the lines per segment go up, the number of frames is reduced and thus the temporal resolution falls. However if the lines per segment go down (improving the temporal resolution) the acquisition times goes up. Thus, in multi-phase imaging there must be a compromise between temporal resolution and acquisition time.

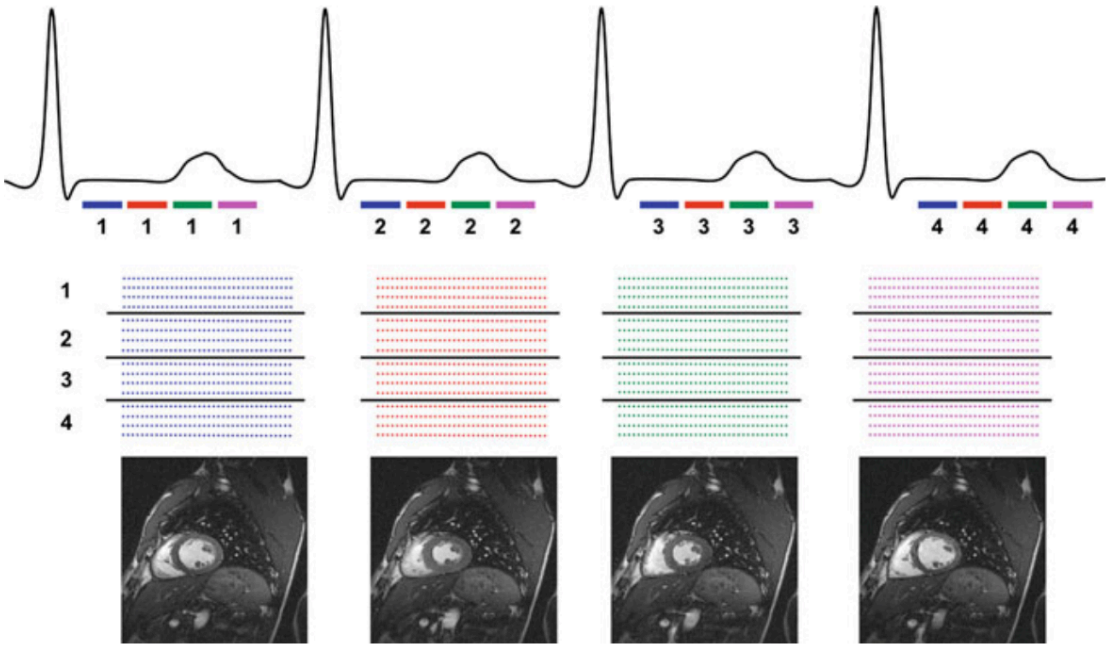

Fig. 4 Prospective multi-phase acquisition. In this example, k-space is divided into four segments—each of which is collected at the same point in the cardiac cycle in four R–R intervals. Each k- space is collected at a different point in the cardiac cycle. Together this data can be reconstructed into a cine image.

End diastole can be imaged if retrospective gating is used (Lenz et al. 1989). In retrospective gating, lines in k-space are continuously collected during the scan. Each line in k-space is then time stamped in relation to the R–R interval it is acquired in. At the end of the scan the average R–R interval is calculated and each individual R–R interval is stretched or compressed to this mean value. This deformation can either be done in a linear manner or in more complex ways in which diastole is stretched more than systole. The end result of this temporal deformation is that all lines in k-space are time stamped relative to the mean R–R interval. They can then be re-binned (in simplistic terms) to produce separate frames. Unfortunately complete filling of k-space requires a certain amount of redundancy, and therefore in retrospective gating more lines are sampled. Thus, retrospective gating has the advantage of imaging throughout the cardiac cycle, although at the cost of slightly longer scan durations.

Not only cardiac motion but also respiratory motion would cause significant artefacts if not taken into consideration. The simplest method of dealing with breathing is to perform imaging during breath holds. Increasing either spatial or temporal resolution will lead to prolonged breath hold times. In longer imaging sequences such as gated whole heart MR angiography, the above-mentioned strategies have little chance of success. These longer acquisitions need a different approach to respiratory motion compensation such as respiratory navigators (Keegan et al. 1999). Fundamentally these are simple MR measurements of diaphragmatic position that enable data acquisition to be restricted to certain points in the respiratory cycle.

Imaging Planes for Cardiac Structures

The transverse or axial plane (Fig. 5) is useful for studying morphology and the relationships of the four cardiac chambers and the pericardium. These images are appropriate for evaluation of the overall morphology of the heart but quantitative measurements of wall thickness, cavity dimensions and functional data cannot be obtained accurately since the planes are not perpendicular to the wall or the cavity (Longmore et al. 1985). Therefore the cardiac imaging planes are more suitable for this purpose. To obtain the correct inclinations for imaging in the cardiac axes, a transverse or axial scout view at the level of the left ventricle (LV) is acquired initially (Burbank et al. 1988). On this image, a new plane is chosen running through the apex of the LV and the middle of the left atrioventricular (AV), mitral valve. This yields the vertical long-axis (VLA) plane (Fig.6b). On this image, a plane chosen to transect the LV apex and the middle of the mitral ring yields the horizontal long-axis (HLA) plane (Fig.6c). The short-axis (SA) plane can now be prescribed perpendicular to both the VLA and HLA (Fig.6d). From a SA plane at the level of the mitral valves, the four-chamber view can be acquired (4Ch). The plane for the 4Ch view passes from the most superior mitral valve,''anterolateral'' papillary muscle to the inferior angle of the right ventricle (RV) anteriorly, usually through the mid-point of the interventricular septum (Fig.6e). A true-SA plane can now be prescribed off the 4Ch view perpendicular to the interventricular septum and parallel to the AV valves (Fig. 7).

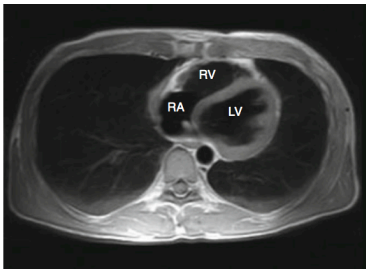

Fig. 5 Axial plane through the mid-thorax

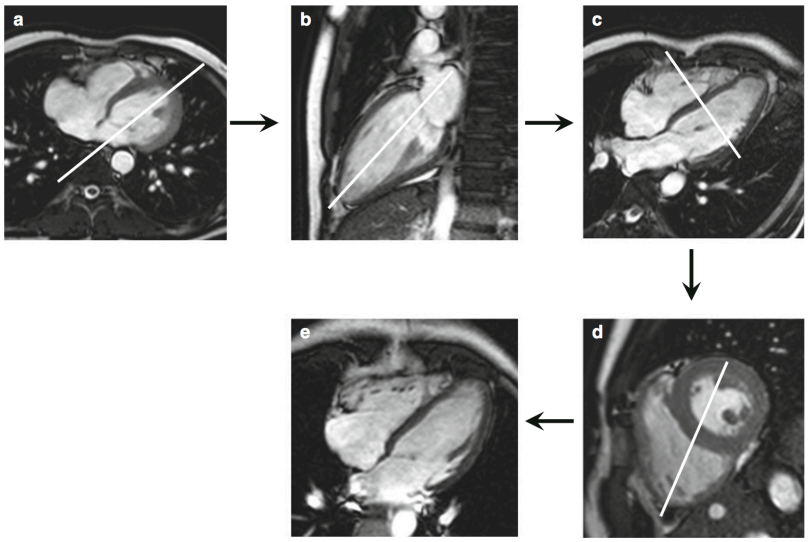

Fig 6. Cardiac axis imaging planes for the left ventricle, images acquired using a SSFP sequence. The vertical long-axis plane (VLA) (b) is aligned from the axial plane (a) through the mitral valve and the LV apex, which may be on a separate more inferior slice. The horizontal long-axis plane (HLA) (c) is aligned from the VLA through the mitral valve and LV apex. The short-axis plane (SA) (d) is aligned from the VLA and HLA planes—perpendicular to both. The 4-chamber plane (e) is aligned from the SA through the anterior mitral valve papillary muscle and the apex of the RV.

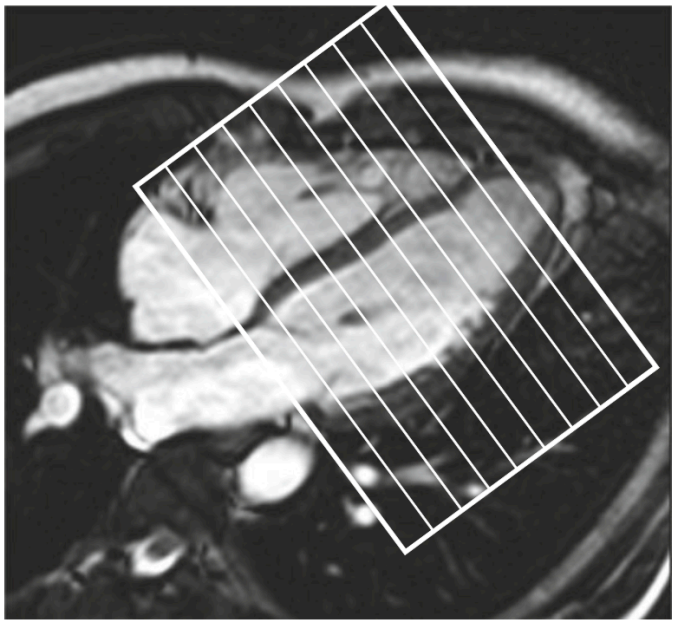

Fig. 7 Alignment of SA stack for analysis of ventricular volumes on the HLA. Note that the basal slice is parallel to the atrioventricular (AV) valves (between the anterior and posterior AV grooves), and almost perpendicular to the interventricular septum.

Left Heart

From the SA plane the VLA (2Ch), HLA (4Ch) and LV inflow/ outflow (3 Ch) can be acquired (Fig. 8). This later LV inflow/outflow image is acquired with a plane that passes across the center of the aortic and mitral valves on the basal SA slice. A view of left ventricular outflow tract (LVOT) can be acquired by passing an imaging plane through and perpendicular to the aortic (Fig.9b). This can be easily achieved by indicating on an LV inflow/ outflow image a perpendicular imaging plane through the middle of the aortic valve. Both the LVOT and LV inflow and outflow planes are well suited for evaluation of aortic valve stenosis and/or regurgitation. A plane through the aortic root (''aortic valve plane''), just above the aortic valve, perpendicular to both the LV inflow/outflow and LVOT views, can be used to assess through-plane aortic flow. This plane is used when quantifying aortic incompetence (Fig.9). The morphology of the aortic valve (e.g., number of valve leaflets and fusion of leaflets), aortic valve area and orifice can be best studied in this plane using a set of adjacent slices through the aortic valve.

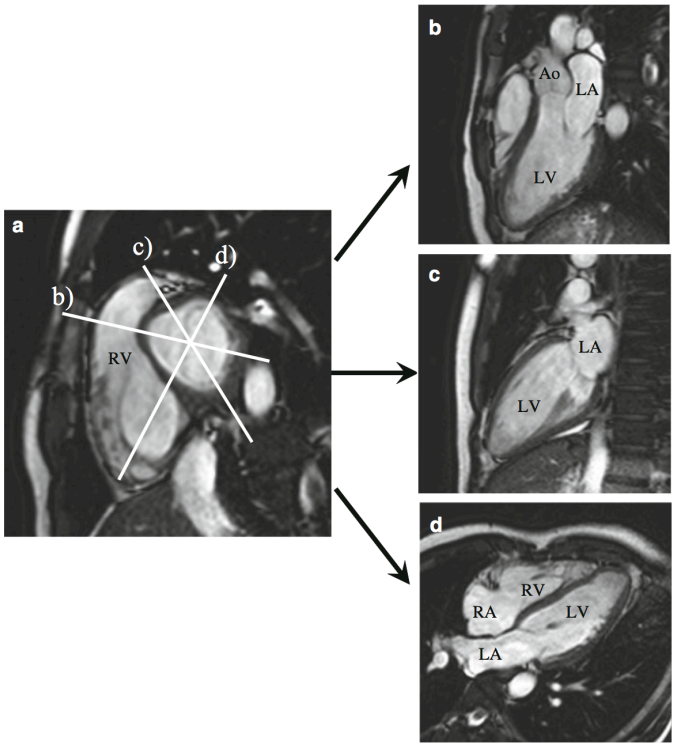

Fig. 8 Imaging planes that can be aligned from the basal SA slice (a): The LV inflow (mitral valve)/outflow (aortic valve) view (b), the VLA(c) and 4-chamber (d) views

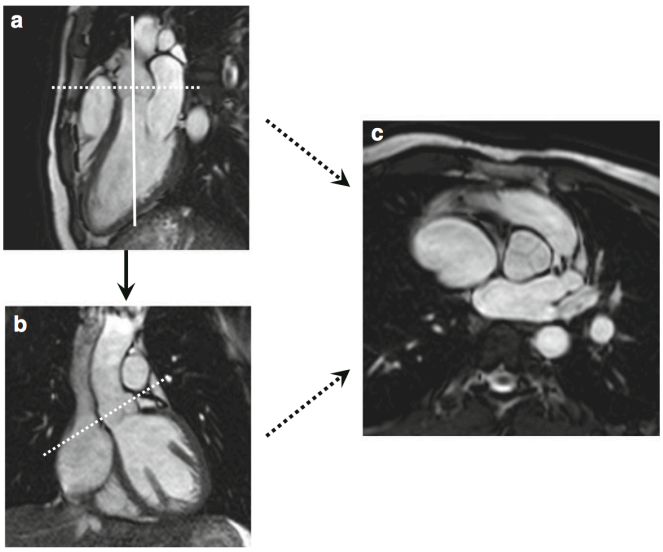

Fig. 9 Alignment of the aortic valve plane (c) for aortic flow assessment from the LV inflow/outflow (a) and the left ventricular outflow tract (LVOT) (b) views (dotted lines). The imaging plane should be placed just above the aortic valve, yet just below the origin of the coronary artery origins. The LVOT view is prescribed perpendicular to the LV inflow/outflow view (complete line on (a)

The mitral valve lies in a double oblique plane. Through-plane imaging of the mitral valve to assess LV inflow curves should therefore be aligned from two views, the VLA and 4Ch (Fig.10). For flow measurements, the plane should lie just beyond the mitral valve leaflets in the LV.

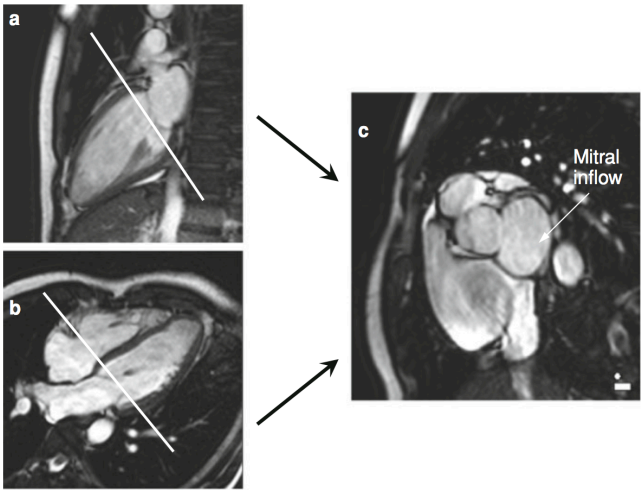

Fig.10 Alignmentof the tricuspid valve plane (c) for RV inflow assessment from the VLA (a) and the 4- chamber planes (b). The imaging plane should be placed just within the RV

Right Heart

A two-chamber view of the right heart can be obtained by placing a plane through the RV apex and the mid-point of the tricuspid valve on the 4Ch view. The right ventricular outflow tract (RVOT) is visualized by aligning a plane that passes through the main pulmonary artery (PA) and the RV inferiorly from a set of axial images (Fig.11c). A plane perpendicular to this, in an axial or oblique axial orientation, will give a second view through the RVOT (Fig.11d). A plane through the main PA, just above the pulmonary valve, perpendicular to both RVOT views, can be used to assess through-plane pulmonary flow. This plane is used when quantifying pulmonary incompetence (Fig.11e). As with the mitral valve, the tricuspid valve lies in a double oblique plane. Through-plane imaging

of the tricuspid valve to assess RV inflow curves should therefore be aligned from two views, the RV 2 chamber view and 4Ch view. For flow measurements, the plane should lie just beyond the tricuspid valve leaflets in the RV.

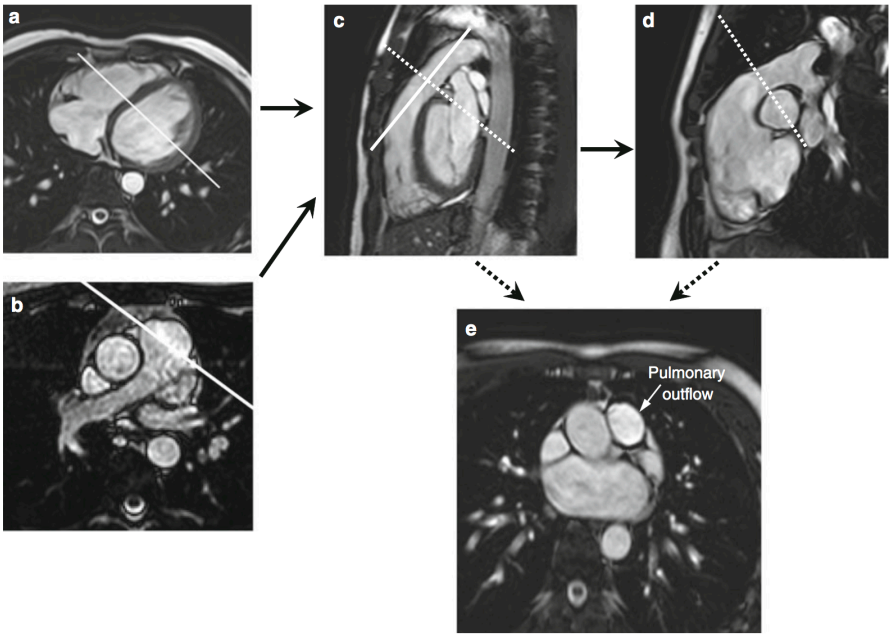

Fig. 11 Alignment of the pulmonary valve plane (e) for pulmonary flow assessment from two perpendicular right ventricular outflow tract (RVOT) (c and d) views (dotted lines). The imaging plane should be placed just above the pulmonary valve. The first RVOT view is prescribed from an oblique plane through the main pulmonary artery and RV on a set of axial images (a and b). The second RVOT plane is prescribed perpendicular to the first RVOT view (complete line on (c)

Main sequences in CMR

There are two fundamental types of sequence commonly used in CMR: gradient echo (GE) and spin echo (SE).

The *spin echo* pulse sequence generates images that have intrinsic black blood contrast. This is because it uses two pulses, the 90° and 180° RF pulses. The transverse magnetisation of blood flowing through the slice that moves out of the slice between the two pulses is not refocused by the 180° pulse and does not contribute to the

generation of a spin echo. This results in a signal void, also known as a 'black blood' or 'dark blood' appearance. This effect is also known as the spin washout effect, referring to the 'washout' of proton spins form the image slice that would otherwise be refocused and contribute to the spin echo signal. Spin echo sequences are mainly used for anatomic imaging and tissue characterization.

In contrast to the spin echo sequence, the *gradient echo* (GRE) sequence only uses one RF pulse to generate the signal and use a partial flip angle (less than 90°). A consequence of partial flip angle is that there is significant longitudinal magnetization present even after a short repetition time (TR). In GRE imaging with a short TR, longitudinal magnetization may not fully recover before the next RF pulse. Thus, the amount of magnetization able to be flipped back into the transverse plane is reduced. However, if the spins are moving (i.e. blood moving in the through plane direction) new unsaturated spins will be present in the slice during the next excitation. This increases the total magnetization available to be flipped into the transverse plane, increasing the signal. Thus, structures containing blood moving in the through plane direction will appear brighter than surrounding stationary tissue. This effect is known as inflow enhancement. The gradient echo pulse sequence is therefore commonly referred to as a bright blood imaging technique.
GRE sequences are commonly used to dynamically image the heart.
The most recent standard cardiac MR sequences are balanced steady-state free precession (b-SSFP), which provide the best contrast between chamber blood (white) and myocardium (dark), and these are now routinely used for imaging of cardiac function.

Anatomical MRI

To acquire anatomical images of the heart and major vessels turbo spin echo (TSE) pulse sequences are commonly used. The spin echo (SE) pulse sequence generates a spin echo signal by the use of an

excitation pulse followed by a 180° RF refocusing pulse. The turbo/fast spin echo pulse sequence generates multiple echoes by applying multiple 180° pulses after the initial 90° pulse. After each 180° pulse there is a corresponding spin echo. The number of echoes acquired for each excitation pulse is known as the *echo train length* (*ETL*) or *turbofactor* and this defines the acceleration factor for the pulse sequence. Typically echo train lengths of 15 or 16 are used in order to reduce the imaging time to within a breath-hold period.

T1-weighted (T1W) and T2-weighted (T2W) MRI

TSE sequences are particularly well suited to T1W and T2W imaging that allows evaluating myocardial signal. In cardiac MRI the main use of T2-weighted imaging is to perform myocardial edema imaging. This is because water has a long T2 and will therefore show up more brightly. Usually T2-weighted sequences include a fat suppression (Simonetti et al. 1996). A robust method of fat suppression is Short Tau Inversion Recovery (STIR) (Simonetti et al. 1996). Inversion recovery (IR) is the most commonly used form of magnetization preparation. IR depends on the fact that different tissues have different T1 characteristics. In IR sequences, an 180° RF pulse (or inversion pulse) is used to flip the magnetization into the opposite direction along the z-axis. From this position the magnetization relaxes back to its original state following the T1 curve of the tissue. As different tissues have different T1 characteristics, each tissue will pass through zero (or the null point) at different times. During RF excitation (which is applied some time after the IR pulse) only tissues with non-zero longitudinal magnetization will produce an MR signal. Therefore if the time between inversion and imaging (TI) is chosen carefully, signal from a given tissue can be completely abolished. STIR relies on the short T1 of fat compared to other tissues. Therefore, the fat magnetization will pass through null point of an IR sequence before the tissue of interest.

If imaging is performed at the null point of fat, the signal from the fat will be suppressed.

Another method of fat suppression is Spectral Inversion Recovery (SPIR). Spectral selective pulses rely on the fact that water and fat precess at slightly different frequencies (approximately 220 Hz difference at 1.5T). Therefore a special RF pulse can be used that only excites fat. In SPIR a spectrally selective 180° pulse is used to invert only the fat magnetization. The water magnetization is unchanged by the spectrally selective 180° pulse. The fat magnetization is then allowed to recover and a TI is chosen that coincides with the null point of fat. Unlike STIR, at the onset of imaging all of the water magnetization is in the longitudinal axis and therefore there is no loss in signal to noise ratio (SNR).

Cine MRI

Cine imaging involves the acquisition of data at multiple time points, known as a *cardiac phases*, throughout the cardiac cycle. The trigger delay for the first time point is set to the shortest possible time after the R wave to enable images to be acquired from the beginning of the cardiac cycle. Data acquired within each cardiac phase fills a separate k-space, resulting in the reconstruction of a separate image corresponding to each cardiac phase. The images for all the cardiac phases are then viewed as a movie sequence or cine, allowing functional assessment of the heart, its wall motion and a visual, qualitative assessment of blood flow.

Cine imaging requires very short repetition times to be used and therefore can only be achieved using gradient echo-based pulse sequences. The main type of gradient echo pulse sequence used for cine imaging is balanced steady state free precession (bSSFP). B-SSFP is a GRE sequence that primarily relies on steady-state magnetization for signal production. If the TR is short, residual transverse magnetization will be present during subsequent excitations, eventually leading to the evolution of steady state

magnetization.

Phase contrast (PC) MRI

Velocity encoded phase contrast (PC) techniques enable non-invasive quantification of blood flow in major vessels or throughout a cardiac valve during the heart cycle. PC-MRI utilizes simple spoiled GRE sequences combined with an additional velocity-encoding gradient. This additional gradient creates a phase image in which pixel intensity is directly proportional to velocity (Fig.12). After RF excitation all magnetization is coherent and in phase. If a gradient is then applied in the z direction, spins in the static tissue will dephase depending on their spatial position. Spins in the moving blood will also accrue phase, but because they are moving through the gradient field they will accrue more (or less depending on the direction of flow). So at this point static spins will have phase due to their spatial position, while moving spins will develop phase because of their position and velocity (Fig.12a). If we now reverse the gradient the phase in the static tissue will return to zero. However, the phase in the moving blood will not go back to zero, rather it will be more or less than zero depending on direction of flow (Fig.12b). This is because the spins in the moving blood are continuously traveling through a varying magnetic field. The end result of these two gradient lobes is that the phase of a spin population is directly proportional to their velocity.

The operator has to set a maximal encoding velocity (Venc). The Venc represents the practical upper limit of velocities that can be depicted and should ideally be set to a numerical value just greater than the true flow velocity. Problems occur if it is set much higher or lower than this value – with the former leading to less sensitivity and the latter causing misrepresentation via the phenomenon of aliasing.

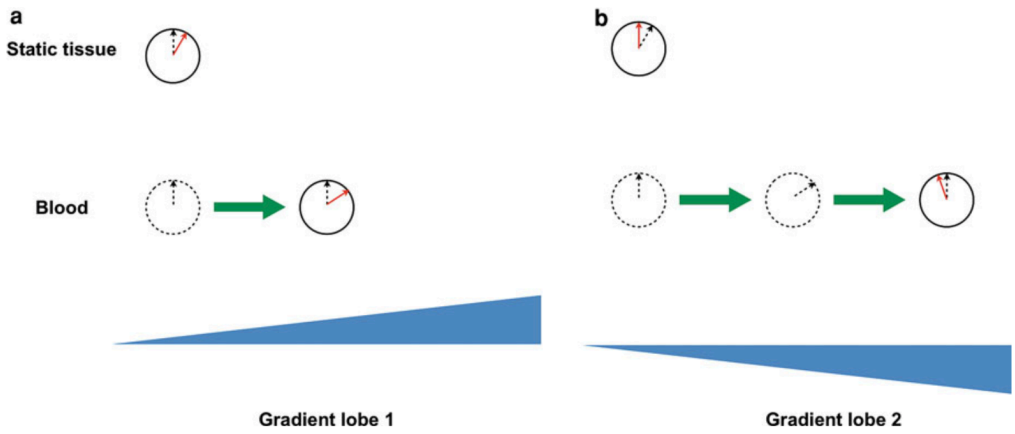

Fig. 12 The phase contrast experiment. A) When a gradient is applied in the direction of flow the static tissue dephases; however in this case the moving spins diphase more because they are moving into a stronger magnetic field. B) When the negative gradient is applied the static spins rephrase, however as the moving spins are moving into an even higher magnetic field they are left with residual phase at the end of the experiment

Late gadolinium enhancement (LGE) MRI

Late gadolinium enhancement (LGE) imaging allows evaluating the signal of the myocardium after intravenous administration of an MR contrast medium to differentiate viable myocardial tissue from non-viable/infarcted myocardial tissue. The *contrast agent* is based on the element *Gadolinium*. Gadolinium is a highly *paramagnetic* substance that mediates the T1 relaxation time of water molecules when it is in close proximity to them. The T1 relaxation time is therefore reduced, demonstrated by an increase in signal intensity when using T1-weighted imaging methods. The contrast agent is carried within the blood pool into the myocardial muscle where it enters extra-cellular space. Wash-in and wash-out of the contrast is relatively fast for normal myocardium, whereas wash-in and wash-out is delayed for infarcted muscle.

Delayed imaging after contrast agent injection using a T1-weighted fast gradient echo pulse sequence is able to demonstrate areas of infarction as areas with increased signal where there is a greater

concentration of contrast agent. Inversion recovery preparation schemes are combined with fast gradient echo pulse sequences. The inversion recovery (IR) technique provides T1-weighting and enhances the signal difference between normal and infarcted myocardium by suppressing the signal from normal myocardium (Fig.13). Contrast-enhanced inversion recovery relies on the fact that tissue containing gadolinium will have a shorter T1 than tissue not containing gadolinium. It is known that gadolinium (Gd) concentration in infarcted myocardium is higher than in normal myocardium. Therefore by the time the magnetization from the normal myocardium passes through the null point of an IR sequence, the infarcted myocardium will already have regained positive longitudinal magnetization. Consequently, if the inversion time (TI) is chosen to coincide with myocardial nulling, infarcted tissue will appear bright (Fig. 13c).

The use of the fast gradient echo pulse sequence allows image acquisition to be kept within a breath- hold period. The images are collected 10-15 minutes after the injection, hence the name *late gadolinium enhancement,* abbreviated *LGE* (previously *delayed enhancement*). Timing of the image acquisition is of paramount importance as too early image acquisition reduces the difference in contrast between normal and damaged myocardium (i.e., myocardial scar, fibrosis) because of insufficient washout of contrast from the normal myocardium, while too late image acquisition can result in an excessive washout of contrast from damaged myocardial tissue.

The quality of LGE imaging depends on the effective suppression of the signal from normal myocardium. This requires very precise selection of the appropriate inversion time, $TI_{myocardium}$, which depends on many factors, including the dose of contrast, the delay after administration and the rate of renal excretion. The TI is therefore chosen by performing a number of fast, low-resolution test image acquisitions at different TIs, typically within the range from

200–250 ms in steps of 25–50 ms. The TI from the test image that demonstrates the best suppression of normal myocardium is then used to perform imaging at full resolution. This can also be achieved by performing a so-called *TI-scout*, which acquires images at multiple time delays after a single inversion pulse within the same acquisition.

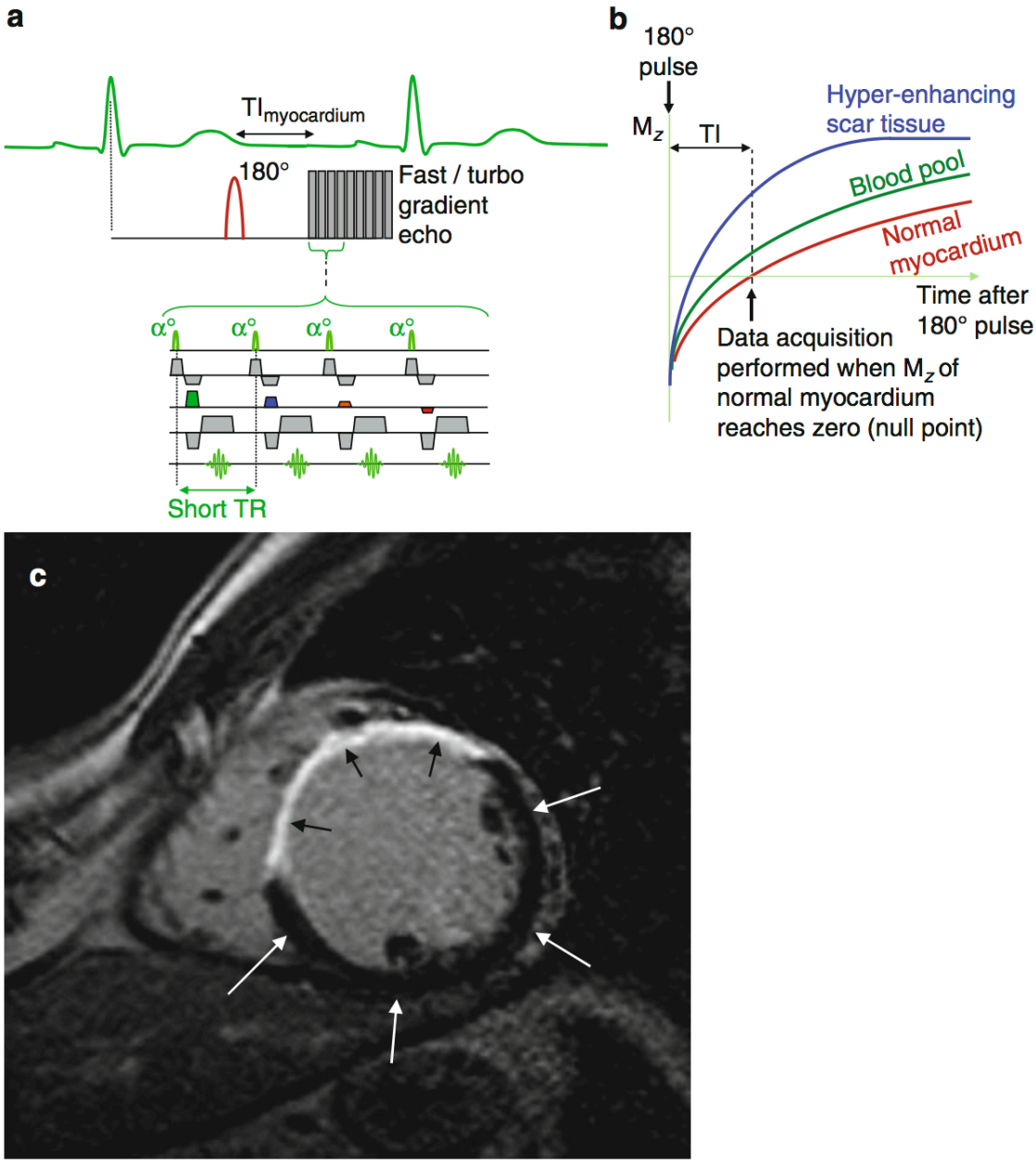

Fig 13. Late Enhancement imaging is performed using an inversion recovery fast (or turbo) gradient echo pulse sequence (**a**). The fast (or turbo) gradient echo pulse sequence allows the image acquisition to be completed within a few heart beats. Image acquisition is normally per- formed in diastole to minimise the effects of heart motion. The 180° inversion pulse is followed by a delay, $TI_{myocardium}$, selected to suppress the signal from normal myocardium. The graph in (**b**) shows the relaxation curves for normal myocardium, the blood pool and scar tissue. The higher concentration of contrast agent within scar tissue results in a faster T1 relaxation rate and therefore an increased signal compared to the blood pool and normal myocardium. Nulling the signal from normal myocardium maximises the scar tissue contrast. The image in (**c**) shows the enhanced signal from scar tissue (*small black arrows*), and the nulled signal within the normal, viable myo- cardium (*white arrows*)

LGE imaging provides high spatial resolution, high contrast images, making CMR the non-invasive gold standard for identifying infarction/replacement fibrosis. In coronary artery disease (CAD), CMR identifies smaller infarcts routinely missed by lower resolution modalities (eg, SPECT) (Wagner et al. Lancet 2003). Ischemic cardiomyopathy is characterized by areas of scarring that typically involve the subendocardium, and depending on the size of the infarct, extend up to the epicardium in a pattern consistent with the "wave front phenomenon" of ischemic cell death (Fig. 14) (Reimer et al. Circulation 1977). Infarct assessment is pivotal in guiding patient selection for revascularisation (those with viable myocardium) and predicting adverse outcome (Kim et al N Engl J Med 2000). The transmural extent of LGE predicts functional improvement following revascularisation: recovery is more likely in segments with ≤50% transmural infarction than those with ≥75% (Kim et al. N Engl J Med 2000). Viability assessment with CMR has the advantage of obviating pharmacological stress. However, an important caveat is that it may overestimate infarct size in the acute phase (2–3 weeks) of acute coronary syndromes (ACSs), as reversible oedema increases gadolinium uptake (Mather et al. Radiology 2011). In ACS, LGE imaging also detects microvascular obstruction, a strong predictor of adverse remodelling and unfavourable prognosis (Khan et al. World J Cardiol 2017;). Extensive microcirculatory damage, thrombosis and oedema-related vessel compression delay gadolinium-based contrast agents penetration into the infarct core, manifesting as a characteristic central black zone surrounded by hyperenhancement (Mather et al. Journal of Cardiovascular Magnetic Resonance 2009). 'Early' gadolinium imaging is useful for identifying thrombus (ventricular/atrial): early after contrast administration, when the blood pool remains bright, avascular thrombus appears as a dark filling defect (Srichai et al. Am Heart J 2006).

In non-ischaemic disease, the pattern/distribution of LGE may offer clues regarding aetiology and prognostic significance (Fig.14).

Myocarditis typically causes subepicardial/midmyocardial scarring, usually (though not always) in a non-coronary distribution with subendocardial sparing. A diagnosis of non-ischaemic dilated cardiomyopathy (DCM) may be confirmed by midwall fibrosis, a recognised risk factor for cardiac death, ventricular arrhythmia and heart failure hospitalisationn (Lehrke et al. Heart 2011). LGE imaging may also prove instructive in hypertrophic states. In hypertrophic cardiomyopathy (HCM), collagen deposition and fibre disarray may cause patchy, midwall (sometime diffuse) LGE, even when overt hypertrophy is absent (Rudolph et al. J Am Coll Cardiol 2009). In HCM, LGE is a risk factor for ventricular arrhythmia and sudden cardiac death (SCD) (Briasoulis et al. Heart 2015). Diffuse fibrosis is also found in hypertensive heart disease and aortic stenosis (though usually less pronounced) (Rudolph et al. J Am Coll Cardiol 2009). In Anderson-Fabry disease (an X-linked lysosomal storage disorder), LGE has an inferolateral midmyocardial predilection (Moon et al. J Cardiovasc Magn Reson 2006). In cardiac amyloidosis, global diffuse enhancement is characteristically seen with a dark blood pool: amyloid fibrils avidly bind GBCA, with consequent difficulty nulling the myocardium. The presence of LGE is correlated with adverse prognosis (Fontana et al. Circulation 2015). Global subendocardial enhancement is also seen in small-vessel vasculitides and endomyocardial fibrosis (eg, hypereosinophilic disease), with the pathognomonic 'apical V sign'. Cardiac sarcoidosis is associated with multiple foci of patchy enhancement, which are predictive of mortality and ventricular arrhythmia (Coleman et al. JACC Cardiovasc Imaging 2017). The presence of mediastinal lymphadenopathy should be sought, as its absence makes this diagnosis unlikely. LGE imaging may also identify atrial scarring/fibrosis (amyloid and atrial ablation). In arrhythmogenic cardiomyopathy (AC), LGE may be present in regions of fibrofatty infiltration and is an established risk factor for SCD.

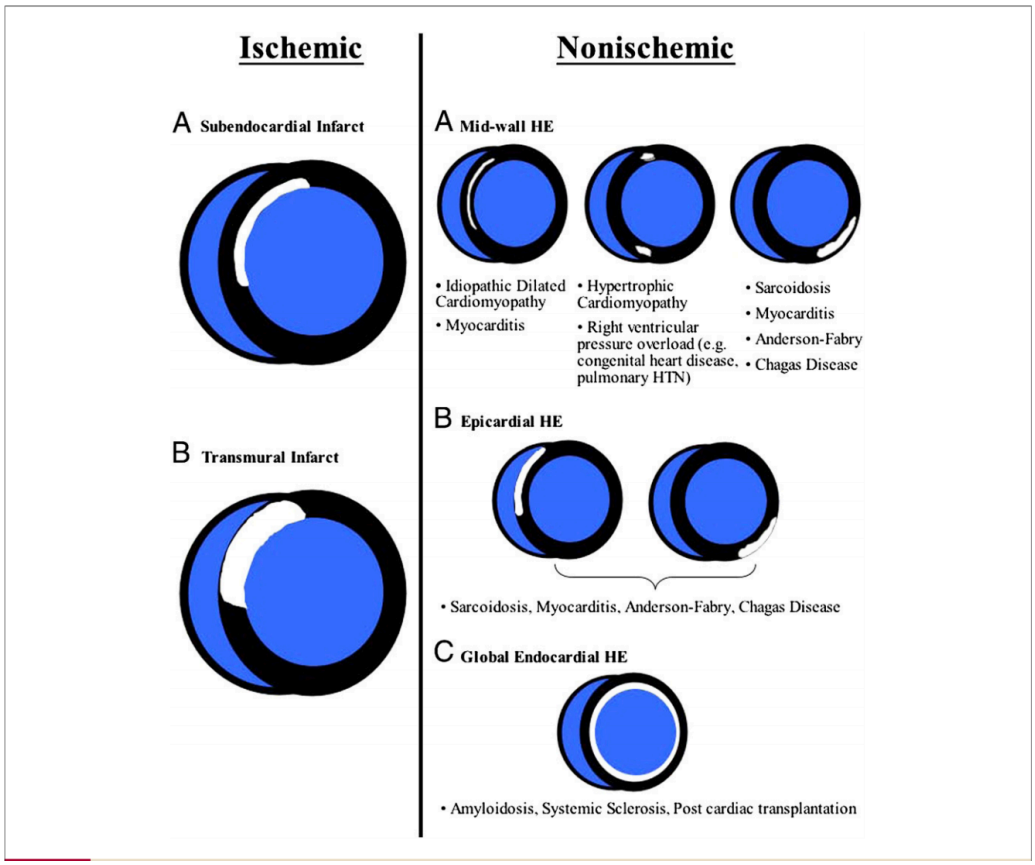

Fig. 14. LGE Patterns for Ischemic and Nonischemic Disorders. A schematic representation of hyperenhancement (HE) patterns that are characteristic for ischemic and nonischemic disorders. Note that the area of HE in ischemic cardiomyopathy always involves the subendocardium. In contrast, midwall or epicardial HE strongly suggests a nonischemic etiology. HTN hypertension.

Image analysis

Ventricular Morphology and Function by CMR.

CMR is regarded as the "gold standard" for quantifying ventricular volume, mass, structure and function. Impressive results for accuracy have been demonstrated by several investigators in various disease states (Boxt et al. J Am Coll Cardiol.1992; Suzuki et al. Am Heart J. 1991). The interstudy reproducibility of CMR-derived parameters of

ventricular function and mass is good for both the left and right ventricle and is superior to two-dimensional and M mode echocardiography (Bottini et al. Am J Hypertens 1995; Semelka et al. Radiology1990).

Ventricular volumes, ejection fraction, and myocardial mass are obtained from a post precessing analysis (Fig. 15) on cine CMR 5-10mm slices covering the LV and RV acquired in short. Endocardial and epicardial contours are drawn during post processing on end-diastolic and end-systolic frames, and LV and RV volumes are calculated as the sum of individual slice volumes. Tracing of the end-diastolic LV epicardial borders in addition to the endocardial borders allows determining LV mass. A previous criticism of this technique has been the time required to analyse the cine data to generate accurate volume and mass data. New software solutions with intensity based thresholding for semiautomated myocardial-blood border definition has enabled analysis to become less time consuming.

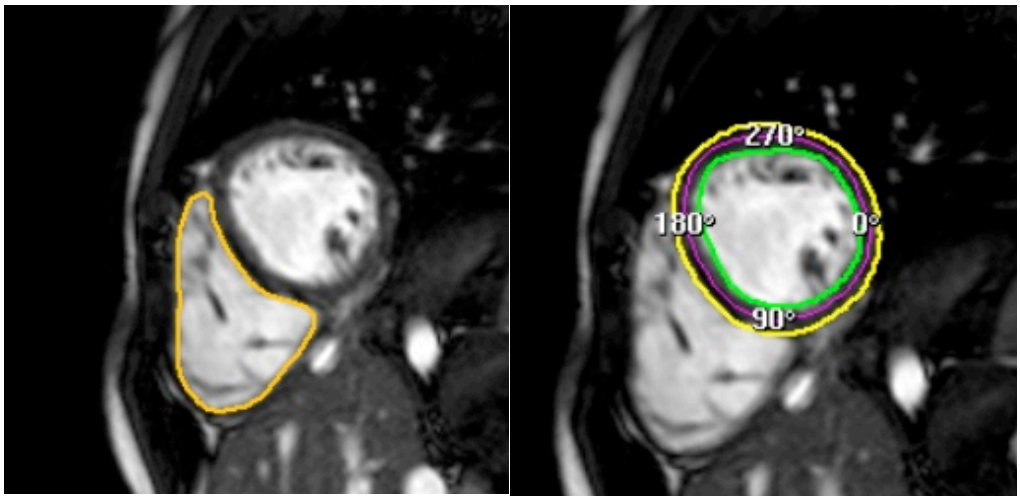

Fig. 15 Analysis of left and right ventricle function.

Flow Analysis

Phase contrast velocity mapping is an MR sequence used to measure velocity and flow in blood vessels, or within the heart, in which each pixel in the image displays the signal phase, which is encoded. Quantification of volume flow requires acquisition of a short axis view of a vessel with blood flow in the through plane direction. The phase map of such a slice can be used to calculate the average spin velocity in each pixel (v_{pix}) at time t. The pixel area multiplied by v_{pix} is the volume flow in each pixel (Q_{pix}) at time t. The sum of Q_{pix} within a region of interest (ROI) drawn around the vessel equals the volume flow at time t (Fig. 16). As phase measurements are made at multiple time points within the cardiac cycle forward flow, regurgitant flow and cardiac output can then be calculated. This imaging technique has been available for over 20 years (Nayler et al. J Comput Assist Tomogr 1986). Velocity encoded imaging has been shown to be a reliable method to measure blood flow in different vessels of the body. Analogous to Doppler echocardiography, this technique allows the calculation of stroke volume, cardiac output, ejection fraction, valvular regurgitant fractions, and quantification of cardiac shunts, while mitral and tricuspid transvalvular flow profiles allow the assessment of ventricular diastolic filling patterns. Cardiac output and the pulmonary-to-systemic flow ratio (Qp:Qs) measured with the use of this technique have been shown to be accurate (Beerbaum et al. Circulation 2001; Robertson et al. Magn Reson Imaging 2001). Phase contrast MR flow is less accurate in patients with either cardiac arrhythmia during acquisition or turbulent blood flow; the presence of these is a general limitation of this technique.

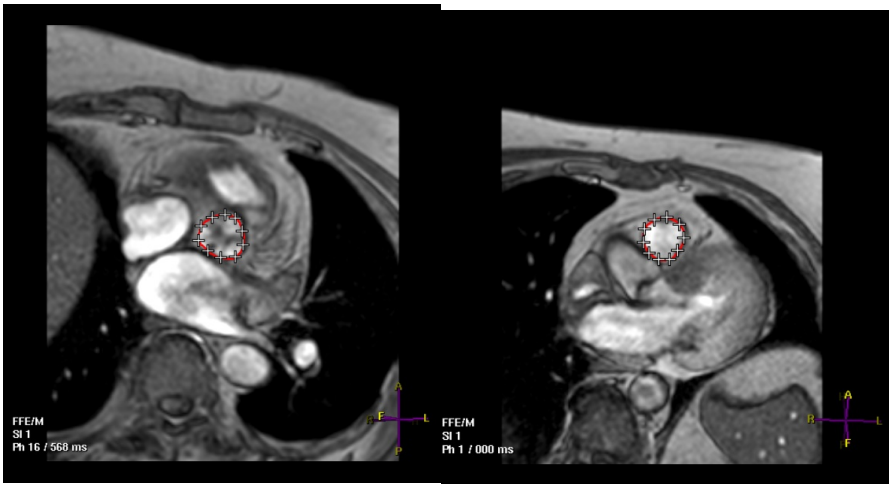

Fig. 16 Flow analysis of aortic and polmonary valve

T1 mapping

There is increasing evidence that the underlying, pathological basis for a variety of non-ischemic cardiomyopathies is myocardial fibrosis. This pathological process of extracellular matrix (ECM) remodeling results in multiple functional consequences including impaired relaxation (Sugihara et al. J Cardiol 1988), precipitation of arrhythmias (Ling et al. J Am Coll Cardiol 2012) and impaired contractile reserve (McLenachan et al. Am J Hypertens 1990). Traditionally, myocardial fibrosis has been recognized in conditions such as hypertensive heart disease, HCM and idiopathic dilated cardiomyopathy (DCM). However, there is increasing identification of myocardial fibrosis as the common causative factor of myocardial dysfunction in many other, particularly metabolic, processes such as obesity, diabetes and aging. Early identification of this underlying, often diffuse, interstitial myocardial fibrosis is important for diagnosis and essential for optimization of reversibility with intervention. Late gadolinium enhancement (LGE-CMR) imaging has become the new gold standard for identification of focal brosis. T1 mapping has the potential to provide a similar quantitative assessment of diffuse myocardial fibrosis.

In general, methods for measuring myocardial T1 consists of three components: 1) a perturbation of the longitudinal magnetization (based on inversion or saturation recovery), 2) an experiment to sample the relaxation curve as the longitudinal magnetization returns to its original level, and 3) a model used to fit the sampled curve and extract the myocardial T1.

Multiple CMR T1 based techniques have been employed for quantitation of diffuse fibrosis. The original scheme known as the MOdified Look-Locker Inversion Recovery (MOLLI) proposed by Messroghli, et al. (Messroghli et al. Magn Reson Med 2004) is illustrated in Figure 17. For each inversion, the MOLLI method samples the IR curve at multiple inversion times using single shot imaging spaced at heart beat intervals. Multiple inversions are used with different trigger delays in order to acquire measurements at different inversion times to sample the IR curve more evenly. Recovery periods are needed between the inversions to ensure that samples from the different inversions are from the same recovery curve, i.e., each inversion starts at the same initial magnetization. The T1-map precision is related to the number and position of samples along the IR curve, and accuracy of the signal model is also affected by the sampling strategy due to the influence of the readout on the apparent recovery.

MOLLI technique was designed to overcome the limitations of motion and prolonged acquisition time. Specifics included an ability to acquire data within one breath-hold at a designated time within the cardiac cycle and the capability of merging images from multiple Look Locker experiments at different consecutive inversion times into one data set. MOLLI sequencing employs a balanced steady-state free precession (SSFP) readout to achieve a higher signal to noise ratio with a narrow image acquisition period of less than 200 msec in end-diastole to minimize motion artifact. Reproducibility of this technique is high (Messroghli et al. Radiology 2006).

Even faster acquisition times have been achieved by Piechnik *et al*. who developed a shortened MOLLI sequence (ShMOLLI) which requires a short breath-hold of only nine heart beats duration

(Piechnik et al. J Cardiovasc Magn Reson 2010). Both sequences are similar but ShMOLLI does not require full recovery of magnetization on sequential inversion pulses and has less heart rate (HR) dependency, which may improve accuracy (Messroghli et al. J Magn Reson Imaging 2007).

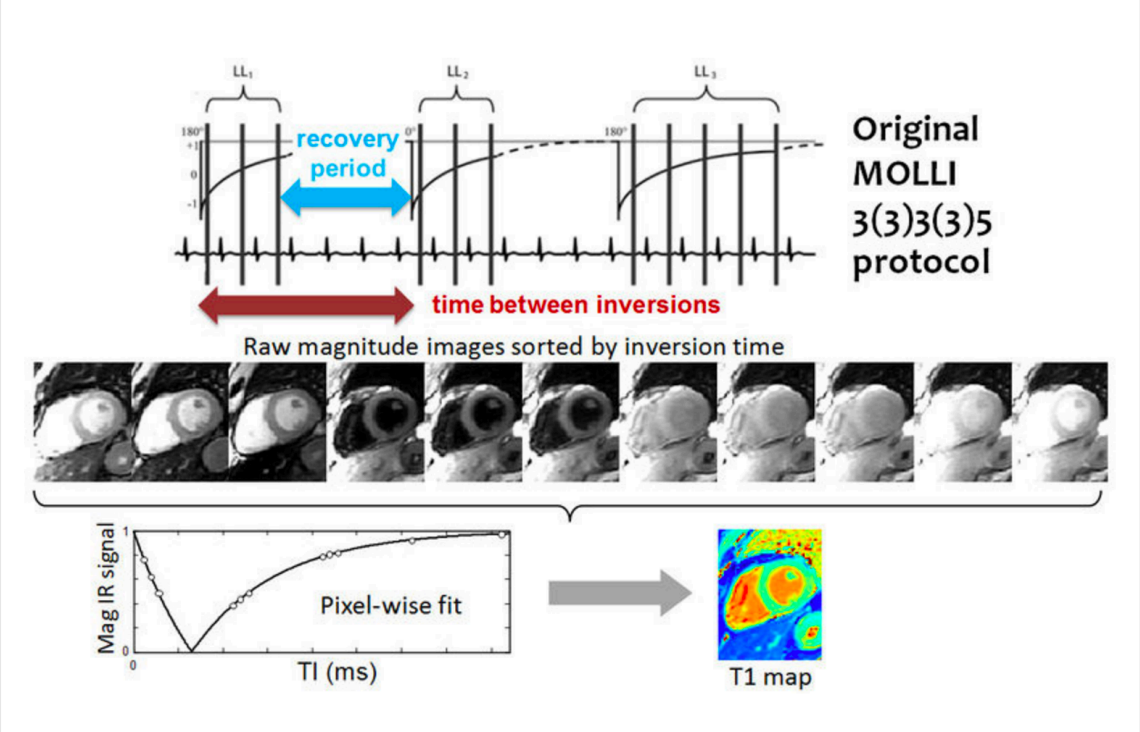

Fig. 17 MOdified Look-Locker Inversion Recovery (MOLLI) scheme for T1-mapping in the heart. The original protocol employed 3 inversions with 3, 3, and 5 images acquired in the beats following inversions, and 3 heart beat recovery periods between inversions, referred to here as 3(3)3(3)5. All images are acquired at the same delay from the R-wave trigger for mid-diastolic imaging. Curve fitting is performed on a pixel-wise basis using the actual measured inversion times.

Typically a series of short-axis images are acquired pre- and approximately 12 minutes after gadolinium-based contrast with between 6 and 12 consecutively longer inversion times depending on the protocol. Offline, standard basal, mid-ventricular and/or apical slices are then selected and can be further divided into conventional

myocardial segments (or discrete regions of interest) and blood-pool for analysis if desired. A curve fitting technique is employed to reconstruct the consecutively acquired images into one data set from which a T1 map of voxels is generated. The signal intensity of each mapped voxel directly represents the T1 relaxation time of the corresponding myocardial tissue. An exponential recovery curve of signal intensities at the different inversion times is then created for each designated region of interest (slice or segment) to determine the myocardial T1 relaxation time.

The ratio of myocardial to blood post-contrast T1 values is expressed as the partition coefficient. By preceding post-contrast T1 mapping with pre-contrast T1 mapping, myocardial extra-cellular volume (ECV) can similarly be derived. This pseudo-equilibrium technique employs the reciprocals of myocardial and blood T1 values pre- and post-contrast and then adjusts for hematocrit to correct for the blood contrast volume of distribution (Messroghli et al. Circ Cardiovasc Imaging 2011; Ugander et al. Eur Heart J 2012). This ECV is expressed as a percentage of the total myocardial extracellular space. A larger ECV represents increased contrast accumulation in an expanded ECM (Fig. 18).

$$ECV = (1 - haematocrit)\,\frac{\frac{1}{post\ contrast\ T1\ myo} - \frac{1}{native\ T1\ myo}}{\frac{1}{post\ contrast\ T1\ blood} - \frac{1}{native\ T1\ blood}}$$

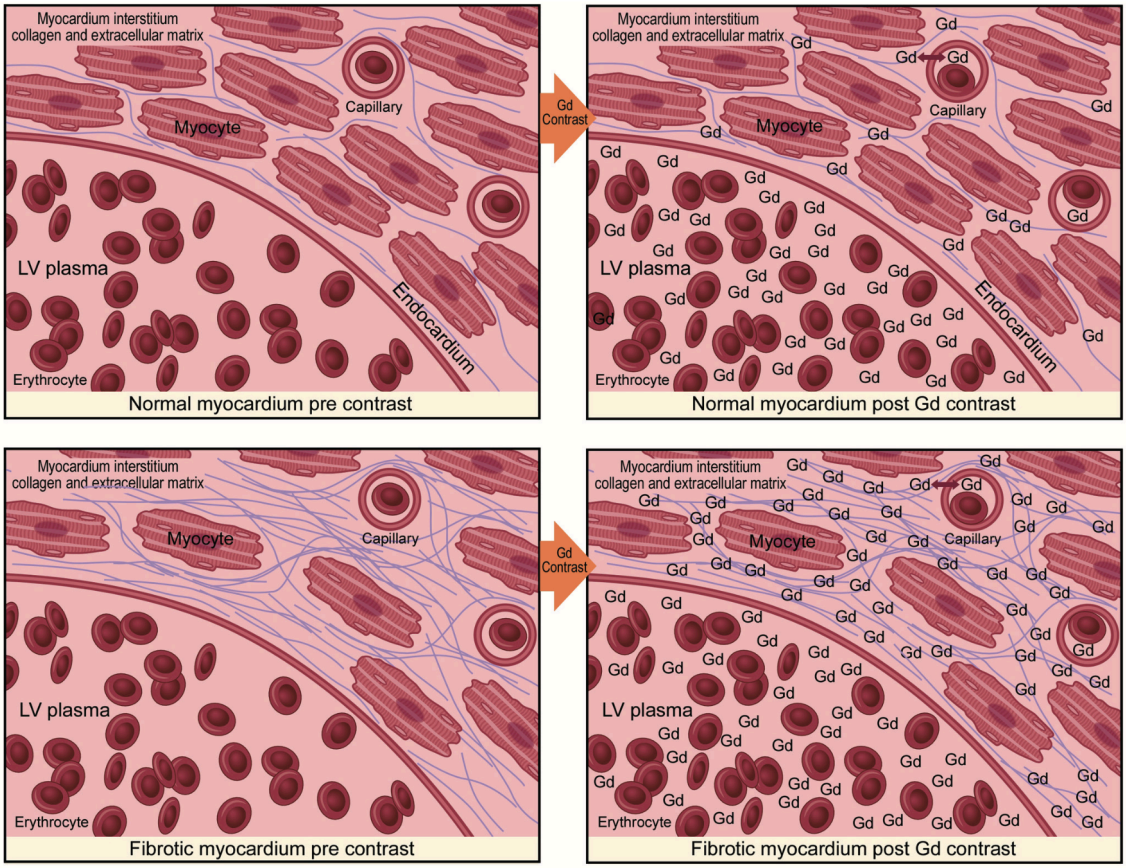

Fig. 18 Pre- and post-gadolinium (Gd) contrast dispersion in normal versus fibrotic myocardium.

Pre-contrast T1 mapping

Pre-contrast techniques measure the intrinsic or native myocardial T1. They have an inherent advantage for subjects with significant renal impairment who may be at increased risk of nephrogenic systemic sclerosis. However, non-contrast T1 mapping is limited by an inability to clearly distinguish interstitial from myocyte signal intensity. This may be of clinical consequence in early disease processes when there is minimal difference in T1 values between healthy and disease states. Standardization of the acquisition phase in the cardiac cycle within and between studies remains an important consideration as acquisition timing can impact on T1 value and ECV due to fluctuation of the myocardial blood volume (Kawel et al. J Cardiovasc Magn Reson 2012). A reduction in T1 time of 43-70%

has been observed from diastole to systole (Wansapura et al. Magn Reson Imaging 2006). Clinical feasibility of T1 mapping markedly increased with the advent of non-contrast MOLLI imaging due to increased reproducibility, higher spatial resolution and reduced motion artifact. However, this technique remains prone to frequency-dependent errors in T1-measurement (Kellman et al. J Cardiovasc Magn Reson 2013).

Post-contrast T1 mapping

Post-contrast techiniques measure T1 time after gadolinium-based contrast injection. There is a distribution difference of contrast between normal and fibrotic myocardium (Fig.18). Areas of fibrosis demonstrate greater gadolinium accumulation, which is represented as a region of high intensity signal with a shorter T1 time than adjacent normal tissue (Dulce et al. AJR Am J Roentgenol 1993). In addition to heart rate and acquisition related confounders, there are several established physiological covariates related to contrast administration, which must be considered. These include: body fat percentage, renal function, delay time in measurement after contrast administration and gadolinium characteristics (such as dose, concentration and water exchange rate).

Partition coefficient and ECV mapping

Estimation of partition coefficient and ECV fraction from T1 mapping reduce the effect of confounding variables as they are calculated from the ratio of change in myocardial T1 relative to blood-pool T1 pre and post-contrast (Jerosch-Herold et al. Am J Physiol Heart Circ Physiol 2008). The advantage of this type of methodology is that it minimizes systematic errors in technique, enables better comparison of scans at different time points and results in less variability at different field strengths and across different vendor platforms. This could be of significant clinic benefit for

monitoring of interval change within individuals, assessing treatment effect and allowing comparison of disease patterns within the general community. The main confounding factor affecting the partition coefficient is hematocrit. However, it can be easily corrected using blood volume of distribution (1-hematocrit) to give the ECV. Although the ECV is a more reliable measure of interstitial space, it remains based on the assumption of contrast equilibrium between blood and myocardium. Clinically, there is a wide spread of ECV values with overlap of values between normal and diseased myocardium (Kawel et al. J Cardiovasc Magn Reson 2012). This makes it problematic for diagnostic purposes and more suited to measurement of interval change within individuals or assessment of more end-stage disease.

Normal ECV values of 25.3 ± 3.5% [1.5 T] have been reported in healthy individuals (Sado et al. Heart 2012) (Fig.19). Apart from amyloid, an increased ECV is most often due to excessive collagen deposition and is thus a more robust measure of myocardial fibrosis. Low ECV values occur in thrombus and fat/lipomatous metaplasia. ECV can either be calculated for myocardial regions-of-interest or visualized on ECV maps.

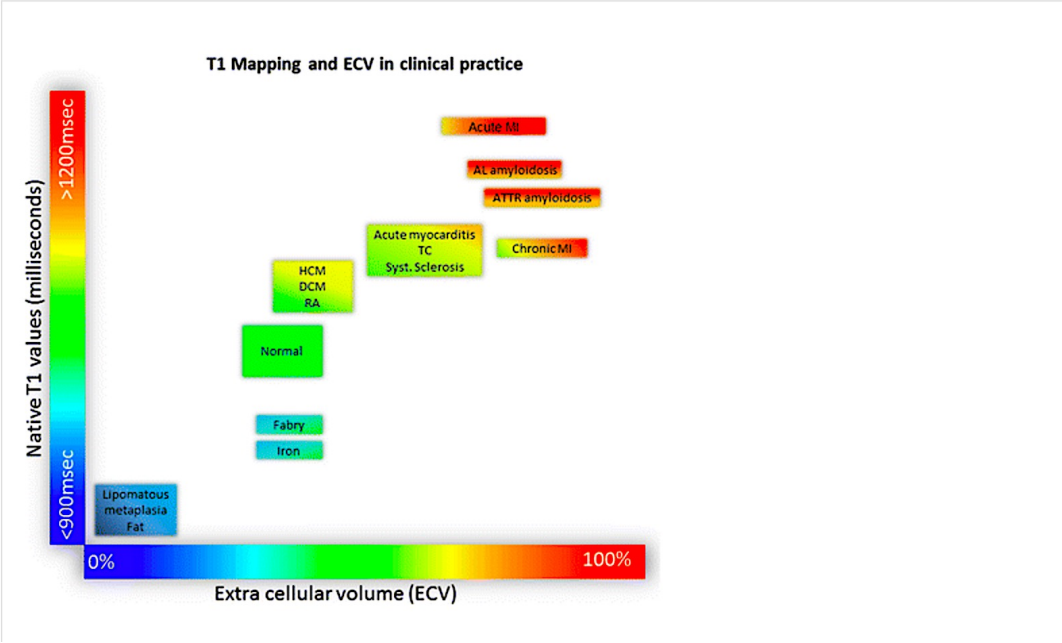

Fig. 19 Tissue characterisation using native T1 and extracellular volume fraction (ECV). Absolute values for native T1 depend greatly on field strength (1.5 T or 3 T), pulse sequence (MOLLI or ShMOLLI), scanner manufacturer and rules of measurements. For the purpose of comparability, only studies using 1.5 T scanners were considered in this figure.

T2 and T2* mapping

Myocardial T2 mapping is a technique used to reconstruct a parametric image based on the T2 value measured in each voxel. The accumulation of water in the myocardium is associated with different types of pathology, such as acute myocardial infarction, myocarditis and graft rejection. Given a long transverse relaxation time of water protons, myocardial T2 mapping appears to be promising to detect intramyocardial water and even quantify myocardial edema.

T2* relaxation refers to the rapid decay of transverse magnetization caused by local magnetic field inhomogeneity. Magnetic field inhomogeneity comes from the inhomogeneity of the static magnetic field or from the differences in magnetic susceptibility between neighboring tissues, such as air-tissue interfaces, metallic implants, paramagnetic contrast agents or iron deposition. Specifically, myocardial T2* mapping is sensitive to tissue iron content, and so it is widely used to quantify the degree of iron deposition in the

myocardium in patients with thalassemia major and repeated blood transfusion.

Indications for CMR

CMR has excellent spatial resolution, due to the various sequences used, and has excellent anatomical definition. This, combined with the lack of interference by body habitus that echocardiography is subject to, make it the current gold-standard for assessment of cardiac structure, size and function. Furthermore, with the assessment of T1 and T2 signal and LGE images, CMR is able to characterize the myocardium beyond any other non-invasive imaging modality. Therefore, CMR has become a highly versatile imaging modality with a wide range of clinical indications. These range from assessment of congenital heart disease to the phenotyping of cardiomyopathies, diagnosis of and risk stratification in ischaemic heart disease and vascular applications. Clinical indications for CMR have been appraised by European and North American societies (Pennell et al. 2004; ACCF/ACR/AHA/ NASCI/SCMR 2010) and several international practice guidelines include CMR (Fig. 20).

Common Indications for CMR

1. Heart failure
2. Ischaemia detection – mostly vasodilator stress perfusion
3. Congenital heart disease – initial assessment and follow-up
4. Diseases of the aorta – especially aneurysm and coarctation
5. Cardiomyopathy – in particular ARVC, DCM, HCM and iron overload
6. Suspected myocarditis
7. Viability assessment – for example post MI
8. Pericardial disease
9. Cardiac masses
10. Course of anomalous coronary arteries
11. Heart valve disease

Fig. 20 Common indications for CMR. DCM, Dilated cardiomyopathy; HCM, hypertrophic cardiomyopathy; ARVC, arrhythmogenic right ventricular cardiomyopathy; MI, myocardial infarction.

Myocardial ischemic disease

Myocardial infarction (MI) is defined as myocardial cell death secondary to prolonged ischemia that results in an inadequate supply of oxygenated blood to an area of the myocardium, particularly when ischemia exceeds a critical threshold that overwhelms cellular repair mechanisms. MI is typically caused by luminal thrombosis superimposed on coronary atherosclerosis; occasionally, it can be caused by coronary spasm, coronary embolism, or thrombosis in nonatherosclerotic vessels. Arteritis, dissection, congenital abnormalities, hypercoagulable states, and cocaine use are uncommon causes.

CMR imaging plays an important role in evaluating the various stages of MI. The infarct progresses like a "wave-front" from the endocardium to the epicardium. Complete necrosis takes 2–4 hours or longer, depending on the presence of collateral circulation, persistent or intermittent coronary arterial occlusion, sensitivity of myocytes to ischemia, preconditioning, and individual demand for myocardial oxygen and nutrients. An infarct is termed microscopic when <10% of the myocardium is involved, moderate when 10%–30% is involved, and large when >30% is involved. Transmural MI affects the full thickness of affected muscle segments, from endocardium through midmyocardium to epicardium. Delayed-enhancement imaging is the most important technique for evaluation of MI. It is the most accurate method for diagnosing MI or nonischemic cardiomyopathies, quantifying the scar, assessing viability, and evaluating thrombus (Hunold et al. Am J Roentgenol 2005). In MI, T2-weighted imaging is most useful for detecting the presence of edema, which is a marker of acute ischemic injury and enables assessment of the "area at risk".

Acute MI

In acute MI (AMI), regional wall-motion abnormalities of the affected vascular territory can be seen on cine images. T2-weighted images show wall thickening and myocardial edema. If there is irreversible damage, hyperenhancement can be seen on LGE images along the distribution of the involved coronary artery due to myocyte death, membrane disintegration or rupture, and intracellular entry of gadolinium. If the myocardial damage is partial, subendocardial hyperenhancement can be seen on LGE images, but if the ischemia continues, necrosis gradually progresses outward to involve the epicardium, with ensuing transmural delayed hyperenhancement. Microvascular obstruction may be present and can be seen as a dark non-enhancing area within the enhancing scar on delayed-enhancement images (Tarantini et al. J Am Coll Cardiol 2005). Perfusion defects can be seen on rest perfusion images in regions of recently infarcted myocardium.

Chronic MI

In established chronic MI (CMI), cine images show wall thinning and regional wall-motion abnormalities in the affected territory. Edema is not seen on T2-weighted images. LGE images show wall thinning and subendocardial or transmural delayed hyperenhancement in a vascular distribution. Perfusion defects may be seen on both rest and stress perfusion images, depending on the degree of transmurality of irreversibly damaged myocardium (Tarantini et al. J Am Coll Cardiol 2005).

Myocardial non ischemic disease

Myocardial non ischemic disease include several disorders, such as DCM, HCM, cardiac sarcoidosis, stress cardiomyopathy, and others, but often show similar clinical presentations which lead to progressive heart failure, a high risk of fatal arrhythmias, and a high mortality rate. Myocardial non ischemic disease has been traditionally diagnosed noninvasively with chest roentgenography, standard 12-lead electrocardiography (ECG), transthoracic and/or transesophageal echocardiography and nuclear imaging, and invasively with coronary angiography, left ventriculography, and endomyocardial biopsy. Recent advantage of CMR has enabled us to assess cardiac morphology, function and tissue characteristics both in ischemic and non-ischemic disease. Thus, CMR can identify cardiac abnormalities not readily recognized by conventional imaging modalities. Moreover, the LGE sequences give important information on differential diagnosis, clinical features, and prognosis (Fig. 14) (Satoh et al. World J Cardiol 2014).

Dilated cardiomyopathy

DCM is the most common isoform of myocardial non ischemic disease and is characterized by dilatation of LV chamber and systolic dysfunction, which leads to progressive heart failure, high risk for fatal arrhythmias and high mortality rate. Although over the half of cases are idiopathic, DCM is not a single tree of disease spectrum but may include several undetermined etiologies, such as chronic myocarditis, tachycardia-induced cardiomyopathy, undiagnosed. CMR represents the gold standard technique in quantifying volumes and ejection fractions of both ventricles, and with its high reproducibility it is suitable in monitoring any changes in cardiac

function over time (Anand et al. Indian Heart 2016). In cine-CMR, all cardiac chambers are enlarged and a decrease in LV ejection fraction (EF) is evident. The LV wall thickness is normal or decreased, but relatively homogenous. In LGE-CMR, DCM has been shown to demonstrate mostly a lack of LGE or the presence of mid-wall enhancement, and a fewer part of cases shows patchy or diffuse striated LGE. The distribution of LGE is unrelated to a particular coronary arterial territory and corresponds to focal fibrosis at autopsy. The mechanisms of myocardial fibrosis in DCM are complex and include inflammation, genetic predisposition, micro-vascular ischemia, and neurohumoral changes. Late-enhancement imaging can supply important prognostic information about the risk of death and major cardiovascular events (Satoh et al. World J Cardiol 2014).

Hypertrophic cardiomyopathy

HCM is a relatively common genetic disorder of the cardiac sarcomere, characterized by an idiopathic LV hypertrophy and affects between 0.1 and 0.2% of the population; furthermore, it is the most frequent cause of sudden death among the young population.

Typically, this disorder demonstrates asymmetric septal hypertrophy, but can also present atypical patterns of hypertrophy involving the mid-ventricle and apex. Hence, HCM has a wide variety of morphological, functional, and clinical features.

Frequently found electrocardiographic alterations are electrical signs of left ventricular hypertrophy (high voltage QRS, left axis deviation, etc.), ventricular repolarization abnormalities, and pathological Q waves. The diagnosis of hypertrophic cardiomyopathy can be made through echocardiographic and echo-Doppler examinations, which

can detect left ventricular wall thickening (diastolic thickness 15 mm). Echocardiography also accurately documents the diastolic dysfunction associated with the cardiomyopathy and any dynamic obstruction of ventricular outflow caused by anomalous movements of the anterior leaflet of the mitral valve. Although transthoracic echocardiography has been the standard tool for the diagnosis of HCM, it has limitations for precise visualization of whole ventricles and quantification of hypertrophy. CMR is capable of identifying regions of LV hypertrophy not readily recognized by echocardiography, especially for apical hypertrophy and apical aneurysm, such as the right ventricle in cases of biventricular involvement (Anand et al. Indian Heart 2016).

Furthermore, CMR is considered the gold standard for the measurement of ventricular mass.

In concentric forms of hypertrophic cardiomyopathy, the use of CMR is fundamental to make the differential diagnosis from other types of cardiomyopathy with a clinically similar presentation, such as non-compaction cardiomyopathy or storage cardiomyopathies: these include the ones occurring in cardiac amyloidosis and Fabry's disease in which there are specific late-enhancement patterns different from those typical of hypertrophic cardiomyopathy. This last diagnostic criterion, combined with morphological information, justifies the use of CMR also in the differential diagnosis of the athlete's heart hypertrophy (Anand et al. Indian Heart 2016).

The pattern of enhancement most frequently found in hypertrophic cardiomyopathy is mesocardial, with a patchy distribution in the areas of greatest hypertrophy, most commonly at the anterior and posterior RV insertion points, and reflects one of the anatomical

substrates of the disease (the disarray that causes expansion of the extracellular space) (Satoh et al. World J Cardiol 2014).

Furthermore, the presence of focal areas of hyperintensity is frequently found in the T2-weighted sequences corresponding to the hypertrophic myocardium. MR perfusion studies may also supply information on ischemic phenomena that reflect microvascular damage with possible implications for risk stratification in patients with known hypertrophic cardiomyopathy. The presence and extent of areas of myocardial fibrosis also seem to be relevant to the stratification of risk of arrhythmic events in such patients. CMR is also indicated in the follow- up of subjects who have undergone surgical treatment, such as subaortic myomectomy, or percutaneous alcohol septal ablation. The accuracy of CMR in identifying myocardial hypertrophy is useful in family screening (Anand et al. Indian Heart 2016).

Arrhythmogenic cardiomyopathy

AC is a heart muscle disease clinically characterized by life-threatening ventricular arrhythmias and pathologically by an acquired and progressive dystrophy of the ventricular myocardium with fibro-fatty replacement. Due to an estimated prevalence of 1:2000-1:5000, AC is listed among rare diseases. A familial background consistent with an autosomal-dominant trait of inheritance is present in most of AC patients; recessive variants have also been reported. AC is a major cause of sudden death in the young and in athletes.

There is no a single gold standard for the diagnosis, which is mainly based on functional and structural alterations of the RV, fibro-fatty replacement of the myocardium, depolarization and repolarization abnormalities, arrhythmias with the left bundle branch block

morphology and family history. Genotype-phenotype correlation studies have recently identified clinical variants characterized by early dominant LV involvement, besides the classical RV variant, thus supporting the use of the broader term AC.

The diagnosis is currently made on the presence of major and minor Task Force criteria that include structural, functional, histological, electrocardiographic, arrhythmic, and genetic factors.

CMR can visualize RV wall better than echocardiography. Functional abnormalities in cine-CMR include regional wall motion defects, focal aneurysms, global RV dilation and dysfunction. In addition, the diagnosis could be supported by the presence of fatty infiltration of RV or LV free wall that can be suppressed in fat suppression sequences (Anand et al. Indian Heart 2016). LGE imaging has been shown to provide additional evidence of fibrosis, which often co-exists in the fat-infiltrated myocardium (Satoh et al. World J Cardiol 2014).

Myocarditis

Myocarditis is most commonly caused by a viral infection resulting in myocardial inflammation and immune-mediated damage in cardiomyocytes. The clinical onset of acute myocarditis may produce extremely variable and non-specific signs, including typical "heart attack-like" signs (acute chest pain, increased troponin and ST segment elevation) and atypical ones including new-onset arrhythmias, rapidly evolving dilated cardiomyopathy, and acute heart failure.

The most characteristic features in CMR are the presence of myocardial edema, diffuse wall motion abnormalities, subepicardial patchy myocardial LGE, and the concomitant involvement of the

pericardium. Edema imaging using T2 black blood sequences plays an important role in the evaluation of patients with suspected myocarditis. The increase in T1 and T2 mapping values also indicate the presence of myocardial edema. In particular, T2 mapping seems to be a very promising sequence in cases of diffuse myocardial edema where focal areas of hyper-intensity are not distinguished (Mahrholdt et al. Circulation 2004).

On LGE-CMR, the subepicardial layer especially in posterolateral wall has LGE, and in severe cases, LGE may be more diffuse and circumferential (Aquaro et al. J Am Coll Cardiol 2017).

Sarcoidosis

Sarcoidosis is a systemic granulomatous disease involving the heart in up to 50% of cases. Cardiac involvement is characterized by non-caseous granulomatous infiltration. CMR is proposed as the diagnostic investigation in studying the heart of patients with sarcoidosis, in the follow-up and assessment of cardiac morphology and function and in determining the disease extension. The focal and diffuse sarcoid infiltrates, responsible for edema and inflammation, are seen as hyperintense areas in T2-weighted sequences with saturation of the fat signal. The left ventricular filling pattern and changes in contractility can also be studied easily with CMR. Finally, analysis of LGE sequences plays a very important role; late enhancement seems to localize to the basal parts of the heart, in particular in the interventricular septum and the lateral wall, with a characteristic distribution (focal or with striae sparing the sub-endocardium) or, in more advanced cases, with a transmural pattern (Komada et al. Nagoya J Med Sci 2016).

Fabry's disease and amyloidosis

About 4% of patients with a morphological diagnosis of hypertrophic cardiomyopathy (on the basis of increased wall thickness) have Fabry's disease. In these patients the activity of α-galactosidase is reduced, leading to an accumulation of GL3 glycosphingolipids. In many cases, CMR shows an intramyocardial area of late enhancement in the basal-lateral wall, an atypical site for cardiomyopathy. The reasons for this distribution lie in the increased wall stress at this site. Some patients have concentric myocardial hypertrophy without LGE and low T1 mapping values, possibly related to early stage disease before the onset of myocardial fibrosis. CMR can be used to evaluate the efficacy of enzyme replacement therapy (Anand et al. Indian Heart 2016).

Other patients with a morphological diagnosis of myocardial hypertrophy show an amyloid restrictive cardiomyopathy characterized by diastolic dysfunction, ventricular hypertrophy and thickening of the interatrial septum. The distinction from other forms of cardiac hypertrophy may be difficult in the early stages of amyloidosis. However, the pattern of distribution of the late enhancement in amyloidosis is distinctive; widespread, global, and mainly subendocardial, with a transmural tendency in more severe cases (Satoh et al. World J Cardiol 2014).

Quantification of nonviable tissue in Late Gadolinium Enhancement

The prognostic role of the Late Gadolinium Enhancement

CMR imaging can be used to comprehensively assess the viability of myocardium in patients with ischemic heart disease and to detect fibrosis in patients with non-ischemic myocardial disease.

Since the introduction of primary percutaneous coronary intervention (PPCI) for the treatment of acute ST-segment elevation myocardial infarction (STEMI), mortality has improved substantially, but the morbidity associated with post–myocardial infarct (MI) heart failure remains significant. CMR is increasingly being used to quantify MI size in randomized controlled trials (RCTs) investigating novel cardioprotective therapies targeting myocardial reperfusion injury to reduce MI size in patients with STEMI treated with PPCI (Tarantini et al. J Am Coll Cardiol 2005). Particularly, the role of LGE in infarct myocardial scar visualization and quantification is critical as it is considered the gold standard for MI size quantification. Experimental models have shown excellent agreement between size and shape in LGE CMR and areas of myocardial infarction by histopathology. A strong correlation between the infarction size and the functional and hemodynamic alterations following myocardial infarction is generally observed and therefore considered a fundamental measure in the assessment of the morphological and functional consequences of infarction (Kim et al. Circulation 1999). MI size, microvascular obstruction (MVO), and myocardial salvage assessed by CMR performed in the first few days post-PPCI have all

been shown to be strongly prognostic. As a result, CMR is increasingly being used for surrogate endpoints in RCTs. A recent meta-analysis of 2,632 patients from 10 RCTs found that MI size measured by LGE-CMR or single photon computed tomography within 1 month post-PPCI showed that for every 5% increase in MI size, there was a 20% increase in the relative hazard ratio for 1-year hospitalization for heart failure and all-cause mortality (Roes et al. Am J Cardiol 2007).

The presence of scar tissue has an important prognostic and therapeutic value as a strong predictor of LV remodeling, cardiac dysfunction, appropriate ICD therapy and mortality (Alexandre et al. J Cardiovasc Magn Reson 2013).

Its quantitative analysis is therefore of potential clinical interest and relies on the segmentation of the myocardial scar tissue in each image, where existing. To this end, several techniques for CMR-LGE image segmentation have been previously proposed. The extent of the hyper enhancement scar tissue has been shown to be able to provide supplementary information beyond conventional risk stratification, thus suggesting that quantitative approaches should be used to measure scar extent and transmurality (Bondarenko et al. J Cardiovasc Magn Reson 2005).

Infarct size from CMR is also a primary endpoint in many clinical trials. Recent studies have also demonstrated how infarct size, shape and location from pre-procedural LGE can be useful in guiding ventricular tachycardias ablation. These procedures are often time-consuming due to the preceding electrophysiological mapping study required to identify slow conduction zone involved in re-entry circuits. Post-processed LGE images provide scar maps, which can

be integrated with electroanatomic mapping systems to facilitate these procedures (Acosta et al. JACC Cardiovasc Imaging 2018).

Clinical implementation of these developments necessitates a reliable, fast, reproducible and accurate segmentation of the infarcted region. Moreover, as use of LGE- based infarct volume estimation becomes more clinically relevant, standardization will facilitate more consistent interpretation (Bondarenko et al. J Cardiovasc Magn Reson 2005).

It was demonstrated that LGE is associated with frequency and occurrence of arrhythmias in patients with HCM (Moon et al. J Am Coll Cardiol 2004). A study conducted by Todiere at al. showed as the extent of LGE ≥10% in patients with HCM is able to recognize additional patients at increased risk for malignant arrhythmic episodes in a population with low-to-intermediate ESC sudden cardiac death (SCD) risk score. For this reason, the same myocardial segmentation techniques used for the detection of myocardial infarct scars have been used, by some authors, for the quantification of myocardial fibrosis, especially in patients with HCM. However, there is no consensus regarding the technique of LGE quantification. Several CMR centers use different signal intensity thresholds as well as visual assessment for LGE analysis in patients with HCM.

Myocardial segmentation techniques on late gadolinium enhancement sequence

The area of hyper-enhancement in the LGE sequences, i.e. myocardial tissue damage, can be quantified in several ways. First, there is the manual method, which consists in manually marking the areas of altered signal considered pathological by the radiologist.

Manual contouring is considered the reference standard, but it can be time-consuming and may be subjective.

In addition to the manual method, semi-automatic software has been developed that allows the quantification in grams and percentage of the LGE area. A common semi-automated method for detecting areas of LGE in the LV is the fixed-model approach, whereby intensities are thresholded to a fixed number of standard deviations (SD) from the mean intensity of nulled myocardium or blood pool. This model is known as the n -SD method, where n = 2 , 3 , 4 , 5 or 6. A second common fixed-model approach is the full-width-at-half-maximum (FWHM) approach, where half of the maximum intensity within a user-selected hyper-enhanced region is selected as the fixed intensity threshold. Using this threshold, a region-growing process is employed from user-selected seeds. These seeds are selected to be within infarcted regions such that they can be segmented with region-growing. In both cases, user interaction is needed for each image to manually select suitable regions of interest (ROIs) used for calculating the threshold values (Karim et al. Med Image Anal 2016).

Several studies report how the FWHM and 6-SD or 5-SD techniques are more reproducible, with no statistically significant differences in the quantification of the volume of LGE compared to the manual segmentation considered the reference standard. The 2-SD technique generates LGE volumes up to 2 times higher than the FWHM, 6-SD and manual techniques (Carminati et al. J Thorac Imaging 2016). However, there is no univocal consensus in the literature. Other authors showed that FWHM underestimates chronic MI size in those with MVO on the acute scan because of very high extracellular volume in the area previously occupied by MVO and should be avoided for assessing chronic MI size (Zhang et al. Clin Radiol

2020). While the 6-SD method appears the most promising and has been shown to have the highest accuracy to predict segment wall recovery in patients with chronic myocardial infarction and is similar to manual quantification in patients with both acute and chronic myocardial infarction. The 6-SD approach also performed well when using 2 different LGE sequences. Furthermore, the reproducibility of these techniques appears to be worse in HCM than in AMI or CMI (Mikami et al. J Cardiovasc Magn Reson 2014).

As the aforementioned approaches require user input, making them prone to inter- and intra- observer variation, other approaches that are automatic have been developed. Hennemuth et al. (2008) modelled the intensities of homogeneous tissue in LGE CMR with a Rician distributions and an expectation- maximization (EM) algorithm was used for fitting the data. Pop et al. (2013) fitted Gaussian mixture models to myocardial tissue pixel intensities and correlated with histology. In Detsky et al. (2009), clustering in a feature space of steady-state and T $*1$ intensity values provided the segmentation which was shown to provide good correlation with FWHM. Tao et al. (2010) employed automatic thresholding using the Otsu method on bi-modal intensity histograms of myocardium and blood pool. The Otsu technique has been shown to accurately delineate MI size. But 2 subsequent studies showed that Otsu overestimated MI size. More recently, the use of the graph-cut technique in image processing has been applied to segment infarct in several methods (Lu et al., 2012; Karim et al., 2014; Karimaghaloo et al., 2012). An advantage of this technique is that constraints can be placed on the resulting segmentation, allowing segmentation boundary regularization with region-based properties. It also predicts which pixels are statistically

most likely to be infarct based on prior probability distribution models.

However, it should be noted that any semi-automated or automated techniques may be affected by the LGE image quality.

Our experience

Introduction

In recent years, new advanced magnetic resonance (MR) techniques in cardiothoracic and abdominal imaging were developed adding a quantitative evaluation to the conventional qualitative image analysis. They are able to quantify MR signal intensity allowing for unbiased and reproducible assessments. Focusing on cardiac MR (CMR) imaging, there is a growing interest in new advanced techniques such as quantification of myocardial tissue damage and the emerging radiomics.

On CMR imaging, late gadolinium enhancement (LGE) sequences are able to detect myocardial tissue damage [1–4]. Moreover, the pattern of myocardial LGE may be helpful in the differential diagnosis of myocardial diseases, in particular in discriminating between ischemic and non-ischemic myocardial injuries [5–7]. In myocardial infarction, the delayed myocardial enhancement in LGE sequences shows a characteristic subendocardial or transmural distribution corresponding to a particular coronary artery territory [2,8–10]. In non-ischemic conditions, such as cardiomyopathies, LGE does not correspond to any particular coronary artery territory and usually shows a subepicardial or mid-wall distribution, with sub-endocardium sparing[1,5,11–13]. In patients with myocarditis, inflammatory lesions frequently show some LGE areas due to the enlargement of the extracellular volume [12,14–16]. The typical LGE pattern in myocarditis is patchy with a prevalent subepicardial/midwall involvement, usually affecting the lateral free wall of the left ventricle[18]. However, sometimes, areas of LGE can

present a non-typical distribution so that the differential diagnosis of myocardial diseases can be a challenging in CMR imaging, usually requiring the knowledge of proper clinical setting[19,20]. In addition, CMR requires a high level of expertise and experience for a proper interpretation of cardiac diseases.

Recently, there has been a growing interest in quantifying the extent of tissue damage seen on LGE-CMR for both ischemic and non-ischemic pathologies, as this is considered to be an unfavorable prognostic factor[15,21,22]. The evaluation of scar tissue plays an important role in the prognosis and treatment of patients affected by ischemic injury, being an important predictor of left ventricular (LV) remodeling, cardiac dysfunction, and ventricular arrhythmias [23–25]. In particular, the amount of post-myocardial infarction scar tissue and its transmural extension are considered to be predictors of mortality, and may be useful in selecting candidates for cardiac defibrillator implantation (ICD) [23,26]. A quantitative evaluation of scar tissue extension is therefore essential, even if it is susceptible to reproducibility issues [27,28]. Nowadays, most scar tissue quantification softwares are based on manual identification of a threshold value for CMR-LGE [5,6,23,28–30] and areas of hyperenhancement within the myocardium are identified without distinguishing between ischemic and non-ischemic alterations[25,28,31-36].

Radiomics is an emerging field of study in which the quantitative data "hidden" inside the standard medical images can be automatically extracted using a panel of sophisticated data characterization algorithms. These objective data, referred to as radiomic features, are often not visible to the human eye and can be used to make more accurate diagnoses, reducing interoperator error, and to predict clinical outcomes[37]. Currently, radiomics is most

commonly applied in oncologic imaging showing great results in cancer screening, diagnosis, and treatment evaluation[38-41]. However, there is a growing interest in using radiomics analysis in cardiac imaging. Texture analysis is the most common type of radiomic analysis performed in CMR imaging[37]. Some studies showed that texture analysis of unenhanced CMR images could be successfully used to identify, differentiate, and diagnose cardiomyopathies[42,43].

On this background, we chose to focus our study on advanced MR techniques in cardiac imaging because experience in this field is still limited, as opposed to abdominal imaging. In this setting, the aim of this study is to test two advanced CMR techniques:

1) The custom made software FLORA (For Late gadOlinium enhanced aReas clAssification), developed by Medical Physics Department and Radiology Department AOUC to identify and classify LGE myocardial lesions automatically and to assess the transmural extent of ischemic lesions.
2) The ability of texture features derived from CMR images in differentiating between myocardial infarction, myocarditis and healthy controls.

Material and Methods

Study population

By searching our Picture Archiving and Communication System (PACS), we retrospectively evaluated all 1243 patients who underwent a CMR examination between March 2018 and November 2020. Of these, analysing LGE sequences, we selected only patients with one of the following inclusion criteria: a confirmed diagnosis of myocardial infarction with evident scar tissue on LGE sequences; a confirmed diagnosis of non-ischemic cardiomyopathy with evident

areas of LGE; no myocardial alterations on CMR, especially in LGE sequences. Exclusion criteria were: poor image quality, the presence of artefacts on LGE-CMR sequences, and incomplete CMR examination (due to claustrophobia or the absence of LGE sequences). The final cohort thus comprised 120 patients with the following characteristics (see Table 1): 40 had a confirmed diagnosis of myocardial infarction with evident scar tissue on LGE sequences; 40 had a confirmed diagnosis of non-ischemic cardiomyopathy; 40 did not show any myocardial alterations on CMR, especially in LGE sequences. The latter group was referred to CMR for the following clinical reasons: 30 patients with ventricular arrhythmias to identify a potential arrhythmogenic substrate (due to the presence of extra systoles on the ECG); 3 with a family history of sudden cardiac death; 2 with a family history of hypertrophic cardiomyopathy; 1 with a left ventricle diverticulum detected at echocardiography; 2 with a slightly increased right ventricle volume at echocardiography; and 2 with a slightly increased left ventricle volume at echocardiography. The final cohort of 120 patients was used to test the custom made software FLORA. Texture features analysis was performed on a subgroup of 60 patients, including 20 patients with myocardial infarction, 20 with myocarditis and 20 without any myocardial alterations on CMR (Table 2).

This retrospective single-center study was conducted in accordance with the Declaration of Helsinki Ethical Principles and Good Clinical Practices and was approved by the Biomedical Research Ethics Committee of our institution. All patients gave their informed consent for the CMR examination with intravenous administration. Patients' records were anonymized and de-identified prior to analysis.

Table 1: Final cohort of enrolled patients to test the custom made software FLORA.

Group of patients	Group details	Number of patients
Ischemic cardiomyopathy	-	40
Non-ischemic cardiomyopathy	Hypertrophic cardiomyopathy	11
	Myocarditis	20
	Myopericarditis	2
	Becker's dystrophy	1
	Sarcoidosis	2
	Dilated cardiomyopathy	3
	Arrhythmogenic left ventricular cardiomyopathy	1
No myocardial alterations on CMR	-	40

Table 2: Subgroup of patients in which texture analysis was performed.

Group of patients	Number of patients
Myocardial infarction	20
Myocarditis	20
No myocardial alterations on CMR	20

CMR protocol

CMR examinations were performed using two different MR scanners. From the final cohort of 120 patients: 90 patients were scanned on a 1.5 T Magnetom Aera (Siemens Medical Solutions, Erlangen, Germany) (30 ischemic, 30 non-ischemic and 30 injury-free); 30 patients were scanned on a 1.5 T Ingenia (Philips Healthcare, Best, The Netherlands) (10 ischemic, 10 non-ischemic and 10 injury-free). From the subgroup of 60 patients: 30 patients (10 myocardial infarction, 10 myocarditis and 10 without any alterations on CMR) were scanned on a 1.5 T Magnetom Aera (Siemens Medical Solutions, Erlangen, Germany); 30 patients (10 myocardial infarction, 10 myocarditis and 10 without any alterations on CMR) were scanned on a 1.5 T Ingenia (Philips Healthcare, Best, The Netherlands).

Breath-hold retrospectively ECGgated cine steady state free processing images were acquired in the short-axis (SA) covered the entire LV (6 mm slices without gap).

SA LGE-CMR images were acquired using breath-holds ECG-triggered inversion recovery gradient echo sequences ten minutes after the administration of 0.1 mmol/kg Gadobutrolo (Gadovist, Bayer HealthCare), infused at 1ml/sec, followed by 20 ml saline with an automated injector. The inversion time was calculated for each patient by considering the null-point of the normal myocardium signal using a Look-locker sequence. Scan parameters for SA-LGE sequences on Siemens/Philips MR scanners were: 2D PSIR LGE, 208x188 image matrix size, pixel size 1.63×1.63 mm^2, slice thickness 8 mm, no slice gap, echo time 1.12 ms, flip angle 40° and 3D PSIR LGE, 256×256 image matrix size, pixel size 1.17×1.17 mm^2, slice

thickness 8 mm, no slice gap, echo time 2.2 ms, flip angle 20° respectively (Table 3).

On the 1.5 T Siemens Magnetom Aera scanner, for T1 mapping, we used ECG-triggered acquisitions modified by Look-Locker inversion recovery (MOLLI), using the scheme 3(3)3(3)5; postcontrast MOLLIs were performed 15–20 min after the gadolinium bolus, using the scheme 4(1)3(1)2.

On the 1.5 T Philips Ingenia scanner, for T1 mapping, we used ECG-triggered acquisitions Shortened MOdified Look-Locker Inversion recovery (ShMOLLI), using the scheme 5(1)1(1)1.

CMR data were analysed using a dedicated workstation (IntelSpace, Philips Medical Systems, Best, The Netherlands).

Table 3: Scan parameter of a cardiac magnetic resonance (CMR) protocol

Parameter	SA cine		SA LGE PSIR		T1 mapping native	
	1.5 T Magnetom Aera	1.5 T Igenia	1.5 T Magnetom Aera	1.5 T Igenia	1.5 T Magnetom Aera	1.5 T Igenia
FOV	360	300	340	300	360	300
TR (ms)	3.1	3.1	713	4.3	311.46	1.97
TE (ms)	1.3	1.53	1.12	2.1	1.12	0.88
Flip angle (°)	60	60	40	20	35	35
Slice thickness (mm)	6	8	8	8	8	10
IT (ms)			300-380	300-380	192	350

PSIR phase sensitive inversion recovery, LGE late gadolinium enhancement, TR time of repetition, TE time to echo, IT inversion time, SA short axis.

FLORA software workflow

FLORA is an automatic tool designed to identify myocardial alterations and distinguish ischemic from non-ischemic LV lesions on CMR-LGE images in the short axis. The software also evaluates transmural extension in the case of ischemic lesions. The software is written in Matlab (2019, version 7.10.0, R2019a, Natick, Massachusetts: The MathWorks Inc). A schematic description of its workflow is provided in Figure (1).

For each patient, a radiologist with seven years of experience in CMR selected a single slice in the SA-LGE sequence in which the myocardial alteration was present/visible (Figure 1a). The myocardium was then segmented by delineatiing both the epicardial and endocardial borders with two regions of interest (ROIs): ROI_{ext}, corresponding to the epicardial border; and ROI_{int}, corresponding to the endocardial border (Figure 1b). Papillary muscles were excluded from the segmentation. This was the only manual operation required while all the remaining operations described further on were fully automatic, and thus completely independent from the operator.

Following slice segmentation, a mask is automatically created and applied to the SA-LGE image to select the pixels located between ROI_{ext} and ROI_{int} corresponding to the myocardium region. Signal intensity profiles, defined in a radial direction, are then extracted using the standard Matlab 'improfile' function, starting from the centroid of ROI_{int} and extending to ROI_{ext} (Figure 1c-d). Using the mask image, all of the profiles' pixel values inside ROI_{int} are set to zero. The histogram of myocardial signal intensities on the LGE image, which is the starting point for the automatic threshold calculation (Figure 1e), is then calculated, dividing the intensity range into 20 bins. The threshold value distinguishes the pixels

belonging to the areas of enhanced signal (i.e. over the threshold) from those of the injury-free myocardium. It is calculated using two different methods: the 'double-gaussian fit' method and the 'fixed-shift' method. It is noteworthy that the automatic threshold estimate must be sensitive enough to detect slight gadolinium enhancement, and robust enough to not be affected by intensity fluctuations due to local variations in the signal-to-noise ratio. A detailed description of the two methods is given in the Supplementary Materials.

Pixels in profiles with an intensity higher than the estimated threshold value, and with at least three other neighboring pixels over the threshold, are identified as pathological. The neighbor check is carried out in the masked image via a 3x3 matrix centered on every pixel to exclude local signal intensity fluctuations. Neighboring pixels over the threshold are also included in the identified pathological region (Figure 1f).

The software code then checks whether the pixel clusters identified as pathological belong in part to ROI_{int} (i.e. if they are partially in contact with the endocardial border). If this occurs with an extension of the overlap of at least 5 mm, the whole cluster is classified as ischemic (red colormap). Otherwise, if there is no overlap, it is classified as non-ischemic (yellow colormap). We also added the orange colormap for non-ischemic lesions reaching the endocardium with an overlap extension < 5mm.

Examples of these classifications are given in Figure 1g.

The software provides both 2D and 3D visualization methods for the classification map. The 2D method consists of the SA-LGE-CMR sliced with the red, yellow and orange colormap superimposed on the detected pathological areas. The 3D method includes a color bar chart with a bar height equal to the pixel intensity. Blue is assigned to

blood pixels; green to injury-free myocardium pixels; red to ischemic lesion pixels; and yellow and orange to non-ischemic pixels (Figure 1g).

Finally, a quantitative estimate of the maximum transmurality for each ischemic area is provided, with values ranging from 0 (no ischemic pattern) to 1 (totally transmural extent of the lesion).

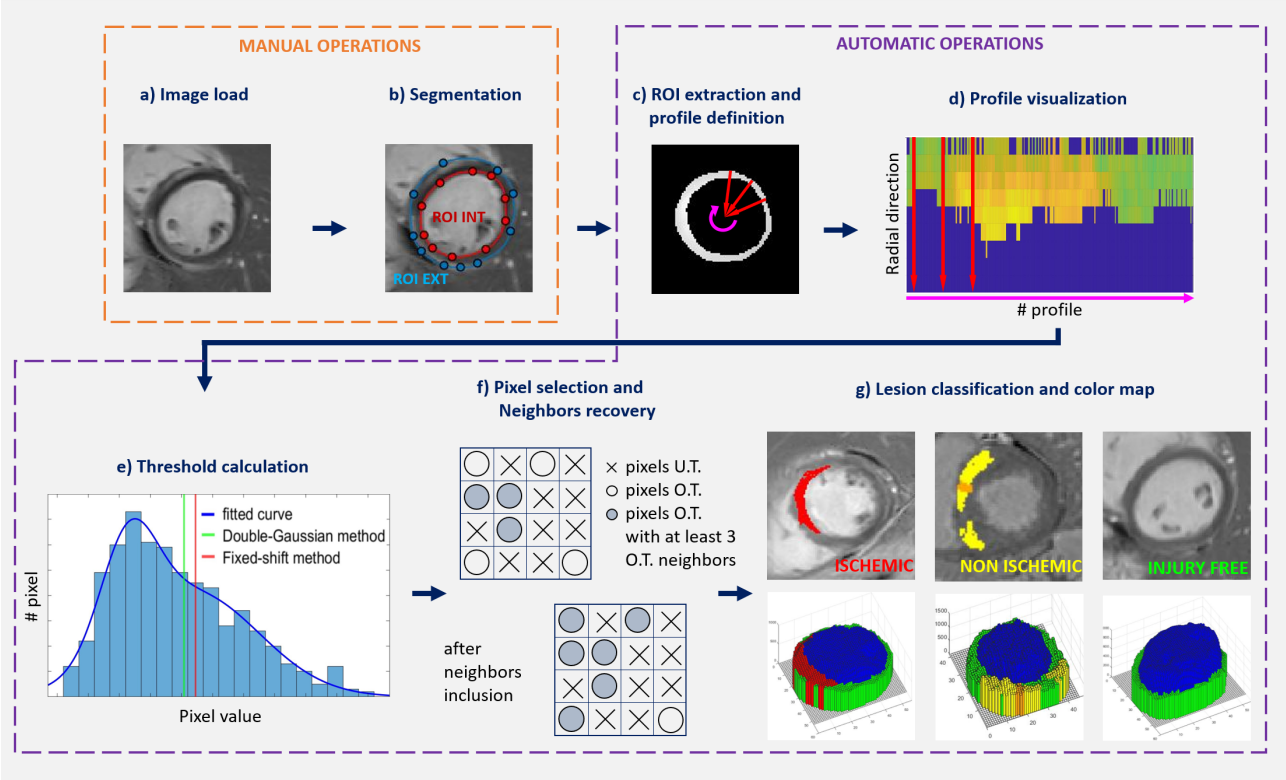

Fig. 1 *Step-by-step representation of the FLORA workflow: the orange-dashed line shows the required manual operations, the purple-dashed line the automatic operations.*

FLORA Software Validation

FLORA's performance was compared with the radiologist's evaluation for the entire 120-patient sample (40 with ischemic lesion, 40 with non-ischemic lesion, and 40 with injury-free myocardium). The following tasks relating to the methods for automatically selecting the threshold were used in the comparison:

1. Lesion identification.

2. Lesion classification: ischemic, non-ischemic, injury-free, mixed pattern (both ischemic and non-ischemic pixel).

3. Assessment of the extent of the identified lesion: concordant, overestimated or underestimated assessment. The assessment was considered overestimated when the extent of the myocardial scar, as indicated by the software, involved more myocardial segments than the radiologist's visual evaluation, when the percentage of transmurality was higher (in the case of ischemic lesion), or when the presence of artifacts or noise was classified as myocardial damage. It was considered understimated when the extent of the myocardial scar involved fewer myocardial segments than the visual evaluation, when the percentage of transmurality was lower, or when small areas of LGE were not recognized.

4. Inter-reader agreement in transmurality evaluation. The distribution of ischemic lesions and the transmurality of fibrosis was evaluated by the radiologist according to the American Heart Association's 17-segment model [44]. The extension of myocardium scar in each segment of the selected silce was scored according to four categories defined by the percentage thickness of affected myocardium: 1=1–25%; 2=26–50%; 3=51–75%; 4=76–100%. A total of 52 segments were evaluated. Afterwards, three radiologists, two with four years and one with 20 of experience in CMR, were asked to perform a blinded estimation of the transmurality extension, with and without the software, in a reduced subgroup of 20 patients with ischemic lesions involving <75 % of myocardial thickness. This was done to asses whether the software could increase the inter-reader agreement in the evaluation of transmurality when LGE images revealed an incomplete transmurality pattern.

Texture analysis

The radiomics workflow included (a) lesion segmentation, (b) features extraction, and (c) features selection (Figure 2).

Image segmentation: SA-CINE, SA-LGE and T1 mapping native images were retrieved from our PACS and loaded into the 3D Slicer software, version 4.10.2 (open source software; https://www.slicer.org/) for segmentation. For each patient, a radiologist with seven years of experience in CMR selected a single slice of the SA-LGE sequence in which the myocardial alteration was visible. The correspondent same slice was selected on the SA-CINE sequence choosing the end-diastolic phase and on the native T1 mapping sequence. The areas to be analyzed were defined by contouring a ROI . The whole myocardium was segmented on the previously selected SA-LGE, SA-CINE and native T1 mapping images by delineating the endocardial and epicardial borders of the LV. In those patients with myocardial infarction and myocarditis, another ROI was drawn on the SA-LGE slice encircling the visible area of fibrosis; the healthy myocardium region was then derived by subtracting the lesion segmentation from the whole myocardium segmentation. Texture analysis was then performed: 1) on the whole myocardium; 2) on the healthy myocardium; 3) on the myocardium with fibrosis.

Texture feature extraction: A total of 93 quantitative features were extracted from the segmented ROIs, including first-order features (providing a global summary of the signal intensities within the segmented volume) such as mean, median, variance, skewness, kurtosis (pointiness), and entropy (randomness or disorder) and second-order features (quantities describing the relationship of

neighbouring voxel signal intensities) calculated from derived matrices such as grey-level co-occurrence matrix (GLCM) and grey-level run-length matrix (GLRLM).

Texture feature selection: Kruscal-Wallis test, with Dunn's test post-hoc analysis, was performed on the segmented ROIs to identify the most significant features in distinguishing between myocardial ischemia, myocarditis and absence of alterations on CMR. In order to reduce data overfitting, a dimensionality reduction was performed on the features obtained from each statistical test. The most significant features for both scanners after dimensional reduction were then selected.

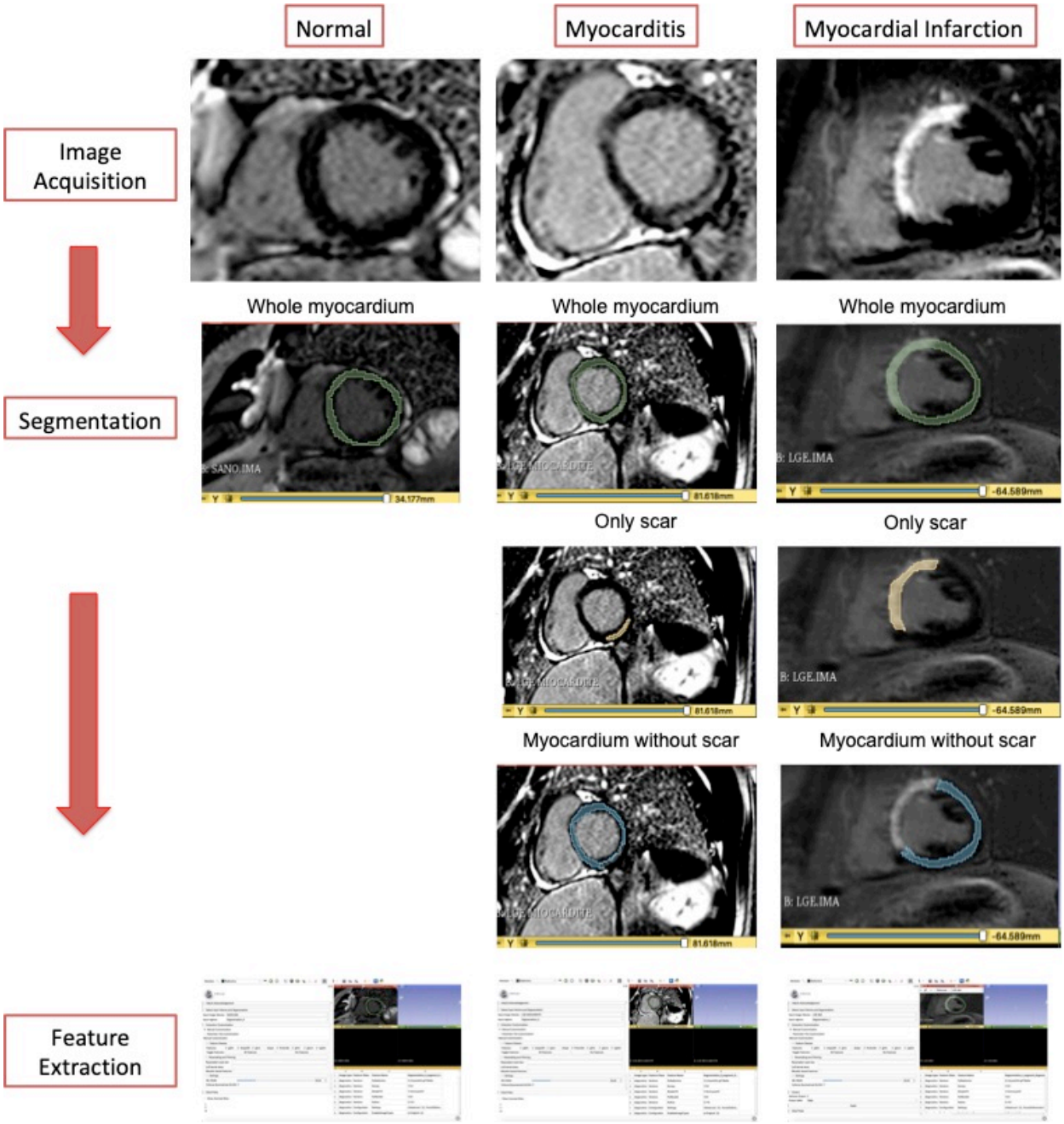

Fig. 2 *Schematic shows radiomics workflow in CMR on late gadolinium enhancement images. First, routine medical-grade images are acquired and reconstructed. Second, images are manually segmented to define ROIs. The whole Myocardium is segmented by delineating the endocardial and epicardial borders of the LV. The region of abnormal myocardium is segmented by encircling the visible area of fibrosis and the healthy myocardium region is derived by subtraction. Third, quantitative radiomics features are extracted from ROIs to build a large set of data. Finally, extracted data are statistically analyzed.*

Statistical analysis

Software-radiologist concordance for Tasks 1 (identification) and 2 (classification) was assessed by means of contingency tables and Cohen's Kappa with SPSS software (IBM SPSS Statistics v.27.0, Armonk, NY, IBM Corp.). The analysis was repeated with results grouped by MR scanner, taking both of the threshold estimating methods into account. The percentage of lesion extent that was correctly estimated, overestimated and underestimated by FLORA was calculated for Task 3. Inter-reader agreement in transmurality evaluation (Task 4), both with and without the use of the software, was assessed using Fleiss Kappa.

Statistical analisys on the features extracted from the SA-LGE, SA-CINE and native T1 mapping segmented images was performed with SPSS software with non-parametric tests, separating patients according to the MR scanner (Siemens and Philips).

Kruscal-Wallis test, with Dunn's test post-hoc analysis, was performed on the segmentations of the whole myocardium to obtain the most significant features in distinguishing between myocardial ischemia, myocarditis and absence of alterations on CMR.

Same analysis was performed on the abnormal myocardium and healthy myocardium regions segmented on the SA-LGE images.

In order to decrease data overfitting, a dimensionality reduction was performed on the significant features obtained from each statistical test using principal component analisys and the Perason's correlation matrix, choosing the less correlated features.

Results

FLORA software

The analysis inclulded 120 patients aged between 18 to 84 years, mean age 52 ± 34; 91men and 39 women.

Examples of ischemic and non-ischemic lesion classification, with the corresponding 3D visualization, are given in Figure 3.

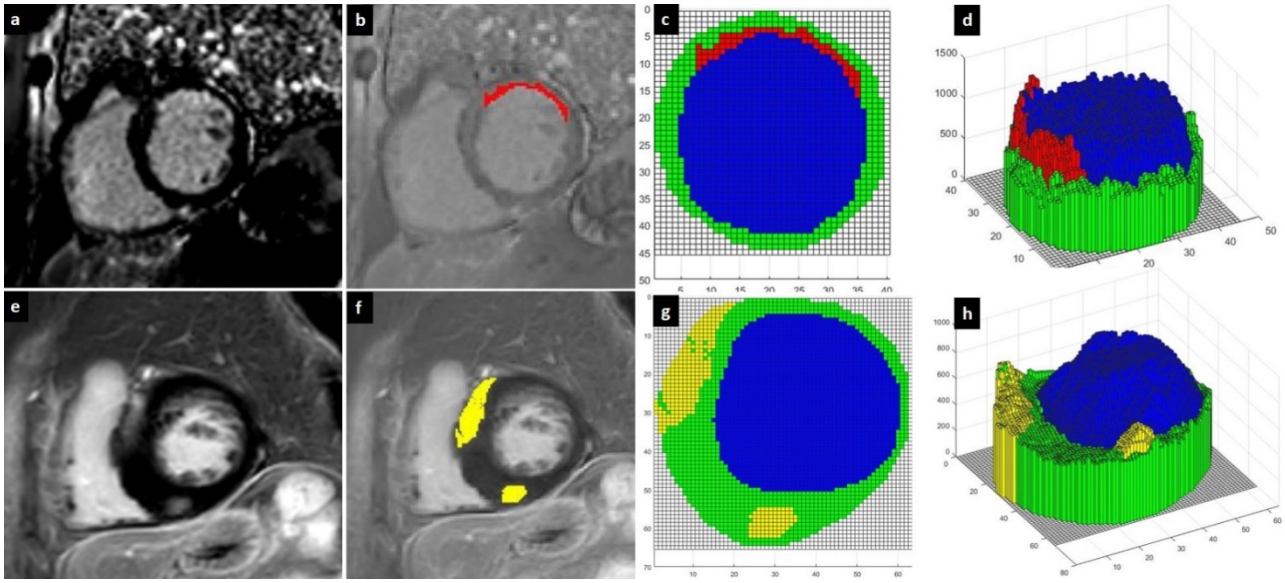

Fig. 3 Images a-d: *A 76-year-old male patient with a previous episode of myocardial infarction. LGE- SA reveals an area of sub-endocardial enhancement in the anterior wall of the mid-cavity (a). The alteration is correctly identified and classified on the 2D image provided by FLORA (ischemic area in red) (b,c), while the 3D image (d) help to assess the degree of involvement of the affected wall.*

Images e-h: *A 65-year-old female with hypertrophic cardiomyopathy involving the interventricular septum. In LGE, the short axis reveals an area of enhancement at the level of the septum, particularly at the anterior and posterior right ventricle insertion points (e). The tissue damage is correctly identified and classified by FLORA as shown in the 2D image (f, g) and in the 3D rendering (h).*

Table 4 gives a comparative indication of the software's performance in identifying lesions for the two methods of automatic threshold estimation (Task 1). Clearly, there were a very low number of false negatives. Cohen's Kappa results for the whole dataset and grouping data by MR scanner were as follows: (double-gaussian fit' method / fixed-shift method): 0.621/0.554 (whole dataset); 0.668/0.549 (Siemens scanner); 0.471/0.571 (Philips scanner). For the Altman classification, the agreement ranged from moderate to substantial. The performance of the double-gaussian fit method, meanwhile, was comparable to that of the fixed-shift method.

These results are due to the relatively high number of false positives. Of the 40 patients classified by the radiologist as injury-free on the LGE sequences, 18/20 (double-gaussian fit method / fixed-shift method) were considered positive by the software due to a low number of pixels, indicating an altered myocardial signal that does not affect the radiological evaluation (evidence of confounding noise). On the other hand, FLORA identified both ischemic and non-ischemic myocardial lesions in almost all cases (80/80 and 79/80 for the double-gaussian fit method and fixed-shift method, respectively, with sensitivity and specificity of 100% / 98.8% and 55% / 50%, respectively).

Table 4: contingency table for lesion identification using the two methods for automatic threshold estimation (Task 1).

		NEGATIVE		POSITIVE	
		Double-gaussian fit method	Fixed-shift method	Double-gaussian fit method	Fixed-shift method
Radiologist	Negative	22	20	18	20
	Positive	0	1	80	79

Table 5 shows the contingency table comparing the software's performance for lesions classified acording to the two methods of automatic threshold estimation (Task 2). The classification works very well for lesions classified as ischemic by the radiologist (Group 1 in Table 5). However, it works less well for cases that do not present signal alterations (Group 3 in Table 5). FLORA correctly classified ischemic lesions (Group 1 in Table 5) in most cases (34/40 with the double-gaussian fit method and 38/40 with the fixed-shift method). The remaining cases (6 and 2, respectively) were classified as a mixed pattern for the presence of ischemic and non-ischemic pixels. Non-ischemic lesions (Group 2 in Table 5) were correctly classified in 28/40 cases using the double-gaussian fit method and 32/40 cases using the fixed-shift method. For the fixed-shift method, the software failed to recognise a subtle mesocardial LGE in a patient with dilated cardiomyopathy in one instance, while the remaining cases were classified as mixed pattern.

Cohen's Kappa was used to assess the software's performance in lesion classification. The results for the whole dataset grouped by MR scanner were as follows (double-gaussian fit method / fixed-shift method): 0.595/0.662 (whole dataset); 0.594/0.669 (Siemens scanner); 0.597/0.642 (Philips scanner). As for the identification task, the agreement ranged from moderate to substantial with higher Cohen's Kappa values, while the fixed-shift method performed better compared to the double-gaussian fit method.

Table 5: Contingency table for lesion classification for the two automatic threshold estimation methods (Task 2).

		1		2		3		4	
		DGF method	FS method	DGF method	FS method	DGF method	FS method	DGF method	FS method
Radiologist	1	34	38	0	0	0	0	6	2
	2	0	0	28	32	0	1	2	7
	3	3	4	3	2	22	20	12	14
	4	0	0	0	0	0	0	0	0

1: ischemic lesion, 2: non ischemic lesion, 3: injury-free, 4: mixed-pattern.

DGF, Double-gaussian fit method, FS Fixed-shift method

Table 6 gives the percentage of overestimated, underestimated and correctly evaluated lesion extent for the whole dataset grouped by MR scanner (Task 3). An example of the extent evaluation is given in Figure 4.

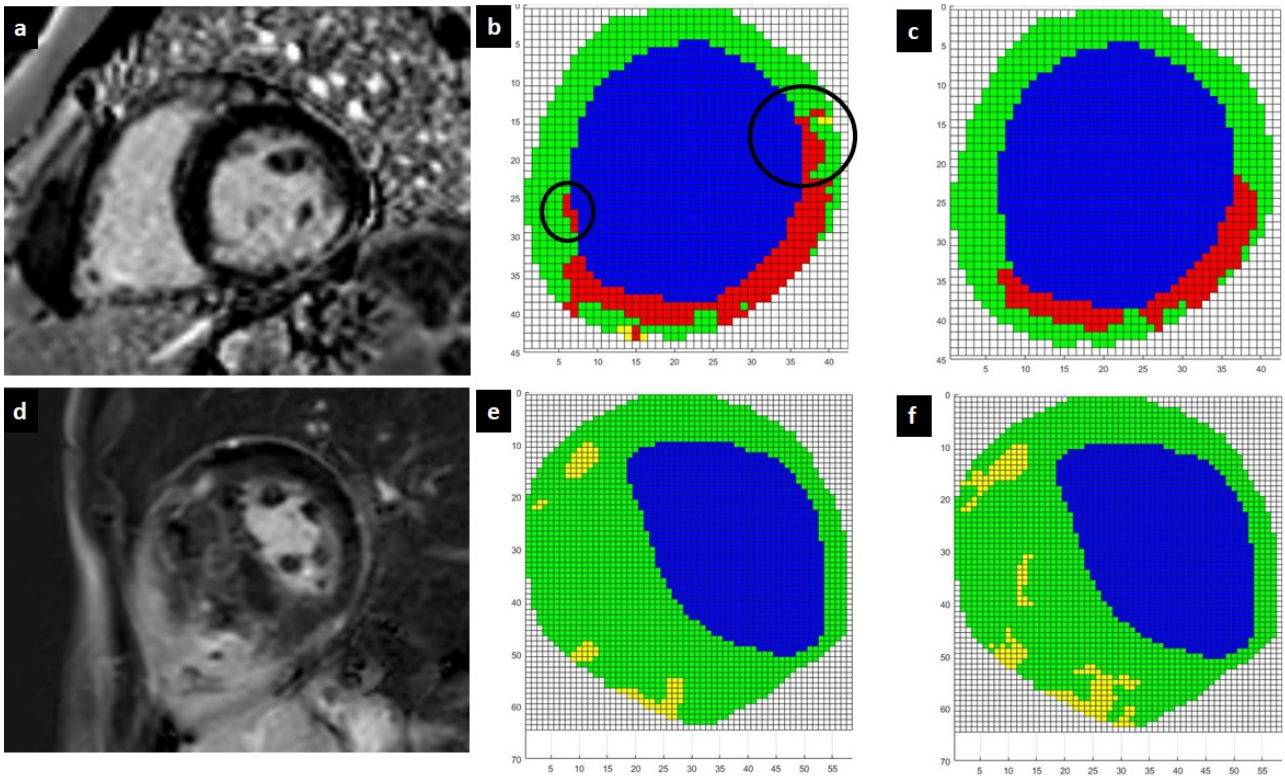

Fig. 4 Images a-c: *57-year-old male with ischemic myocardial damage. LGE-SA reveals an ischemic scar of the inferior and infero-lateral wall of the left ventricle (a). Using the double-gaussian fit method, FLORA overestimates the ischemic lesion in the 2D image, marking altered pixels in segments not identified by the radiologist (black circles) (b). These are correctly identified with the fixed-shift method (c).*

Images d-f: *25-year-old male with hypertrophic cardiomyopathy involving the interventricular septum. LGE-SA reveals diffuse enhancement of the interventricular septum (d). FLORA underestimates myocardial fibrosis more frequently with the double-gaussian fit method (e) than with the fixed-shift method (f).*

There was good agreement between the FLORA software and the radiologist for the evaluation of the extent of the lesion (Cohen's Kappa for double-gaussian fit method / fixed-shift method: 0,855 / 0,931).

Table 6: Percentage of correctly evaluated lesion extent (Task 3).

	Scanner 1		Scanner 2	
	Double-gaussian fit method	Fixed-shift method	Double-gaussian fit method	Fixed-shift method
Correctly evaluated	67%	76%	77%	70%
Overestimated	23%	12%	17%	13%
Underestimated	10%	11%	6%	17%

Table 7 gives the Fleiss's Kappa values used to assess the inter-reader agreement in transmurality estimation (Task 4) for patients with transmurality extent < 75% after visual evaluation. The agreement levels increased significantly when radiologists were assisted by the software, increasing from slight to moderate/substantial.

Table 7: Fleiss's Kappa to assess inter-reader agreement in evaluating scar tissue transmural extent (Task 4).

Transmurality grade	No software assistance	Software assistance: double-gaussian fit method	Software assistance: fixed-shift method
1	0.100	0.484	0.484
2	0.130	0.643	0.481
3	0.190	0.744	0.553
4	-	1.000	-

Transmurality grade (percentage of affected myocardial). 1:1–25%, 2: 26–50%, 3: 51–75%, 4: 76–100%.

Texture analysis

The total amount of significant features derived from each of the selected images on both the MR scanners and the features selected after the dimensionality reduction with the correspondig p-value (p) are reported below. When a three group comparison was made, the two groups that passed the Dunn's test are also reported.

- On the SA-LGE images the significant features extracted were:
    a. From the analysis of the the whole myocardium comparing the three groups (myocardial ischemia (I), myocarditis (M) and no alterations on CMR (S)): for the Ingenia scanner a total of 59 features, 5 after dimensional reduction: Contrast (GLCM) ($p = 0.001$; I-S, I-M), Correlation ($p < 0.001$; I-S) Skewness ($p = 0.015$; I-S), Maximum ($p < 0.001$; I-S, I-M), JointEnergy ($p = 0.011$; I-S, I-M); for the Aera scanner a total of 62 features, 7 after dimensional reduction: Contrast (GLCM) ($p = 0.005$; I-S, M-S), Imc1 ($p < 0.001$; I-S), Skewness ($p = 0.005$; I-S, M-S), RobustMeanAbsoluteDeviation ($p < 0.001$; I-S, M-S), RootMeanSquared ($p < 0.001$; I-S, M-S), Entropy ($p < 0.001$; I-S, M-S), Mean ($p < 0.001$; I-S, I-M); the significant features for both scanners after dimensional reduction were Contrast (GLCM) and Skewness (Table 8; Figure 5).
    b. From the analysis of the healthy myocardium comparing the three groups (myocardial ischemia (I), myocarditis (M) and no alterations on CMR (S)): for the Ingenia scanner a total of 13 features, 2 after dimensional reduction: Skewness ($p = 0.020$; I-S), Stregth ($p = 0.002$;

I-S, I-M); for the Aera scanner a total of 45 features, 6 after dimensional reduction: GrayLevelVariance (GLDM) ($p = 0.002$; I-S, M-S), RobustMeanAbsoluteDeviation ($p = 0.010$; I-S), Mean ($p = 0.018$; I-S), SizeZoneNonUniformity ($p = 0.032$; I-S), LargeAreaHighGrayLevelEmphasis ($p = 0.037$; I-S), Coarseness ($p = 0.010$; I-S); no significant feature for both scanners after dimensional reduction was found.

c. From the analysis of the myocardium with fibrosis comparing myocardial ischemia and myocarditis: for the Ingenia scanner a total of 59 features, 5 after dimensional reduction: MCC ($p < 0.001$), ClusterProminence ($p < 0.001$), MeanAbsoluteDeviation ($p < 0.001$), Minimum ($p = 0.019$), SmallAreaLowGrayLevelEmphasis ($p = 0.009$); for the Aera scanner a total of 59 features, 4 after dimensional reduction: HighGrayLevelEmphasis ($p = 0.029$), Idmn ($p= 0.024$), RobustMeanAbsoluteDeviation ($p = 0.013$), 10Percentile ($p < 0.001$); no significant feature for both scanners after dimensional reduction was found.

- On the SA-CINE images the significant features extracted were:

a) From the analysis of the whole myocardium comparing the three groups (myocardial ischemia (I), myocarditis (M) and no alterations on CMR (S)): for the Ingenia scanner a total of 2 features, 1 after dimensional reduction: MCC (Maximal Correlation Coefficient) ($p= 0.013$; I-S); for the Aera scanner a total of 19 features, 5 after dimensiona reduction: GrayLevelNonUniformity

(GLDM) (p= 0.002; I-S, I-M), DependenceVariance (p=0.001; I-M), ClusterShade (p= 0.013; I-S), LargeAreaHighGrayLevelEmphasis (p= 0.0013; I-S), Coarseness (p= 0.012; I-M); no feature significant for both scanners after dimensional reduction was found.

- On native T1 mapping images the significant features extracted were:
    a) From the analysis of the whole myocardium comparing the three groups (myocardial ischemia (I), myocarditis (M) and no alterations on CMR (S)): for the Ingenia scanner a total of 16 features, 3 after dimensional reduction: ShortRunHighGrayLevelEmphasis (p = 0.008; I-M), ClusterShade (p = 0.032; I-M), RobustMeanAbsoluteDeviation (p = 0.010; I-S); for the Aera scanner a total of 52 features, 5 after dimensiona reduction: ClusterShade (p = 0.006; I-S), MeanAbsoluteDeviation (p = 0.002; I-S), Variance (p < 0.001; I-S, M-S), GrayLevelNonUniformity (GLSZM) (p = 0.017; I-S), LargeAreaLowGrayLevelEmphasis (p = 0.023; I-S); the feature significant for both scanners after dimensional reduction was Cluster Shade (Table 8; Figure 5).

Table 8 : List of significant quantitative texture features for the Kruskal-Wallis test between the three pathology groups for both MR scanners after dimensionality reduction. For each feature the p-value, the median and the Tukey's first and third quartile values are reported separately for the two MR scanners and for each pathology group. Pathology groups: 1 = myocardial infarction, 2 = myocarditis, 3 = no alterations on CMR.

Sequence	Feature	P-value		Pathology	Median		1st / 3rd Quartile		Brief feature description
		Ingenia	Aera		Ingenia	Aera	Ingenia	Aera	
SA-LGE 3 groups	Contrast (GLCM)	0.001	0.005	1	33.6	14.3	27.0 / 49.1	7.7 / 16.4	First-order feature; it is a measure of the local intensity variation. It is higher in the regions without any regular intensity pattern
				2	13.1	10.6	8.9 / 19.5	7.8 / 22.6	
				3	13.0	5.0	10.0 / 14.2	4.2 / 5.8	
SA-LGE 3 groups	Skewness	0.015	0.005	1	0.99	0.63	0.84 / 1.34	0.42 / 1.38	First-order feature; it measures the asymmetry of the distribution of values about the Mean value. A zero value indicates the values are symmetrically distributed.
				2	0.89	0.76	0.76 / 1.03	0.55 / 1.02	
				3	0.21	0.10	-0.09 / 0.63	0.03 / 0.32	
T1 3 groups	ClusterShade	0.032	0.006	1	-665	206	-952 / -97	81 / 321	Second-order feature; it is a measure of image symmetry and non-uniformity: a higher value implies greater asymmetry about the mean.
				2	28	85	-231 / 66	34 / 124	
				3	-213	8.0	-1442 / 41	-0.9 / 25	

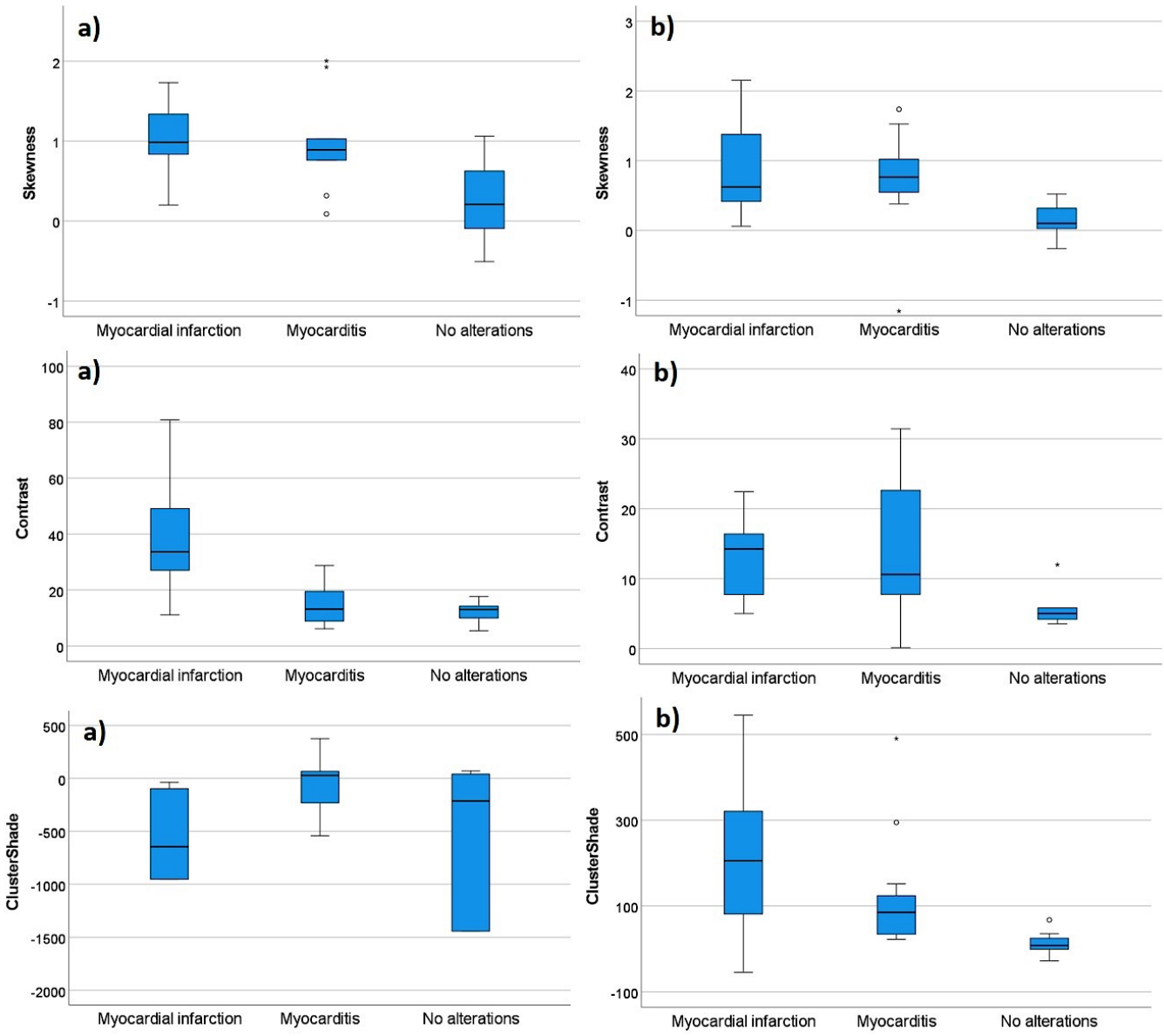

Fig. 5 *Contrast (GLCM), Skewness and ClusterShade boxplots for the three groups of pathology and the two different MR scanners: a) for Philps Ingenia 1.5 T scanner and b) for Siemens Aera 1.5 T scanner.*

Discussion

The FLORA tool was designed for the identification, classification and evaluation of the extent and degree of transmurality (for ischemic lesions only) using LGE – a validated method for assessing

myocardial damage and a prognostic marker in patients with myocardial ischemia[45,46]. The 'areas of "irreversible" damage appearing as transmural bright alterations on LGE images should be correctly classified, and a distinction between ischemic and non-ischemic lesions should be done. Many existing studies focus on developing new types of LGE sequences [10,47]. In recent years, dark-blood LGE sequences have been proposed. In these sequences the scar-blood contrast is increased, thus improving the visibility of subendocardial scars [6]. However, these images are usually still analyzed by a visual assessment. Furthermore, if large areas of transmural LGE are identified, it is more difficult to determine the degree of transmurality or to differentiate the ischemic areas from other not ischemic lesions that show extended LGE. Moreover, currently available software solutions allow for scar tissue quantification by manually setting a LGE threshold. These are of limited use in clinical practice and don't help radiologists in classifying the areas of LGE.

FLORA showed moderate to good agreement with the radiologist in the identification and classification of myocardial signal changes in LGE sequences. The best and perhaps most promising result from the study is that FLORA produced hardly any false negatives (i.e. it showed very high sensitivity), which is an important feature for this type of software.

The best results were obtained in the classification of ischemic myocardial damage, which was correctly identified in 85% and 95% of cases for the double-gaussian fit method and the fixed-shift method, respectively. In the remaining cases it was classified as a mixed-pattern due to the presence of some occasional yellow pixels (classified as non-ischemic) resulting from small artifacts on the

LGE-SA images. In one case, the identification of yellow pixels in the middle of the ischemic area was due to the presence of no-reflow areas in the segmentation. Despite this, the extent of the ischemic myocardial scar was correctly recognized in these cases. In just two cases, both related to the use of the double-gaussian fit method to determine the threshold, the image indicated the presence of further areas of miocardial alteration, in addition to the ischemic area. FLORA thus displayed low specificity, mainly due to the incorrect classification of few isolated pixels that did not affect the radiologist's final diagnosis.

FLORA was able to provide an automatic quantitative evaluation of the extent of trasmurality of an ischemic lesion, which may be of assistance to radiologists. We have shown that there is a low agreement among radiologists in defining the degree of transmurality of an ischemic lesion when the myocardial damage affects less than 75% of the myocardial thickness. In these cases, visual estimation of the extent of transmurality was more difficult and thus less reproducible. Agreement among readers in the quantitative evaluation of the extent of transmurality of ischemic lesions increased from slight to moderate/substantial with the assistance of FLORA, indicating that the software can reduce inter-reader variability in scar-tissue quantitative evaluation using LGE for patients with ischemic lesions. This last aspect is crucial, given the importance of a reliable quantitative evaluation of the degree of transmurality of the ischemic lesion, both for patient's prognosis and for defining the correct course of treatment[48,49] .

Non-ischemic changes were also correctly recognized in most cases. However, some of them were classified as mixed pattern (30% and 17.5% of cases for the double-gaussian fit method and fixed-shift

method, respectively). This is because non-ischemic alterations typically have a non-sub-endocardial enhancement pattern, often located in the mid-wall or epicardial regions [5,50]. The sub-endocardium can also be involved, especially when the myocardial damage is very extensive, but it does not follow any coronary distribution, and involvement is patchy and of limited extension. There is thus more difference in the software's representation of the tissue damage in the non-ischemic group, compared with the ischemic group.

Furthermore, the results did not depend significantly on the MR scanner used, suggesting that the results obtained for the validation dataset may also be confirmed in other CMR examinations. Multicenter validations on larger populations are certainly necessary.

The software was also able to increase the detection of sub-endocardial sparing areas, allowing for a better classification between ischemic and non-ischemic lesions (Figure 6). Extensive alterations featuring significant edema, as it happens for example in myocarditis or in sarcoidosis, can erroneously be classified as ischemic areas.

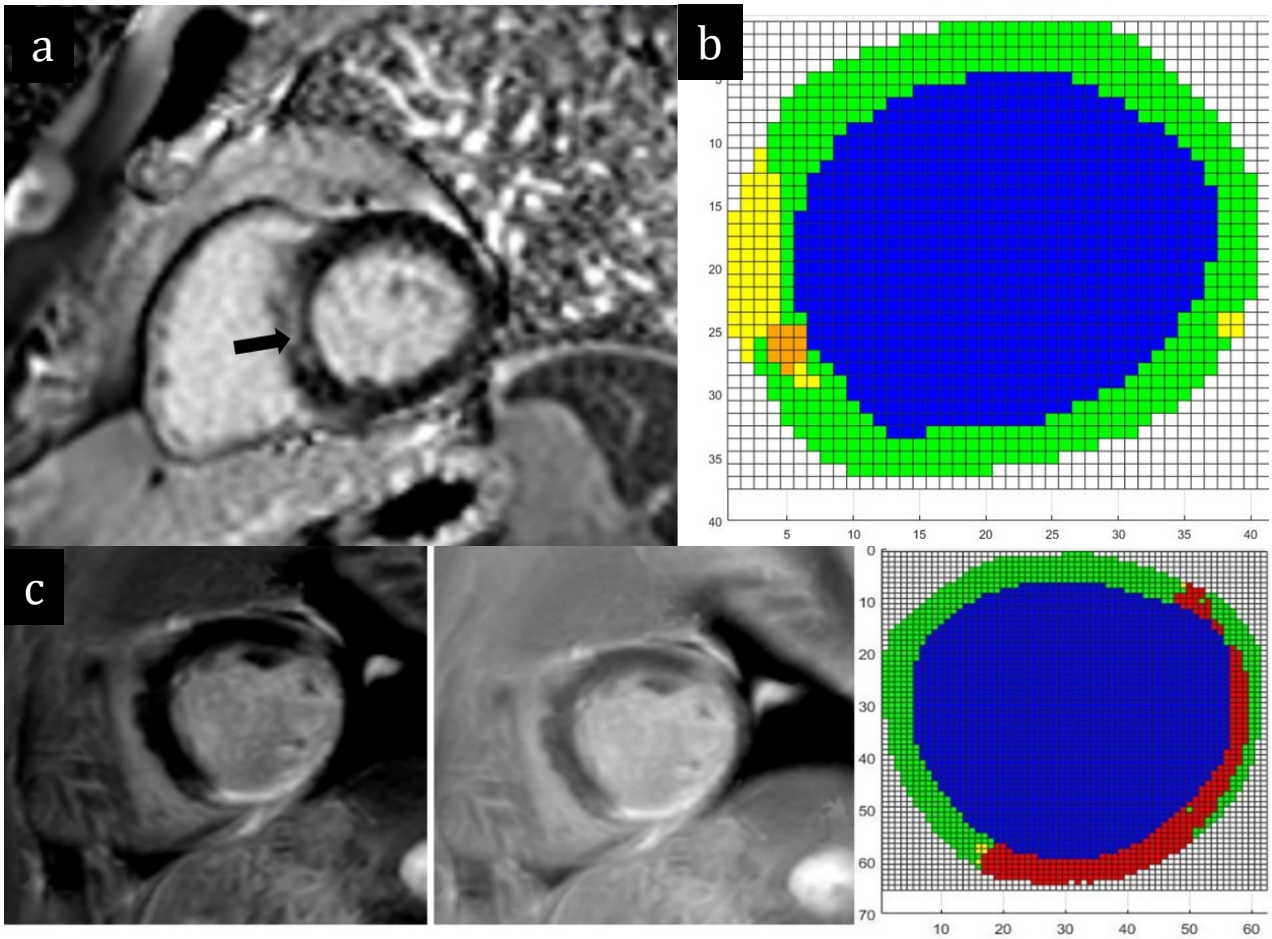

Fig. 6 *60-year-old male suffering from myocarditis with an area of enhancement in the interventricular septum at the base of the LV on LGE-SA (black arrow) (a). FLORA increases the detection of sub-endocardial sparing areas and correctly classifies myocardial damage as non-ischemic (b) vs ischemic (c).*

FLORA's worst performance was in occasional incorrect classification of injury-free myocardial areas (medium specificity). This depends on the fact that a very high sensitivity was preferred, even at the expense of observing some false positives.

In our study population only one false negative was observed: it was a patient suffering from dilated cardiomyopathy, who had very thin walls with low intramyocardial enhancement in the septum. This is probably due to the small number of pixels present in a very thin myocardium.

Another limitation is that FLORA can confuse some motion artifact patterns with areas of altered LGE signal (Figure 7). However, this does not significantly affect the use of the software, as images with artifacts are easily identified by the radiologist. This misclassification can thus be easily identified. Furthermore, even if an automatic threshold recognition method is used, the radiologist's intervention for myocardium segmentation is always required. This leads to a minimal interobserver variability, however lower than that observed in visual evaluation. Finally, another important limitation of this study is that the FLORA software results were compared only with the standard radiologist's evaluation. In future, it could be very interesting compared FLORA performance with a semiquantitative software analysis of LGE areas currently available.

Nevertheless, the FLORA software results have an important clinical significance. In particular, FLORA can reduce inter-reader variability in the radiologist's final diagnosis especially if there are LGE areas with non-characteristic distribution and/or the radiologist have a low level of expertise and experience. Moreover, FLORA could be an useful tool to speed-up analysis time using an automatic approach.

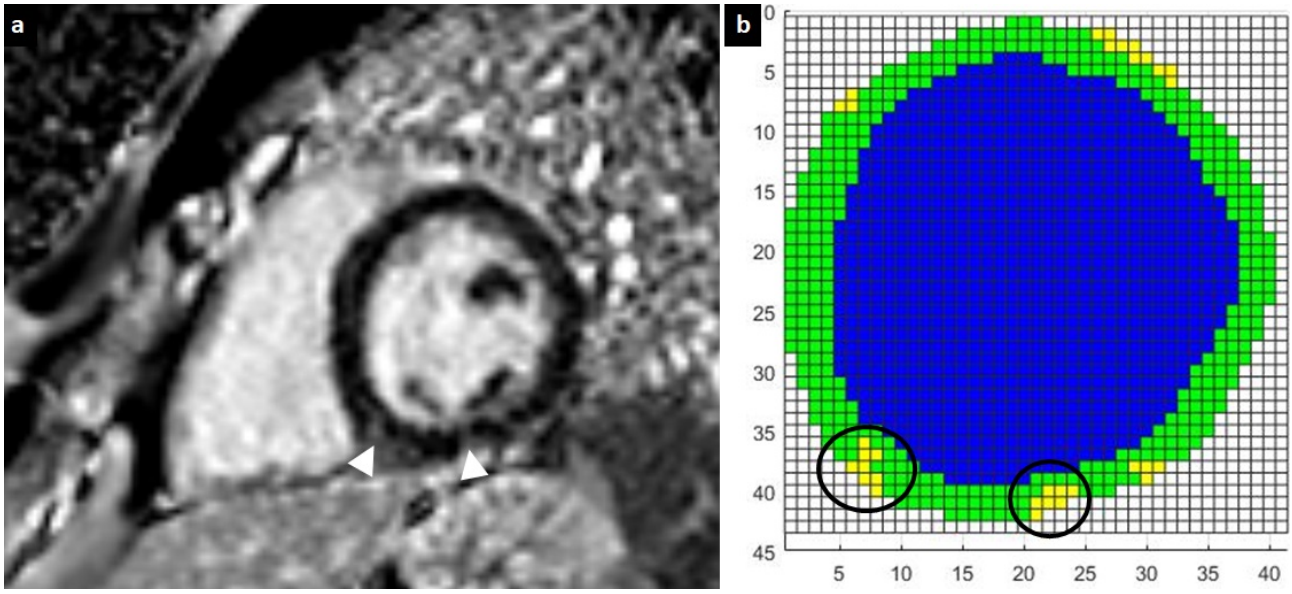

Fig. 7 *Small artifacts on the LGE SA sequence (white arrowhead) in a patient classified as injury-free by the radiologist (a) are recognized by FLORA as areas of non-ischemic altered signal (black circles) (b).*

FLORA's future developments will focus on radiomics techniques being integrated into the classification kernel of the software. For this reason, we started to evaluate the diagnostic value of texture features analysis in differentiating between myocardial infarction, myocarditis and healthy controls. To our knowledge, there are only few studies concerning the diagnostic value of texture analysis based on CMR images. The main finding of our study was the identification of three features significant for both MR scanners after dimensional reduction. Specifically, from the analysis of the whole myocardium on the SA-LGE images, we identified Contrast (GLCM) and Skewness as texture features significant for both scanners after dimensional reduction while, from the analysis of the whole myocardium on native T1 mapping images, ClusterShad was identified as a significant feature for both MR scanners.

In particular, on the SA-LGE images, for both scanner employed, a statistically significant difference in Contrast (GLCM) was observed between myocardial infarction and healthy controls ($p < 0.05$) so that myocardial infarction showed more irregular intensity patterns compared to patients with no alterations on CMR. Moreover, in patients with no alterations on CMR, Skewness was close to 0 (the values were symmetrically distributed) while in myocardial infarction and in myocarditis it was close to 1 (the values were asymmetrically distributed, with a distribution that presents a tail at the higher pixel values, corresponding to those relating to the myocardial scar).

In addition, from the analysis of the whole myocardium on SA-LGE images, myocardial infarction showed more irregular intensity patterns (Contrast GLCM), higher maximum value of signal intensity (Maximum), and a less homogeneous pattern (Joint Energy) for the Philips Ingenia scanner and a higher mean value of signal intensity (Mean) for the Siemens Aera scanner compared to myocarditis. We found a greater difference between myocardial infarction and healthy control compared to myocarditis, with 5 texture parameters resulting statistically different for the Philps Ingenia scanner (Contrast GLCM, Correlation, Skewness, Maximum, Joint Energy: all $p<0.05$), and 7 for the Siemens Aera scanner (Contrast GLCM, Skewness, Imc1, Root Mean Squared, RobustMeanAbsoluteDeviation, Entropy and Mean: all $p<0.05$). Entropy was higher in both the myocardial infarction and myocarditis groups compared to group with no alterations on CMR, because it reflects how irregular or “random” the pixel intensity distribution is. In addition, myocarditis and myocardial infarction showed a greater magnitude of the intensity values (RootMeanSquared) and a higher value of RobustMeanAbsoluteDeviation than healthy controls.

RobustMeanAbsoluteDeviation is a first-order feature and it is the mean distance of all intensity values from the Mean Value calculated on the subset of image array with gray levels in between, or equal to the 10th and 90th percentile. Therefore, texture analysis was shown to be a promising tool in discriminating between these myocardial diseases with the largest number of texture parameters with a statistically significant difference identified on the SA-LGE images. This is an important result because radiomics presents a novel quantitative image analysis technique with potential to improve the diagnostic accuracy and confidence of CMR, especially when radiologists with low level of expertise and experience evaluate images. In this setting, texture analysis could be uses as a tool for self-training programs.

From the texture analysis of native T1 maps, we identified ClusterShade as a texture feature significant for both scanners obtained after dimensional reduction. ClusterShade is a second-order feature and it is a measure of the uniformity of the image; a higher cluster shade implies greater asymmetry about the mean. However, for the Ingenia scanner, myocarditis showed a higher value of ClusterShade than myocardial infarction while, for the Aera scanner, myocardial infarction showed a higher value of ClusterShade than patients without alterations on CMR (Figure 5). This difference between the two scanner employed could be explained by the limited number of study subjects, as it is shown in the blox plots by the high degree of dispersion in the data, or by a higher variability due to different parameters of acquisition. Major sources of variability for radiomics features are MR scanners, image acquisition and reconstruction parameters, and ROI delineation. Many image acquisition–related factors, including spatial resolution, signal-to-

noise ratio, MR field strength and image slice thickness, are a potential source of confounding elements in texture analysis. However, little to no study has been done to discern how these factors specifically affect cardiac MRI radiomics[51,52]. Beyond ClusterShade, we identified other significant features after dimensional reduction for the Ingenia scanner (ShortRunHighGrayLevelEmphasis, $p = 0.008$; RobustMeanAbsoluteDeviation, $p = 0.010$) and for the Aera scanner (MeanAbsoluteDeviation, $p = 0.002$; Variance, $p < 0.001$; GrayLevelNonUniformity GLSZM, $p = 0.017$; LargeAreaLowGrayLevelEmphasis, $p = 0.023$). Therefore, standardized acquisition and reconstruction protocol will be needed to reduce the limits of bias and variance and to create the most robust models.

In our study, no texture features derived from the SA-CINE images with a statistically significant difference for both scanners after dimensional reduction was found. This result is not in accordance with other studies that demonstrate the ability of CMR texture analysis based on non-contrast cine images to differentiate between myocardial diseases and healthy myocardium. Baessler et al, in two different studies, showed significant differences between patients with hypertrophic cardiomyopathy and healthy controls and between individuals with myocardial infarction and healthy controls through texture analysis of non-contrast cine images[53,54]. In addition, Larroza et al. demostrated the ability of texture analysis of non-contrast cine images to accurately identify the non-viable myocardium in patients with myocardial infarction with 92% sensitivity and AUC of 0.849[55]. Schofield et al., in their study on 216 patients, found that texture analysis of unenhanced short axis cine images shows promise in

discriminating between the aetiologies of left ventricular hypertrophy[42]. Actually, considering each MR scanner separately, we found some statistically significant features after dimensional reduction: on the Ingenia SA-CINE images, MCC was statistically different between myocardial infarction and patients without alterations on CMR (p=0.013); on the Aera SA-CINE images, GreyLevelNonUniformity GLDM (Gray Level Dependence Matrix), DependenceVariance, and Coarseness were statistically different between myocardial infarction and myocarditis, while GreyLevelNonUniformity GLDM, ClusterShade and LargeAreaHighGrayLevelEmphasis were statistically different between myocardial infarction and healthy controls. However, none of these features were common to both MR scanners and this finding is very important because differences in radiomics features reflect variations in image acquisition and processing, and not only in tissue characteristics. As we pointed out above, one of the most important challenges for radiomics is the reproducibility of the features so there is a urgent need to identify radiomics features that are robust to real-life variations in CMR images[56]. In their review on Radiomics, Gillies et al. highlighted that a restrospective radiomics investigation must be validated against a completely independent data set, preferably from another institution[41].

Beyond the integration between FLORA and radiomics, another future development of our work could be to evaluate the prognostic value of texture features especially in patients with myocardial infarction. Indeed, a study has shown correlation of texture features to arrhythmia risk in post-myocardial infarction patients[57]. A recent study of Cheng et al. evaluated the prognostic value of texture features based on LGE-CMR images in 67 hypertrophic

cardiomyopathy patients with systolic dysfunction. They found that some texture features linked to LGE heterogeneity are strongly associated with adverse events in their study population[58]. Finally, from the integration between FLORA and radiomics we could developed an automated machine learning algorithm for LGE quantification in hypertrophic cardiomyopathy help in risk stratification. Recently, Augusto et al. have been developed an automated machine learning method of measuring left ventricular maximum wall thickness in hypertrophic cardiomyopathy that have shown to be superior to human experts with potential implications for a more accurate diagnosis and risk stratification[59].

The main limitation of this preliminary study on radiomics is being a retrospective single-centre study with a limited number of subjects because the most rigorous radiomics investigation requires a prospective multicenter trial with standardized acquisition and reconstruction protocols. In addition, multiple texture parameters are challenging to rationalise and their meaning may not be intuitive to comprehend. More studies are needed to correlate the meaning of texture parameters and myocardial alterations.

Conclusions

Advanced MR techniques present a novel quantitative image analysis with potential to improve diagnosis and enhance diagnostic capabilities compared to conventional qualitative MR imaging.

The use of CMR image analysis software such as FLORA may give an important contribution to the standardization of diagnostic and prognostic parameters. The new semiautomated software FLORA showed a very high sensitivity in the identification of myocardial

LGE. It showed moderate to good agreement with the radiologist in the classification of myocardial LGE correctly identifying most of the ischemic lesions. FLORA can reduce inter-reader variability in the determination of the degree of transmurality of the scar in patients with ischemic lesions. Therefore, FLORA has proven to be an applicable tool that improves and facilitates the classification of LGE areas allowing their quantification.

Radiomics with texture analysis could help in the complex CMR tissue characterisation discriminating between myocardial diseases and improving diagnostic accuracy and confidence. Our study showed that some texture features are potentially useful in discriminating between myocardial infarction, myocarditis and healthy controls. In particular, we found three features after dimensional reduction that were significant for both the scanners employed. Larger cohort of patients and the use of standardized acquisition and reconstruction protocols are further needed to validate our findings.

References

1. Moon JCC, Reed E, Sheppard MN, Elkington AG, Ho SY, Burke M, Petrou M, Pennell DJ. The histologic basis of late gadolinium enhancement cardiovascular magnetic resonance in hypertrophic cardiomyopathy. *J Am Coll Cardiol* 2004;**43**:2260–2264.
2. Kim RJ, Fieno DS, Parrish TB, Harris K, Chen EL, Simonetti O, Bundy J, Finn JP, Klocke FJ, Judd RM. Relationship of MRI delayed contrast enhancement to irreversible injury, infarct age, and contractile function. *Circulation* 1999;**100**:1992–2002.
3. Pradella S, Grazzini G, Amicis C De, Letteriello M, Acquafresca M, Miele V. Cardiac magnetic resonance in hypertrophic and dilated cardiomyopathies. *Radiol Medica* Springer Milan; 2020;**125**:1056–1071.
4. Becker MAJ, Cornel JH, Ven PM van de, Rossum AC van, Allaart CP, Germans T. The Prognostic Value of Late Gadolinium-Enhanced Cardiac Magnetic Resonance Imaging in Nonischemic Dilated Cardiomyopathy: A Review and Meta-Analysis. *JACC Cardiovasc Imaging* 2018;**11**:1274–1284.
5. Hunold P, Schlosser T, Vogt FM, Eggebrecht H, Schmermund A, Bruder O, Schüler WO, Barkhausen J. Myocardial late enhancement in contrast-enhanced cardiac MRI: Distinction between infarction scar and non-infarction-related disease. *Am J Roentgenol* 2005;**184**:1420–1426.
6. Holtackers RJ, Heyning CM Van De, Nazir MS, Rashid I, Ntalas I, Rahman H, Botnar RM, Chiribiri A. Clinical value of dark-blood late gadolinium enhancement cardiovascular magnetic resonance without additional magnetization preparation. *J Cardiovasc Magn Reson* Journal of Cardiovascular Magnetic Resonance; 2019;**21**:1–11.
7. Assomull RG, Prasad SK, Lyne J, Smith G, Burman ED, Khan M, Sheppard MN, Poole-Wilson PA, Pennell DJ. Cardiovascular Magnetic Resonance, Fibrosis, and Prognosis in Dilated Cardiomyopathy. *J Am Coll Cardiol* 2006;**48**:1977–1985.
8. Tarantini G, Cacciavillani L, Corbetti F, Ramondo A, Marra MP, Bacchiega E, Napodano M, Bilato C, Razzolini R, Iliceto S. Duration of ischemia is a major determinant of transmurality and severe microvascular obstruction after primary angioplasty: A study performed with contrast-enhanced magnetic resonance. *J Am Coll Cardiol* Elsevier Masson SAS; 2005;**46**:1229–1235.
9. Palmisano A, Vignale D, Benedetti G, Maschio A Del, Cobelli F De, Esposito A. Late iodine enhancement cardiac computed tomography for detection of myocardial scars: impact of experience in the clinical practice. *Radiol Medica* Springer Milan; 2020;**125**:128–136.
10. Fahmy AS, Neisius U, Tsao CW, Berg S, Goddu E, Pierce P, Basha TA, Ngo L, Manning WJ, Nezafat R. Gray blood late gadolinium enhancement cardiovascular magnetic resonance for improved detection of myocardial scar. *J Cardiovasc Magn Reson* Journal of Cardiovascular Magnetic Resonance; 2018;**20**:1–11.
11. Satoh H. Distribution of late gadolinium enhancement in various types of cardiomyopathies: Significance in differential diagnosis, clinical features and prognosis. *World J Cardiol* 2014;**6**:585.
12. Patel AR, Kramer CM. Role of Cardiac Magnetic Resonance in the

Diagnosis and Prognosis of Nonischemic Cardiomyopathy. *JACC Cardiovasc Imaging* 2017;**10**:1180–1193.
13. Schiau C, Schiau Şerban, Dudea SM, Manole S. Cardiovascular magnetic resonance: contribution to the exploration of cardiomyopathies. *Med Pharm Reports* 2019;**92**:326–336.
14. Aquaro GD, Perfetti M, Camastra G, Monti L, Dellegrottaglie S, Moro C, Pepe A, Todiere G, Lanzillo C, Scatteia A, Roma M Di, Pontone G, Perazzolo Marra M, Barison A, Bella G Di. Cardiac MR With Late Gadolinium Enhancement in Acute Myocarditis With Preserved Systolic Function: ITAMY Study. *J Am Coll Cardiol* 2017;**70**:1977–1987.
15. Doltra A, Amundsen B, Gebker R, Fleck E, Kelle S. Emerging Concepts for Myocardial Late Gadolinium Enhancement MRI. *Curr Cardiol Rev* 2013;**9**:185–190.
16. Luetkens J a., Homsi R, Sprinkart AM, Doerner J, Dabir D, Kuetting DL, Block W, Andri?? R, Stehning C, Fimmers R, Gieseke J, Thomas DK, Schild HH, Naehle CP. Incremental value of quantitative CMR including parametric mapping for the diagnosis of acute myocarditis. *Eur Heart J Cardiovasc Imaging* 2016;**17**:154–161.
17. Amano Y, Tachi M, Tani H, Mizuno K, Kobayashi Y, Kumita S. T2-Weighted Cardiac Magnetic Resonance Imaging of Edema in Myocardial Diseases. *Sci World J* 2012;**2012**:1–7.
18. Ferreira VM, Schulz-Menger J, Holmvang G, Kramer CM, Carbone I, Sechtem U, Kindermann I, Gutberlet M, Cooper LT, Liu P, Friedrich MG. Cardiovascular Magnetic Resonance in Nonischemic Myocardial Inflammation: Expert Recommendations. *J Am Coll Cardiol* 2018;**72**:3158–3176.
19. Mahrholdt H, Goedecke C, Wagner A, Meinhardt G, Athanasiadis A, Vogelsberg H, Fritz P, Klingel K, Kandolf R, Sechtem U. Cardiovascular Magnetic Resonance Assessment of Human Myocarditis: A Comparison to Histology and Molecular Pathology. *Circulation* 2004;**109**:1250–1258.
20. Faletti R, Gatti M, Baralis I, Bergamasco L, Bonamini R, Ferroni F, Imazio M, Stola S, Gaita F, Fonio P. Clinical and magnetic resonance evolution of “infarct-like” myocarditis. *Radiol Medica* Springer Milan; 2017;**122**:273–279.
21. Kalisz K, Rajiah P, Roifman I, Gutierrez J, Wang E, Biswas L, Sparkes J, Connelly KA, Wright GA, Khan MAMA, Yang EY, Zhan Y, Judd RM, Chan W, Nabi F, Heitner JF, Kim RJ, Klem I, Nagueh SF, Shah DJ, Slonimsky E, Konen O, Segni E Di, Konen E, Goitein O, Raja AA, Farhad H, Valente AM, Couce JP, Jefferies JL, et al. Evolving concepts in dilated cardiomyopathy. *J Am Coll Cardiol* European Radiology; 2018;**19**:364–375.
22. Patel AR, Kramer CM. Role of Cardiac Magnetic Resonance in the Diagnosis and Prognosis of Non-Ischemic Cardiomyopathy. 2018;**10**:1180–1193.
23. Alexandre J, Saloux E, Dugué AE, Lebon A, Lemaitre A, Roule V, Labombarda F, Provost N, Gomes S, Scanu P, Milliez P. Scar extent evaluated by late gadolinium enhancement CMR: A powerful predictor of long term appropriate ICD therapy in patients with coronary artery disease. *J Cardiovasc Magn Reson* 2013;**15**:1–11.
24. Roes SD, Kelle S, Kaandorp TAM, Kokocinski T, Poldermans D, Lamb

HJ, Boersma E, Wall EE van der, Fleck E, Roos A de, Nagel E, Bax JJ. Comparison of Myocardial Infarct Size Assessed With Contrast-Enhanced Magnetic Resonance Imaging and Left Ventricular Function and Volumes to Predict Mortality in Patients With Healed Myocardial Infarction. *Am J Cardiol* 2007;**100**:930–936.
25. Zhang LJ, Dong W, Li JN, Mi HZ, Jiao J, Dou RY, An J, Liu JL, He Y, Song XT. Quantification of late gadolinium enhancement cardiovascular MRI in patients with coronary artery chronic total occlusion. *Clin Radiol* 2020;**75**:643.e19-643.e26.
26. Acosta J, Fernández-Armenta J, Borràs R, Anguera I, Bisbal F, Martí-Almor J, Tolosana JM, Penela D, Andreu D, Soto-Iglesias D, Evertz R, Matiello M, Alonso C, Villuendas R, Caralt TM de, Perea RJ, Ortiz JT, Bosch X, Serra L, Planes X, Greiser A, Ekinci O, Lasalvia L, Mont L, Berruezo A. Scar Characterization to Predict Life-Threatening Arrhythmic Events and Sudden Cardiac Death in Patients With Cardiac Resynchronization Therapy: The GAUDI-CRT Study. *JACC Cardiovasc Imaging* 2018;**11**:561–572.
27. Bondarenko O, Beek AM, Hofman MBM, Kühl HP, Twisk JWR, Dockum WG Van, Visser CA, Rossum AC Van. Standardizing the definition of hyperenhancement in the quantitative assessment of infarct size and myocardial viability using delayed contrast-enhanced CMR. *J Cardiovasc Magn Reson* 2005;**7**:481–485.
28. Flett AS, Hasleton J, Cook C, Hausenloy D, Quarta G, Ariti C, Muthurangu V, Moon JC. Evaluation of techniques for the quantification of myocardial scar of differing etiology using cardiac magnetic resonance. *JACC Cardiovasc Imaging* 2011;**4**:150–156.
29. Mikami Y, Kolman L, Joncas SX, Stirrat J, Scholl D, Rajchl M, Lydell CP, Weeks SG, Howarth AG, White JA. Accuracy and reproducibility of semi-automated late gadolinium enhancement quantification techniques in patients with hypertrophic cardiomyopathy. *J Cardiovasc Magn Reson* 2014;**16**:1–9.
30. Ko SM, Hwang SH, Lee HJ. Role of cardiac computed tomography in the diagnosis of left ventricular myocardial diseases. *J Cardiovasc Imaging* 2019;**27**:73–92.
31. Bulluck H, Hammond-Haley M, Weinmann S, Martinez-Macias R, Hausenloy DJ, Cerqueira MD, Weissman NJ, Dilsizian V, Jacobs AK, Kaul S, Laskey WK, Pennell DJ, Rumberger JA, Ryan TJ, Verani MS, Anand S, Janardhanan R, Bondarenko O, Beek AM, Nijveldt R, McCann GP, Dockum WG Van, Hofman MBM, Twisk JWR, Visser CA, Rossum AC Van, Holtackers RJ, Heyning CM Van De, Nazir MS, Rashid I, et al. Comparison of myocardial fibrosis quantification methods by cardiovascular magnetic resonance imaging for risk stratification of patients with suspected myocarditis. *J Cardiovasc Magn Reson* Journal of Cardiovascular Magnetic Resonance; 2020;**21**:1–11.
32. Carminati MC, Boniotti C, Fusini L, Andreini D, Pontone G, Pepi M, Caiani EG. Comparison of image processing techniques for nonviable tissue quantification in late gadolinium enhancement cardiac magnetic resonance images. *J Thorac Imaging* 2016;**31**:168–176.
33. Grassi R, Miele V, Giovagnoni A. Artificial intelligence: a challenge for third millennium radiologist. *Radiol Medica* Springer Milan;

2019;**124**:241–242.
34. Assen M van, Muscogiuri G, Caruso D, Lee SJ, Laghi A, Cecco CN De. Artificial intelligence in cardiac radiology. *Radiol Medica* Springer Milan; 2020;**125**:1186–1199.
35. Bulluck H, Hammond-Haley M, Weinmann S, Martinez-Macias R, Hausenloy DJ, Anand S, Janardhanan R, Bondarenko O, Beek AM, Nijveldt R, McCann GPGP, Dockum WG Van, Hofman MBM, Twisk JWR, Visser CA, Rossum AC Van, As- NYH, Holtackers RJ, Heyning CM Van De, Nazir MS, Rashid I, Ntalas I, Rahman H, Botnar RM, Chiribiri A, Basha TA, Liew C, Tsao CW, Delling FN, Addae G, et al. Late gadolinium enhancement imaging in assessment of myocardial viability: Techniques and clinical applications. *J Cardiovasc Magn Reson* Journal of Cardiovascular Magnetic Resonance; 2018;**20**:1–11.
36. Zabihollahy F, Rajan S, Ukwatta E. Machine Learning-Based Segmentation of Left Ventricular Myocardial Fibrosis from Magnetic Resonance Imaging. *Curr Cardiol Rep* Current Cardiology Reports; 2020;**22**:1–8.
37. Hassani C, Saremi F, Varghese BA, Duddalwar V. Myocardial Radiomics in Cardiac MRI. AJR Am J Roentgenol. 2020 Mar;214(3):536-545. doi: 10.2214/AJR.19.21986.
38. Shiradkar R, Ghose S, Jambor I, et al. Radiomic features from pretreatment biparametric MRI predict prostate cancer biochemical recurrence: preliminary findings. J Magn Reson Imaging 2018; 48(6):1626–1636.
39. Lambin P, Rios-Velazquez E, Leijenaar R, et al. Radiomics: extracting more information from medical images using advanced feature analysis. Eur J Cancer 2012; 48(4):441–446.
40. Kumar V, Gu Y, Basu S, et al. Radiomics: the process and the challenges. Magn Reson Imaging 2012; 30(9):1234–1248.
41. Gillies RJ, Kinahan PE, Hricak H. Radiomics: images are more than pictures, they are data. Radiology 2016; 278:563–577
42. Schofield R, Ganeshan B, Fontana M, et al. Texture analysis of cardiovascular magnetic resonance cine images differentiates aetiologies of left ventricular hypertrophy. Clin Radiol 2019; 74:140–149
43. Shao XN, Sun YJ, Xiao KT, et al. Texture analysis of magnetic resonance T1 mapping with dilated cardiomyopathy: a machine learning approach. Medicine (Baltimore) 2018; 97:e12246
44. Cerqueira MD, Weissman NJ, Dilsizian V, Jacobs AK, Kaul S, Laskey WK, Pennell DJ, Rumberger JA, Ryan T, Verani MS. Standardized myocardial sementation and nomenclature for tomographic imaging of the heart: A Statement for Healthcare Professionals from the Cardiac Imaging Committee of the Council on Clinical Cardiology of the American Heart Association. *Circulation* 2002;**105**:539–542.
45. Bulluck H, Hammond-Haley M, Weinmann S, Martinez-Macias R, Hausenloy DJ. Myocardial Infarct Size by CMR in Clinical Cardioprotection Studies: Insights From Randomized Controlled Trials. *JACC Cardiovasc Imaging* 2017;**10**:230–240.
46. Jimenez Juan L, Crean AM, Wintersperger BJ. Late gadolinium enhancement imaging in assessment of myocardial viability: Techniques and clinical applications. *Radiol Clin North Am* Elsevier Inc;

2015;**53**:397–411.
47. Basha TA, Akçakaya M, Liew C, Tsao CW, Delling FN, Addae G, Ngo L, Manning WJ, Nezafat R. Clinical performance of high-resolution late gadolinium enhancement imaging with compressed sensing. *J Magn Reson Imaging* 2017;**46**:1829–1838.
48. Kim RJ, Wu E, Rafael A et al. The use of constrast-enhanced magnetic resonance imaging to identify reversible myocardial dysfunction. *N Engl J Med* 2000;**343**:1445.
49. Bondarenko O, Beek AM, Nijveldt R, McCann GP, Dockum WG Van, Hofman MBM, Twisk JWR, Visser CA, Rossum AC Van. Functional outcome after revascularization in patients with chronic ischemic heart disease: A quantitative late gadolinium enhancement CMR study evaluating transmural scar extent, wall thickness and periprocedural necrosis. *J Cardiovasc Magn Reson* 2007;**9**:815–821.
50. Anand S, Janardhanan R. Role of cardiac MRI in nonischemic cardiomyopathies. *Indian Heart J* Cardiological Society of India; 2016;**68**:405–409.
51. Mayerhoefer ME, Szomolanyi P, Jirak D, Materka A, Trattnig S. Effects of MRI acquisition parameter variations and protocol heterogeneity on the results of texture analysis and pattern discrimination: an application-oriented study. Med Phys 2009; 36:1236–1243
52. Saha A, Yu X, Sahoo D, Mazurowski MA. Effects of MRI scanner parameters on breast cancer radiomics. Expert Syst Appl 2017; 87:384–391
53. Bassler B, Mannil M, Maintz D, Alkadhi H, Manka R. Texture analysis and machine learning of non-contrast T1-weighted MR images in patients with hypertrophic cardiomyopathy—preliminary results. Eur J Radiol 2018;102:61–7.
54. Baessler B, Mannil M, Oebel S, Maintz D, Alkadhi H, Manka R. Subacute and chronic left ventricular myocardial scar: accuracy of texture analysis on nonenhanced cine MR images. Radiology 2018;286:103–12.
55. Larroza A, Lo´pez-Lereu MP, Monmeneu JV, Gavara J, Chorro FJ, Bodı´ V et al. Texture analysis of cardiac cine magnetic resonance imaging to detect non-viable segments in patients with chronic myocardial infarction. Med Phys 2018;45:1471–80.
56. Raisi-Estabragh Z, Izquierdo C, Campello VM, Martin-Isla C, Jaggi A, Harvey NC, Lekadir K, Petersen SE. Cardiac magnetic resonance radiomics: basic principles and clinical perspectives. Eur Heart J Cardiovasc Imaging. 2020 Apr 1;21(4):349-356. doi: 10.1093/ehjci/jeaa028.
57. Kotu LP, Engan K, Borhani R, et al. Cardiac magnetic resonance imagebased classification of the risk of arrhythmias in post-myocardial infarction patients. Artif Intell Med 2015 Jul;64(3):205e15.
58. Cheng S, Fang M, Cui C, Chen X, Yin G, Prasad SK, Dong D, Tian J, Zhao S. LGE-CMR-derived texture features reflect poor prognosis in hypertrophic cardiomyopathy patients with systolic dysfunction: preliminary results. Eur Radiol. 2018 Nov;28(11):4615-4624. doi:

10.1007/s00330-018-5391-5.
59. Augusto JB, Davies RH, Bhuva AN, Knott KD, Seraphim A, Alfarih M, Lau C, Hughes RK, Lopes LR, Shiwani H, Treibel TA, Gerber BL, Hamilton-Craig C, Ntusi NAB, Pontone G, Desai MY, Greenwood JP, Swoboda PP, Captur G, Cavalcante J, Bucciarelli-Ducci C, Petersen SE, Schelbert E, Manisty C, Moon JC. Diagnosis and risk stratification in hypertrophic cardiomyopathy using machine learning wall thickness measurement: a comparison with human test-retest performance. Lancet Digit Health. 2021 Jan;3(1):e20-e28. doi: 10.1016/S2589-7500(20)30267-3.

Supplementary Materials

In this section the threshold calculation methods described in the text are detailed.
A histogram, composed of 20 bins, is created from the values of the pixels belonging to the myocardium. From this histogram a fit is made with a double Gaussian function:

$$F = A_1 * e^{-\frac{(x-\mu_1)^2}{s_1^2}} + A_2 * e^{-\frac{(x-\mu_2)^2}{s_2^2}}$$

where A_1, μ_1 and $\sigma_1 = s_1/\sqrt{2}$ are respectively the amplitude, the mean and the standard deviation of the first gaussian function and A_2, μ_2 and $\sigma_2 = s_2/\sqrt{2}$ the amplitude, the mean and the standard deviation of the second gaussian function. The starting parameters of the Matlab fit function are set so that the distribution around the maximum of the histogram is fitted with the first gaussian function.
The Double-gaussian method choose the threshold value (T_G) depending on the occurrence of the following conditions:

- if $\mu_1 + \sigma_1 > \mu_2$ and $\mu_2 - \sigma_2 < \mu_1$, then $T_G = \mu_1 + 2\sigma_1$;
- if $\mu_1 + 2\sigma_1 < \mu_2 - \sigma_2$, then $T_G = \mu_1 + 2\sigma_1$;
- if $\mu_1 + 2\sigma_1 < \mu_2 - \sigma_2/2$ and $\mu_2 - 2\sigma_2 > \mu_1 + \sigma_1$, then $T_G = \mu_2 - \sigma_2/2$;
- if none of the previous conditions are satisfied, T_G is the minimum between $\mu_1 + 2\sigma_1$ and μ_2.

The Fixed-shift method threshold (T_F) is chosen based on the bin of the histogram containing the maximum value (B_{MAX}), according to the following conditions:

- if $B_{MAX} < 15$ and σ_1 is greater than the range of 3 bins, T_F is the value of the 5th bin after the B_{MAX};
- if $B_{MAX} < 15$ and σ_1 is lesser than the range of 3 bins, T_F is the value of the 4th bin after the B_{MAX};
- if none of the previous conditions are satisfied, T_F is the middle position between the B_{MAX} and the last bin.